REMOTE SENSING OF TREE STRUCTURE AND BIOMASS IN NORTH AUSTRALIAN MESIC SAVANNA

by

Grigorijs Goldbergs

(Bachelor of Science, Master of Geo-Information Science)

A thesis submitted in fulfilment of the requirements for the degree of

DOCTOR OF PHILOSOPHY

Research Institute for the Environment and Livelihoods,

College of Engineering, IT and Environment

Charles Darwin University, Darwin, Australia,

May 2019

Thesis declaration

I hereby declare that the work herein, now submitted as a thesis for the degree of Doctor of Philosophy at the Charles Darwin University, is the result of my own investigations, and all references to ideas and work of other researchers have been specifically acknowledged.

I hereby certify that the work included in this thesis has not already been accepted in substance for any degree, and is not being currently submitted in candidature for any other degree.

Grigorijs Goldbergs Date: ***02 April 2019***

Acknowledgements

This study is the result of my involvement with many people who strive for the best in themselves and others, and I would like to express my gratitude and appreciation for all the people who helped me in various ways as I undertook this research.

In particular, I sincerely thank the members of my supervisory panel for their guidance, constructive criticism, advice and support – Assoc. Prof Shaun R Levick, Dr Stefan W Maier, Dr Andrew Edwards and Adj. Prof Jeremy Russell-Smith. I have been very fortunate to work with You and learned much from You!

I would also like to thank Prof. Lindsay Hutley, Matthew Northwood, Jayshree Mamtora, Emmylou Trombley, Mike Lawes and Prof. Andrew Campbell (ACIAR) from CDU and RIEL staff for their support and getting me through my PhD process.

I would like to thank the following organisations for their in-kind and financial support: Research Institute for the Environment & Livelihoods (RIEL) and Darwin Centre for Bushfire Research of Charles Darwin University; Bushfire and Natural Hazards Cooperative Research Centre (BNHCRC), made available by the Commonwealth of Australia through the Cooperative Research Centre program.

I would like to especially thank my friend and former college Muditha Heenkenda for her advice and help through the early stage of my PhD.

I also would like to express my deepest gratitude to the following people who bringing me up to be the person I am today: Nina Pušpure and Jānis Laicāns, my secondary school teachers; Dr Jānis Klētnieks, great Latvian scientist, my supervisor and mentor; Helēna Gerilovič̆a, my ‘soul’ doctor and close friend.

Finally, I appreciate the encouragement provided by my family during this study. Special thanks and love to my great son Edvards for his patience in putting up with a stressed and overworked father on the other side of the world. But most of all, thanks to my wife Alina for her tolerance, support, love and understanding.

I dedicate this work to the memory of my mother, Vera.

Abstract

The quantification of Above Ground Biomass (AGB) plays a major role in issues related to greenhouse gas emissions and carbon sequestration, pertaining to global warming and the effects of climate change. In *Eucalyptus miniata/tetrodonta* dominated open-forest in Australia's northern tropical savanna, AGB mapping is challenging, due to the complex structure of the canopy stand, highly dynamic woody cover, vast spatial extent, vulnerability to climatic effects and the impacts of extensive fire.

Remotely sensed data allow for the mapping, quantification and monitoring of AGB at various scales. Quantification of AGB in tropical savanna by common medium and coarse spatial resolution optical sensor data is inappropriate to monitor finer-grained ecological processes responsible for measuring carbon stocks at an individual tree level and are limited in detecting vertical vegetation structure. There is limited research on the utility of airborne LiDAR (Light Detection and Ranging) and alternative high resolution (< 0.5 m) remote sensing tools for Australian savanna structural assessment. The main goal of this research is to evaluate the efficiency of small footprint airborne LiDAR and determine whether Unmanned Aerial Systems (UAS) and Very High Resolution (VHR) satellite stereo remote sensing data can be used to extract tree biophysical and vertical structural parameters for the purposes of accurately estimating biomass stocks in Australian mesic savannas.

This study utilized a two-phase LiDAR analysis procedure integrating both Individual Tree Detection (ITC) and Area-Based Approaches (ABA) to better understand how the uncertainty of biomass estimation varies with scale. Regression analysis was applied on remote sensing data to develop biomass estimation models based on tree height allometry. This study demonstrated that where field-plot data are spatially limited, it is possible to use a hierarchical integration approach based on AGB uncertainty calculation and calibration to upscale AGB estimates from individual trees to broader landscapes.

Although airborne LiDAR provided higher tree detection rates and accurate estimates of tree aboveground biomass, this research found that a 3D point cloud obtained from light-weight optical UAS imagery by an image dense matching technique is an

adequate low-cost alternative for the detection of dominant and co-dominant tree stands, at least at a local scale in Australian tropical savanna.

This study offers some insight into factors causing the poor dense image matching by high-resolution stereo satellites. The structural complexity of Eucalypt crowns, represented by clumped-leaf-grain structure and erectophile foliage, are the main factors determining the efficiency of tree/canopy detection using stereo satellite imagery.

Table of contents

Chapter 6

List of Figures

List of Tables

List of Abbreviations

ABA	Area-Based Approach
AGB	Above-Ground Biomass
BRDF	Bidirectional Reflectance Distribution function
CHM	Canopy Height Model
DBH	Diameter at Breast Height
DSM	Digital Surface Model
DTM	Digital Terrain Model
EMR	Electromagnetic Radiation
GCP	Ground Control Point
GE1	Geo Eye 1
GIS	Geographic Information Systems
GPS	Global Positioning System
GSD	Ground Sample Distance
IMU	Inertial Measurement Unit
ITC, ITD	Individual Tree Detection
LiDAR	Laser scanning Light detection and Ranging
NT	Northern Territory
RS	Remote Sensing
SAR	Synthetic-Aperture Radar
SGM	Semi-Global Matching
SfM	Structure from Motion
UAS	Unmanned Aerial Systems
VHR	Very High Resolution
WV1	World View 1

Chapter 1

Introduction

Page intentionally left blank

1.1 Introduction

1.1.1 The ecological and land management requirements for spatially explicit forest information

The spatial-temporal mapping of forests to assess their status and productivity is of increasing importance given their role in the global carbon cycle and the wide range of ecosystem services they can provide locally (Franklin 2001; Rogers et al. 2012). Sustainable management, monitoring and use of forest resources, be it for wood-based bioenergy, climate change mitigation, conservation, or maintenance of water quality, and biodiversity, will become increasingly important given climate change, population pressure and associated land use change (Becker et al. 2006; Newton 2007). Management of production forests is largely related to wood production, soil management, and water use (Gaston and Spicer 2013). However, natural forest/woodland ecosystems have a far broader range of required management outcomes. Over the last two decades, the magnitude and dynamics of forest carbon sequestration has become a key topic within the global change community. Forests cover 30% of the planet's land area, and a critical component of tracking sequestration is the reliable mapping of tree biomass and the monitoring of cover and structural change over time (Koch 2010). Biomass is a key component of global biochemical cycles, especially in the carbon cycle. Since about 50% of the forest biomass is carbon, forest biomass provides a good estimate of the carbon pools in forests (Köhl et al. 2006).

Based on Australia's international climate change agreement commitments, including the United Nations Framework Convention on Climate Change (Australia is a party to the UNFCCC which came into force from 21 March 1994) and the Montreal Process (Working Group on Criteria and Indicators for the Conservation and Sustainable Management of Temperate and Boreal Forests), Australia is required to provide progressively reliable, precise and quantitative data on vegetation structure, dynamics and condition over the entire continent (Richards and Brack 2004). This presents many research challenges given the breadth of information required, and especially with regard the current huge array of information sources. To manage forests sustainably, meet national and global reporting commitments, and provide input to climate change research, it is critical to develop efficient and cost-effective methodologies that will allow for precise quantification of vegetation biomass and dynamics (Bradshaw et al. 2013; Wood et al. 2006). In this matter, tools for mapping the extent of vegetation cover and structure are of central importance.

Traditional practices for collecting vegetation biomass information are costly and time-consuming providing low spatial coverage, and, in most cases, require destructive fieldwork, which is impractical for large and remote areas. Remote sensing complements traditional field methods through data analysis which enables precise estimation of vegetation biomass and dynamics across high spatial coverage and different scales by avoiding destructive sampling and reducing time and cost from data acquisition to final output. The application of Remote Sensing (RS) and Geographic Information Systems (GIS) technologies to forest assessment is the focus of ongoing research, and the techniques continue to develop rapidly (Newton 2007).

1.1.2 Performance and challenge of remote sensing-based biomass estimation

When remote sensing data are used to quantify vegetation biomass, the level of detail obtained depends mostly upon the spatial resolution of the used sensor, the electromagnetic spectrum within observations are recorded (spectral resolution), the sensitivity of the sensor's detector to detected Electromagnetic Radiation (EMR) (radiometric resolution) and whether the sensor is active (emit their own energy) or passive (detect external EMR, e.g. optical sensors) (Newton 2007).

Satellite-based earth observations offer methods for estimating biomass and carbon stocks, but at relatively coarse spatial scales only. Satellite sensors that produce two-dimensional images are insufficient to monitor finer-grained ecological processes responsible for the carbon stocks on an individual tree level and are limited in detecting three-dimensional spatial patterns of vegetation (Lu 2006). Consequently, the sensor scales of the most widely available optical satellite imagery, Landsat (Ground Sample Distance (GSD) 30 m) and MODIS (GSD 250 m), are not appropriate for direct measurements of carbon stocks (Asner et al. 2012a). Despite the fact that new Sentinel multispectral satellite sensors (GSD 10m) have great potential for long-term high-frequency vegetation monitoring applications (Malenovský et al. 2012), this thesis aims at pointing out the use of the modern high-resolution (1 m resolution and better) remote sensing tools which allow the retrieval of the vertical structural characteristics of vegetation.

In recent years, there has been increasing use of active sensors like Synthetic-Aperture Radar (SAR) and airborne Laser scanning Light Detection and Ranging (LiDAR) systems to estimate various 3D characteristics of canopy and crown structure such as crown base height, Crown Fuel Weight (CFW), and Canopy Bulk Density

(CBD), based on height metrics and regression models (Popescu and Zhao 2008; Skowronski et al. 2011). Laser scanning, combined with up-to-date advanced data processing methods, has the potential to deliver very precise and reliable full 3D biomass structure information to estimate carbon storage.

However, LiDAR data acquisition is still expensive, and not often readily available. As an alternative, stereo airborne and satellite imagery may also offer the ability to rapidly assess canopy height, in an accurate and repeatable manner (Aguilar et al. 2014a). The development of high-performance Structure from Motion (SfM) (Ullman 1979) and image-matching techniques, e.g. Semi-Global Matching (SGM) (Hirschmuller 2008), allows for the generation of high-quality Digital Surface Models (DSM). By using high-performance image-matching and photogrammetry techniques, 3D tree canopy information may be easily and automatically extracted from satellite and aerial images in stereo and multi-image mode depending upon complexity and density of vegetation (Baltsavias et al. 2008). Accuracy depends primarily on the image scale, image texture, imaging geometry, and compactness of the tree canopy. Nowadays, the adaptable stereo imaging capability of the newest civilian Very High Resolution (VHR) satellites (e.g. WorldView-2 or Pléiades) and their improved geometric resolution generate accurate CHMs by means of standard photogrammetric procedures (Aguilar et al. 2014a).

Remote sensing tools and statistical algorithms, used for regional and global biomass estimates, are eventually depend on measurements of individual trees (Asner et al. 2012b; Saatchi et al. 2011). To develop robust biomass estimates, one key parameter for estimating tree biomass is tree height (due to allometric relationships developed between tree height, tree diameter and wood density), which can be

obtained from the CHM, derived from LiDAR and VHR optical imagery by means of photogrammetric processing of stereo-pairs or triplets. In this research, a methodology using these RS tools was modified from previous studies and applied to Australian tropical savanna, one the world's most extensive and intact woodland ecosystems (Woinarski et al. 2007).

Chave et al. (2005) reported that standard deviation of all divergences between observed and predicted stand biomass, across 27 tropic study sites included Australian tropical savanna, was within 11.8–15.6%. Thus, the major objective of this research is to investigate efficiency of RS tools for estimating biomass within threshold 15 % of plot mean AGB. In given thesis, the word "efficiency" means the evaluation of accuracy, reliability and effectiveness of RS tools and corresponding data.

1.1.3 Description of Australian tropical savannas

North Australian tropical savannas cover ~2,000,000 km^2, occupying nearly one third of the Australian continent, accounting for approximately 12% of the world's tropical savannas and 33% of terrestrial carbon (Williams et al. 2004). Australian tropical savannas are restricted to the tropical and subtropical zones of the Australian continent, from north-eastern Queensland across the Gulf of Carpentaria, the Top End of the Northern Territory (NT), and west to the Kimberley in Western Australia **(Figure 1.1)** (O'Donnell 2005). Australia's tropical savanna habitats are relatively pristine, partly due to low population density (0.25 people km^{-2}; Australian Bureau of Statistics (2017)) and lower levels of exploitation of natural resources (Williams et al. 2005a). NT savannas are often remote; support unique flora and fauna, and vast areas are inaccessible.

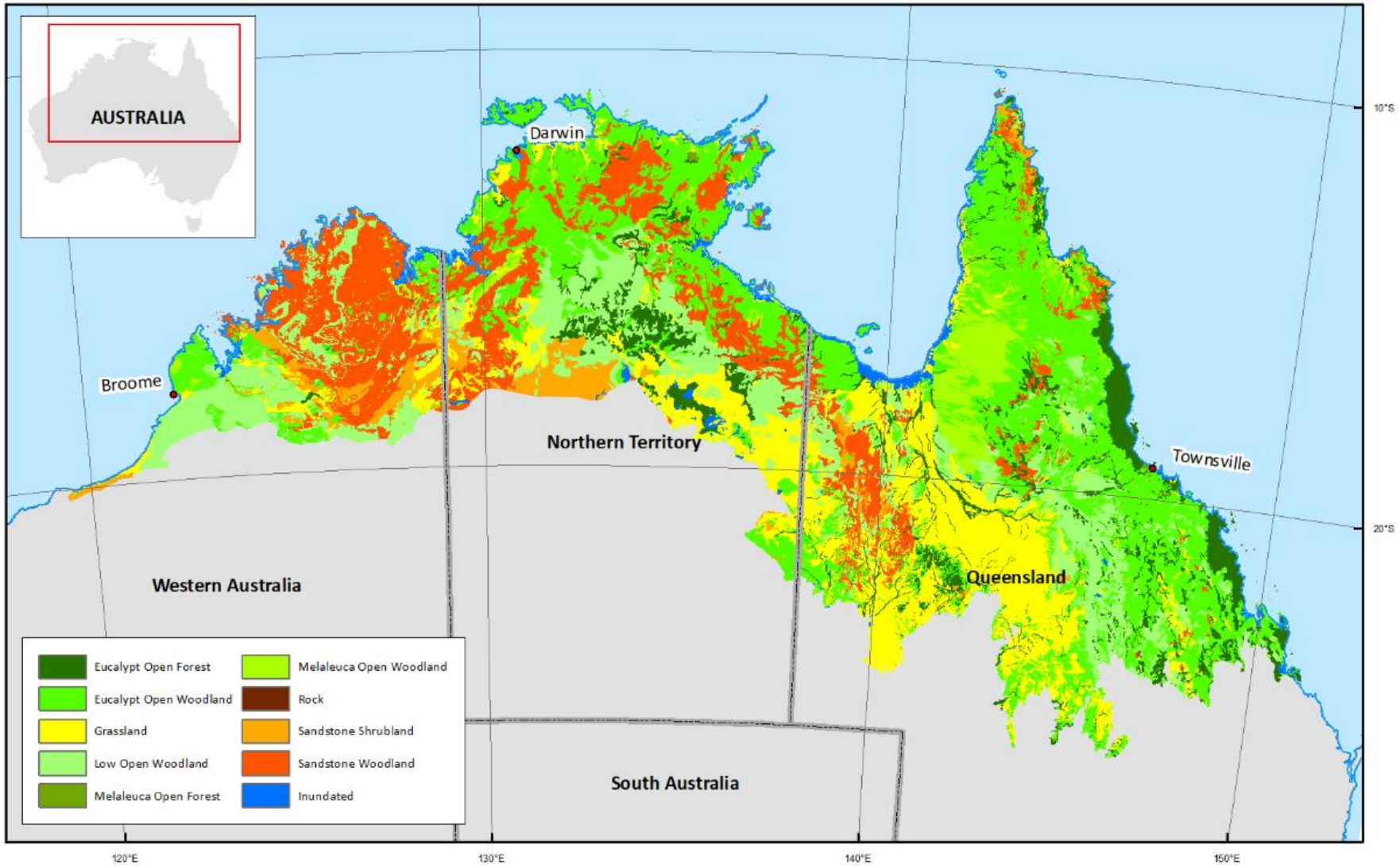

Figure 1.1: The extent of the tropical savannas in northern Australia illustrating the main vegetation groups (Fox et al. 2001).

The composition and structure of these savannas is largely determined by soil water availability, plant available nutrients and fire frequency (Williams et al. 1997). Above the 1000-mm rainfall isohyet, tropical 'mesic' savannas are dominated by *Eucalyptus miniata* and *Eucalyptus tetrodonta* open forests **(Figure 1.2)**. These two species provide more than 70% of overstorey leaf area index and standing biomass (O'Grady et al. 2000), less than 30% canopy cover, and a stem height range from 10 to 25m depending on soil type and depth. *Eucalypts* have extensive root systems, enabling them to use water from deep soil layers and maintain relatively high transpiration and photosynthetic rates during the dry season (O'Grady et al. 1999). The dry season, lasting from May to October, is a period of little or no rainfall. Temperatures and solar radiation remain high throughout the year and mean monthly temperatures throughout the year vary only slightly from annual means.

Figure 1.2: Photograph of the tropical 'mesic' savanna, dominated by *Eucalyptus spp*.

Recent remote sensing and inverse model studies of carbon sources and sinks (Beringer et al. 2011; Collins et al. 2009; Cooke et al. 2009; Kanniah et al. 2011) have identified these heterogenous Australian tropical savannas as being highly dynamic in space and time in terms of woody cover change and carbon sequestration due to their vast spatial extent, high productivity, vulnerability to climatic effects (cyclones etc.), fires and insufficient fire management (Moore et al. 2015). This presents many research challenges given the breadth of information required, and especially with regard the quantification of vegetation above-ground biomass. Thus, to manage Australian savannas sustainably, meet national and global reporting commitments, and provide input to climate change research, it is critical to develop methodologies which will allow for precise quantification of savanna stocks and dynamics.

There is limited data describing carbon stocks and their aboveground dynamics across northern tropical savannas in Australia. However, such information is crucial for developing comprehensive carbon sequestration and accounting strategies and for conserving tropical savannas (Kanniah et al. 2010). Despite these importances, tropical savannas are under studied compared to the other major biomes and there have been relatively few studies focusing on the savanna vegetation structural parameters and biomass estimation by using high-resolution remote sensing techniques.

1.1.4 Fires in Australian savannas

Fire is a key driver of savanna structure and dynamics in savanna across the globe, and an it particularly important in north Australia. In Australia, between 300,000 km^2 and 700,000 km^2 are affected by fire annually (Maier and Russell-Smith 2012a). Fire is frequent, particularly in the mesic savannas, where fire regimes are

dominated by grass fires rather than crown fires, and where fire seasons are determined by monsoonal weather patterns. Peak fire activity generally occurs during the mid to late dry and early wet season (August to December) (Meyer et al. 2012). Current fire regimes cause severe damage to the environment, have serious effects on biodiversity, ecology, and, at the same time, are substantial sources of greenhouse gas emissions (Russell-Smith et al. 2009). It is widely recognised that biomass burning is a globally significant driver of carbon CO_2 cycling and an important source of greenhouse gases (van der Werf et al. 2010). As above ground biomass (AGB) is approximately 48% carbon, there is a clear need for techniques to efficiently and reliably quantify three-dimensional (3D) AGB structure and biomass change related to changes in the frequency, timing and intensity of fires. As well, savanna fire management requires accurate, spatially precise and up-to date information on vegetation fuel distribution and vertical structure.

Due to low population densities in significant parts of the Australian mainland, fire-affected areas typically occur in remote and inaccessible situations. In such cases, remote sensing has become an essential tool for fire management and applied research, especially in central Australian rangelands and the fire-prone tropical savannas of northern Australia. The availability of a robust approach for measuring carbon stocks in savanna vegetation could provide an opportunity to enhance landscape-scale fire management through carbon sequestration in living vegetation / biomass, in ‘savanna burning’ projects (Australia. 2018). This could greatly assist indigenous community groups, and other land managers (e.g. conservation and pastoral) in remote northern Australia to develop viable environmental service initiatives and support enhanced community resilience (Greiner R et al. 2012).

Page intentionally left blank

1.2 Thesis aims, objectives and research questions

Section 1.1 identified the need for precise biomass quantification and dynamics by using high resolution remotely sensed data in Australian savannas. Airborne small footprint LiDAR has shown promise to date in being able to meet many of the requirements for accurate tree biophysical and vertical structural parameters extraction. However, there is limited research on the utility of LiDAR and alternative high resolution remote sensing tools for Australian savanna structural assessment. Therefore, the main goal of this research is to evaluate the efficiency of small footprint LiDAR and determine whether VHR optical remote sensing data (airborne and VHR stereo satellite imagery) can be used to extract tree biophysical and vertical structural parameters for the purposes of accurately estimating biomass (RMSE <15 % of plot mean AGB), and hence carbon stocks, in Australian mesic (>1,000 mm mean seasonal rainfall) savannas.

To achieve this goal, the following research aims have been identified, each with a series of objectives.

Aim 1: To evaluate how the uncertainty of Above-Ground Biomass (AGB) estimation varies at plot-level spatial scales by integrating both individual tree and area-based LiDAR methods.

Objectives:

I. To establish allometric relationships between field-derived individual tree AGB and LiDAR-derived crown area and tree height.

II. To test the individual tree delineation canopy maxima and watershed segmentation algorithms efficiency and quantify commission/omission errors.

III. To integrate individual tree and area-based methods for savanna biomass and biomass uncertainty estimation.

Aim 2: To assess the extent to which SfM three-dimensional (3D) point clouds—obtained from consumer-grade light-weight and low-cost (< $2000) unmanned aerial systems (UAS) - can efficiently estimate tree structural parameters in order to quantify biomass in Australian tropical savannas, and be a feasible low-cost alternative to airborne LiDAR scanning for canopy parameter retrieval.

Objectives:

I. To analyse the influence of the spatial resolution of canopy height models on tree detection accuracy, by using the structure from motion (SfM) and image matching techniques for generating 3D point clouds from stereo imagery.

II. To assess the applicability and accuracy of canopy maxima and watershed segmentation tree detection algorithms applied to SfM-based CHMs.

Aim 3: To assess the accuracy of extrapolation, from local to broader scales, the canopy structural parameters information obtained from SfM three-dimensional (3D) point clouds by using stereo imagery from commercially available VHR satellites.

Objectives:

I. To evaluate and compare the completeness and vertical accuracy of extracted digital surface models (DSM) from pure along-track GeoEye1 (GE1) and WorldView2 (WV2) VHR satellite stereo pairs.

II. To examine the influence of eucalypt canopy structure, imagery acquisition geometry and other related factors on SfM performance and canopy detection accuracy.

Aim 4: To provide recommendations and a conceptual framework for estimating canopy structural parameters in open canopy Australian tropical savannas based on analysis and comparison of high resolution remote sensing data (LiDAR, airborne and VHR satellite imagery).

Objective:

I. To analyse the influence of image spatial resolution for individual tree crown and canopy identification in Australian savannas, by using image matching techniques applied on stereo imagery.

1.3 The Study area

This study will be undertaken in Litchfield National Park, 100 km south-west of Darwin, Northern Territory, between latitudes 13^0 08' S and 13^0 14' S and longitudes 130^0 44' E and 130^0 51' E,. Covering approximately 25 km^2, the Litchfield Savanna Supersite (LSS) represents high rainfall tropical savanna, the dominant ecosystem type across northern Australia (TERN 2012). The rainfall is highly seasonal with most rain falling from October to April. During the fire season (May to September), the understorey progressively cures with increasing biomass flammability. The landscape is predominantly composed of savanna woodlands dominated by *Eucalyptus* and mixed perennial/annual grasses (Landsberg J et al. 2011) **(Figure 1.2).**

1.4 Outline of the thesis

There are seven chapters in this thesis, composed of three peer-reviewed manuscripts, a general introduction (Chapters 1 and 2), a discussion of the findings of the research with recommendations and conclusions (Chapter 6). The three manuscripts have been published in international peer-reviewed journals. The manuscripts are organized into three separate chapters (3 to 5), each of which stands alone and addresses one or more research objectives.

The current chapter, Chapter 1, presents a brief introduction to the central research questions of this thesis, provides descriptions of Australia's savanna and their definition at the national level, and outlines the requirements for precise biomass quantification by using high resolution remotely sensed data in Australian savanna.

Chapter 2 provides a review of high resolution remotely sensed tools and methods for precise biomass quantification and dynamics, vegetation structure, and the importance of scale and resolution.

Chapter 3 is a peer reviewed publication entitled: *Hierarchical integration of individual tree and area-based approaches for savanna biomass uncertainty estimation from airborne LiDAR* published in **Remote Sensing of Environment** (Goldbergs et al. 2018a). The paper describes, in detail, the two-phase LiDAR procedure to integrate both individual tree detection (ITC) and area-based approaches (ABA), designed for above ground biomass and its uncertainty estimation in tropical savannas, facilitating regional savanna inventories, monitoring and mapping.

Chapter 4 is a peer reviewed publication entitled: *Efficiency of Individual Tree Detection Approaches Based on Light-Weight and Low-Cost UAS Imagery in Australian Savannas* published in **Remote Sensing (**Goldbergs et al. 2018b**).** The paper assesses the extent to which SfM three-dimensional (3D) point clouds obtained from consumer-grade light-weight and low-cost (< $2000) unmanned aerial systems (UAS) can efficiently and effectively detect individual trees, measure tree heights, and provide AGB estimates in Australian tropical savannas.

Chapter 5 is a peer reviewed publication entitled: *Limitations of high resolution satellite stereo imagery for estimating canopy height in Australian tropical savannas* published in **International Journal of Applied Earth Observations and Geoinformation** (Goldbergs et al. 2019). The paper focuses on estimating canopy height by means of photogrammetric processing of stereo-pairs from commercially available VHR satellites, and analyses the factors influencing image-based CHM quality and completeness.

Chapter 6 summarises the findings of this thesis and discusses the theoretical and practical implications of the research, limitations, and the future directions for savanna biomass estimation and vegetation vertical structure assessment by utilising high resolution remotely sensed data.

Page intentionally left blank

Chapter 2

Remote sensing-based vegetation biomass estimation

Page intentionally left blank

2.1 Methods for vegetation above-ground biomass estimation

Total biomass includes both the above and below ground biomass. Living trees embody the major portion of the carbon pool represented by the aboveground biomass (AGB; i.e. stems, branches, twigs and foliage). Due to the difficulty of collecting field survey data of below ground biomass, most biomass studies have focused on AGB. In this thesis, if no additional information is provided, 'biomass' represents only AGB. A variety of methods are used to perform the estimation of biomass, from field-based measurements to remote sensing methods **(Table 2.1).**

The most common technique for deriving woody biomass is through field-based destructive sampling and the calculation of allometric relationships among tree component volumes or weights. This tree-based allometry is a principal tool in carbon accounting and indirectly estimates the above- and/or below-ground biomass (Williams et al. 2005b). The conversion of stem Diameter of Breast Height (DBH) (1.3 m above mean tree base) to tree biomass using allometric equations is a well-established practice (Chave et al. 2005; Montagu et al. 2005) and is the standard approach for studying woody biomass dynamics (Lasky et al. 2014; Paul et al. 2013; Preece et al. 2015). Destructive harvesting is time consuming and expensive, and in some cases, restricted access to certain species and tree sizes, limits the number of trees sampled. Remote sensing methods can offer a rapid and cost-effective alternative method for estimating the local AGB in forests (Lefsky et al. 2002; Lucas et al. 2008; Næsset and Økland 2002), and more consideration of such approaches is needed in tropical savannas (Asner et al. 2008).

Table 2.1: Summary of main methods for above-ground biomass estimation (adapted from Lu et al. (2016))

Category	Methods and tools	Description	Advantages	Disadvantages
Field based measurements methods	Destructive sampling (harvest method)	Individual tree and its parts cut, dried and weighed	Most accurate and direct biomass estimation approach. Primary method for establishing allometric models	Destroys trees; time consuming and labour-intensive; limited number of samples; limitations for cutting mature and heavy stems
	Allometry	Tree species with regression models between AGB and tree-canopy variables	Accurate; non-destructive after allometry established; applied to any tree-canopy of corresponding species; can be applied to previous field measurements	Site and species specific; in most cases needs the destructive sampling to establish relations
Active sensor Remote sensing	airborne LiDAR Provides own pulsed light energy to illuminate the object;	LiDAR metrics based on statistical measures of point clouds or estimated products (individual trees, CHM, etc.) regressed against AGB	Most accurate 3D object description; high sample density; able to penetrate trees/canopies; day-night operation	High operating costs per area unit; Very large datasets that are difficult to interpret; does not penetrate cloud, absorbed by water
	Radar (SAR) emits electromagnetic radiation at microwave frequencies	Backscattering coefficients; creates an integrated regular grid of elevation samples	Penetrates forest canopy, clouds and haze; more appropriate for large area coverage; day-night operation	Less accurate than LiDAR; signal phase delay problem; limited spatial resolution

Table 2.1 continued

Category	Methods	Description	Advantages	Disadvantages
Passive (optical) sensor Remote sensing	Imagery (mono) spectral and spatial feature analysis	Vegetation tree-canopy cover extraction based on spectral bands, vegetation indices, pixel-based and object-based image segmentation and classification	High diversity in image radiometry, spatial and temporal resolution, suitable for wide range of applications; flexibility in combination of spectral and spatial imagery features;	Data only related to horizontal vegetation structure; dependence on weather conditions and sun parameters
	Structure from Motion (SfM) and stereo image matching	AGB estimate based on variables of generated image-based dense 3D point clouds or estimated products (individual trees, CHM, etc.)	Estimates vertical vegetation structure and parameters; High diversity in cover, spatial and temporal resolution (from UAS to satellite)	No tree/canopy penetration; dependence on weather conditions and sun parameters; requires skilled data analyst
Remote sensing	Integration of optical and/or active sensor data	Active sensor data combined with optical-sensor multispectral bands as extra variables	Gain strength of both sensors to improve predictions of AGB; contains vertical and horizontal information of vegetation structure	Increased acquisition and processing costs. More research needed to evaluate efficiency on sensor integration

Remote sensing uses two primary types of sensors – active and passive. Passive sensors detect external electromagnetic radiation (mostly sunlight) that is emitted or reflected by the observed object. Active sensors emit their own energy and measure the detection radiation that is reflected or backscattered from the target. Sensors of all types can be placed to different platforms: land based (mobile or fixed), Unmanned Aerial Systems (UAS), airborne and satellite. All platforms can be assisted by navigational systems, such as Global Positioning System (GPS) and an Inertial Measuring Unit (IMU) to perform an accurate geo-positioning of the sensor (Konecny 2014). Satellite sensors acquire a large swath with high temporal recurrence, allowing sequential monitoring with less precise estimates. In their turn, terrestrial and airborne sensors provide data with highest 3D spatial resolution and accurate estimation of forest attributes for low coverage area.

AGB can be measured only indirectly from remote sensing data, by using the correlations between biomass and tree or canopy variables, such as crown diameter or tree-canopy height (Lu 2006). An indicator with high predictive efficiency for biomass estimation is the tree height, which is highly correlated with wood volume (Koch 2010). Each sensor platform provides data over different spatial scales and enables AGB estimates with different levels of uncertainty and errors (Popescu et al. 2013).

The requirement for exact and spatially accurate data on the height and on the three-dimensional (3D) structure of vegetation has long been recognized in the fields of forestry and projects on carbon accounting (Hyyppä et al. 2008; Newton 2007). Different remote detecting methods have been produced to address these issues, producing different levels of achievement. In the past two decades, many researchers have reported that active sensors like LiDAR and SAR have a much greater potential

than passive sensors in retrieving data of 3D vegetation structure through vegetation penetration capability and interacting with all the vegetation stratum (Englhart et al. 2011; Lu et al. 2016; Maltamo et al. 2014).

The past decade has seen an increase in biomass studies and remote sensing applications in Australian tropical savannas (**Table 2.2**). Most studies in the field of biomass estimation have only focused on the retrieval of horizontal vegetation structure information, like crown/canopy and land cover classifications, and vegetation indices. However, most studies lack research on very high resolution active and passive sensors which could provide vertical structure information, e.g. estimation of canopy/tree heights or height metrics for biomass calculations. There are few studies relating to the application of LiDAR (Lucas et al. 2008; Shendryk et al. 2016) and no previous study has investigated the use of stereo imagery for characterising Australian savanna vertical vegetation structure and estimation of plot-scale/individual tree AGB. Thus, this study assesses and investigates the usefulness of LiDAR, airborne and VHR satellite stereo imagery data for the purposes of accurately estimating biomass in Australian mesic savannas.

Table 2.2: Examples of biomass studies and remote sensing applications in Australian tropical savannas

Sensor	Type	Data spatial resolution	Estimated parameters and applications	Data samples	References
Airborne Synthetic Aperture Radar (AirSAR)	active	5m-10m	AGB estimation based on sensor backscatter intensity (pixel-based) correlation with DBH/basal area	0.0625 - 1ha plots	(Collins et al. 2009)
Airborne LIDAR; terrestrial LiDAR	active	0.5-20 pts/m2	AGB estimation based on correlation with extracted individual tree heights and LiDAR point cloud height metrics	0.0625 - 1ha plots	(Lucas et al. 2008; Shendryk et al. 2016)
Aerial photography	passive	0.35-0.50 m	AGB based on allometry from vegetation cover; supervised classification of orthophotos; mangrove canopy height from stereo imagery	Individual tree and canopy level	(Fensham and Fairfax 2003; Lucas et al. 2002; Mitchell et al. 2007)
WorldView2 (WV2)	passive	0.5 PAN 2 m MS	Mangrove Canopy and tree top delineation from parameterized object-based and local maxima algorithms; Inverse Watershed Segmentation; regression with LAI; vegetation maps	Individual tree and canopy level	(Heenkenda et al. 2016; Heenkenda et al. 2015) (Whiteside and Bartolo 2015)
QuickBird	passive	0.6 PAN 2.4m MS	parameterized object-based segmentation and local maxima (NDVI) tree crown delineation	Dominant trees	(Whiteside et al. 2011b; Whiteside et al. 2014)

Sensor	Type	Data spatial resolution	Estimated parameters and applications	Data samples	References
Airborne Hyper-spectral scanner (Specim AISA+)	passive	0.5-2.5m	Vegetation parameters; canopy parameters; spectral parameters such as vegetation indices, LAI, etc.	Canopy level	(Beringer et al. 2011)
Advanced Very High-Resolution Radiometer (AVHRR)	passive	1.1 km	Fire detection and mapping based on temperature from thermal bands; NDVI	Pixel-based	(Russell-Smith et al. 2003)
ASTER	passive	15 m	Object-based (OB) image segmentation and land cover classification	Pixel-based	(Whiteside et al. 2011a)
Landsat TM ETM+	passive	30 m	Fire mapping (RED,NIR,sNIR bands) and fire severity mapping	Pixel-based	(Edwards et al. 2018; Goodwin and Collett 2014)
MODIS	passive	1 km	NDVI; Gross primary productivity (GPP) along with Leaf Area Index (LAI), fraction of absorbed Photosynthetically Active Radiation (fPAR), light use efficiency (LUE) and meteorological variables;	Pixel-based	(Beringer et al. 2011; Kanniah et al. 2011; Kanniah et al. 2009)
MODIS	passive	250m, 500m, 1 km	Active fire detection and mapping based on temperature from thermal bands;	Pixel-based	(Edwards et al. 2013; Maier 2010)

2.2 LiDAR remote sensing of vegetation

Lidar (Light Detection and Ranging) is an active remote sensing technology, which emit and detect the reflected light energy to measure distance to the object. LiDAR captures the horizontal and vertical distribution of plant physiognomy at high spatial resolution in 3D dense point cloud form (**Figure 2.1**); the most appropriate data to estimate biomass by indirect allometry (Maltamo et al. 2014). Depend on used platform, LiDAR can be divided into Airborne Laser Scanner (ALS), Terrestrial Laser Scanner (TLS) and satellite-mount LiDAR. In contrast to the viewing perspective from above provided by satellite and airborne sensors, terrestrial LiDAR provides a clear view of the tree stem and can directly determines the Diameter at Breast Height (DBH). ALS can estimate biomass from local to regional scale and allows better understanding of the variation in forest structure and biophysical parameters at multiple spatial scales (Popescu and Hauglin 2014). In this thesis, if no additional information is provided, 'LiDAR' represents only airborne laser scanner.

LiDAR processed data (primarily tree height) is increasingly being used as the basis for biomass estimation of whole woodland and their components (individual plants and their parts). Many studies utilising either small footprint (< 0.5 m radius) or large footprint (5 - 10 m) waveform airborne LiDAR have demonstrated an ability to recover structural elements such as tree and canopy height, canopy cover and volume at accuracies nearly equivalent to, and sometimes better than, through field survey (Gobakken and Næsset 2005; Lefsky et al. 1999; Riaño et al. 2003). Most existing RS techniques rely on developing allometric models between height metrics and field-estimated forest biomass (Asner et al. 2013; Meyer et al. 2013). When measuring tree

heights using LiDAR data, several factors impact measurement accuracy, including: size and reflectivity of the tree, sampling density, LiDAR pulse diameter, and shape of the tree crown.

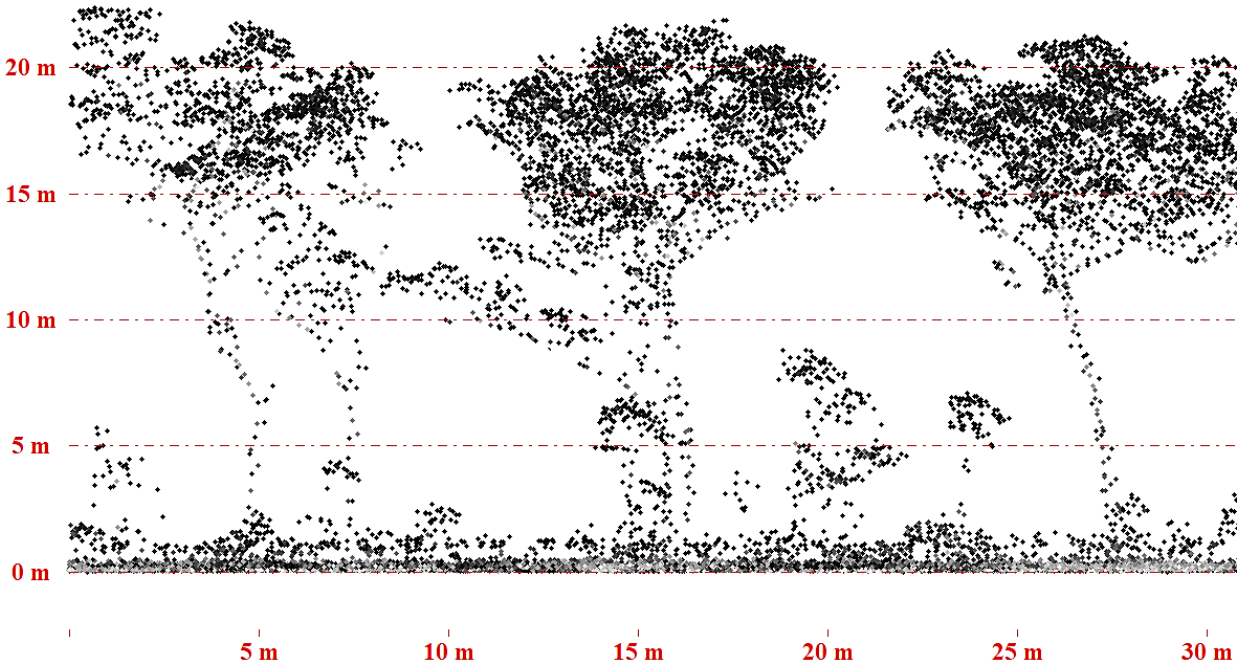

Figure 2.1: LiDAR point cloud profile in study area dominated by Eucalypt tree species.

According to the characteristics of the sensor and the accuracy requirements of the vegetation data to be extracted, two main approaches for deriving biomass information from LiDAR data have been applied so far: the area-based approach (ABA) (also known as the raster-based approach), based on statistical canopy height distributions; and the single tree approach, relying on individual tree detection (Barbati et al. 2009). In area-based estimation, canopy height data derived from LiDAR are calibrated against field measurements and then regressed against the 3D point cloud height distributions to predict the corrected standing volume or above ground biomass of the defined area (Corona and Fattorini 2008; Levick et al. 2016). Plot size and plot spatial arrangement, respectively, strongly influence the accuracy of AGB estimates obtained

from LiDAR by ABA (Gobakken and Næsset 2009). By contrast, the individual tree detection (ITC) approach is based on crown modelling of height data derived from LiDAR. Tree-level inventories are obtained from a sequence of steps that include individual tree detection (from a CHM) and delineation, and estimation of tree attributes. The individual tree heights and crown sizes derived from the LiDAR data are used in the allometric models for AGB estimation (Edson and Wing 2011; Popescu et al. 2003).

The accuracy of AGB estimation depends on multiple factors including both tree-level detection rates and tree structural parameter' estimation errors. The frequency of systematic omission (missed trees) and commission (over-segmentation) errors is affected by the crown detection algorithm and the tree structure (Vauhkonen et al. 2011). Same time in area-based approaches, the accuracy of predicted forest structure metrics decreases as the pulse density decreases (Jakubowski et al. 2013). Thus, undetected and false trees, errors in the allometric model predictions and forest structure metrics degrade the final accuracy of stand- and plot-level AGB estimates (Korpela et al. 2007).

Promising results for estimating biomass of tropical forests and savannas have been reported (Asner and Mascaro 2014; Chen et al. 2015; Colgan et al. 2012; Silva et al. 2014) Using discrete-return LIDAR data (6.4 pts m^{-2}), Colgan et al. (2013) was able to reach biomass estimation accuracy 14 – 22% of plot mass in South Africa savannas. Asner et al. (2008) found that for plot-level estimates of aboveground biomass the Mean Canopy Height (MCH) and Quadratic Mean Canopy Height (QMCH) LiDAR metrics were the best for Hawaii tropical forests. Hernández-Stefanoni et al. (2014) showed that increasing plot size, rather than total sample area, improves height-based

LiDAR-derived biomass estimations. Based on LiDAR metrics, Réjou-Méchain et al. (2015) provided accurate tropical forest AGB estimation with error of 14% at a 1-ha plot-level resolution and of 23% at a 0.25-ha resolution. Silva et al. (2014) predicted AGB stocks in fast growing *Eucalyptus* plantations in Brazil with similar accuracy ~14% (7.70 Mg ha^{-1}) of plot biomass, by ABA approach.

In Australia, both airborne and ground-based LiDAR surveying of ecosystems has been gaining traction over the last decade (Miura and Jones 2010; Shendryk et al. 2016; Tickle et al. 2006; Turner 2006). Lucas et al. (2008), by using area-based approach, shown strong correlation (r^2 = 0.90, RMSE = 11.8 Mg ha^{-1},) between field AGB and the Jackknife estimates from LiDAR, in Queensland mixed species forests. Ediriweera et al. (2014) investigated the efficacy of merging LiDAR and Landsat5 TM methods to predict and improve plot-scale AGB estimates in subtropical rainforest and eucalypt-dominated forest in north-eastern Australia with AGB relative estimation accuracy 12 – 18% of plot AGB.

Estimation of AGB by LiDAR has been mostly restricted due to the recognition that a considerable amount of field data are required to verify and calibrate the relationship between laser-derived height metrics and forest characteristics by the ABA (Yu et al. 2010). The level of field-based data required cannot be easily justified or realized in the low populated and remote vast Australian mainland savannas. However, the individual tree-based LiDAR methods using laser densities of > 5 pts m^{-2} can provide the data needed for the ABA at much lower cost, and provided that the data can be adequately calibrated against a stratified sample from ground-based assessments in the field (Vastaranta et al. 2012).

Similarly, tree-canopy detection efficiency is strongly affected by forest conditions, particularly vegetation structure and species, stem density, canopy cover and pattern. Thus, the common LiDAR procedures and regression models cannot be simply transferred from one site to another without calibration, refinement and verification of the procedures. The efficient way to reduce or prevent the systematic errors and overcome extensive field work is the combination of ABA and ITC approaches (Lindberg et al. 2010; Vastaranta et al. 2012)

Chapter 3 offers some important insights into LiDAR procedures to integrate both individual tree detection (ITC) and area-based approaches (ABA), designed for above ground biomass and its uncertainty estimation in tropical savanna.

2.3 Estimating canopy structural parameters from stereo imagery.

A significant obstruction to the operational implementation of LiDAR for woodland evaluation is the high cost of data acquisition, coverage (areal extent) and temporal resolution limitations (in comparison with satellite sensors), storage and processing software requirements (Asner et al. 2012a). The major initial cost component of data acquisition is aircraft deployment, especially if standby costs are included. Data storage costs these days are generally minimal compared to the overall project value; however software development (time and staff) and hardware costs are usually internalised within the organisations (Lee 2008). In contrast with airborne remote sensing, satellite datasets have the following advantages: relatively high and regular temporal resolution; greater areal extent (large areas are covered by one satellite scene) and lower data acquisition costs. As an alternative, optical-based sensor

aerial and satellite stereo imagery may also offer the ability to rapidly assess canopy height, in an accurate and repeatable manner (Aguilar et al. 2014b).

Stereo photogrammetry measures the three-dimensional position of a point relative to a reference datum from two different perspectives (images) (Pulfrich 1922). Repetition of this procedure for the various points, describing the object and its surface, results in an image-based 3D point cloud that can be used to generate a Digital Surface Model (DSM). Recent developments in technology have allowed the processing of a large amount of imaging data using the techniques known as Structure-from-Motion (SfM) (Ullman 1979) and Multi-View Stereopsis (MVS) by matching corresponding image features occurring in a series of overlapping photographs. Particularly, the introduction of Semi-Global image Matching (SGM) technique has been key in using optical cameras as a stand-alone solution for dense DSM production (Hirschmuller 2008).

The use of stereo photogrammetry in forestry was originally focused on the construction of two cartographic products: Digital Terrain Models (DTMs) and Digital Surface Models (DSMs), which are used to describe the underlying terrain and top of canopy surfaces respectively. These products are used to generate canopy height models (CHM) that subsequently provide accurate estimates of important vegetation parameters such as canopy heights, stand volume, and the vertical structure of the vegetation canopy. The estimation of canopy heights is performed by the subtraction of bare ground values (DTM) from the canopy layer (DSM). An accurate estimation of a CHM relies heavily on a good approximation of the ground surface underneath (Fatoyinbo 2012). The extraction of 3D information from VHR satellite sensor imagery is the subject of a large photogrammetric investigation undertaken for the last

decade, and mainly conducted in comparing CHM accuracies from different VHR sensors and evaluating different image matching algorithms (Aguilar et al. 2014b).

While technological innovations such as Simultaneous Localization and Mapping (SLAM) and deep MVS (Huang et al. 2018; Saputra et al. 2018) can improve image matching capacity, issues related to sun elevation angle (e.g. shadows) and sun-to-image geometry remain key factors in any optical image product that is acquired and used for point cloud and DSM generation (White et al. 2013). For vegetation applications, photogrammetric image matching, except terrestrial-based imagery, extracts the 3D points only for the upper canopy surface and is incapable of providing sub-canopy structure information (Baltsavias et al. 2008). This is the main difference, and limitation, when comparing image-based and LiDAR point clouds. In addition, the DSMs generated from LiDAR have better vertical accuracy than the DSMs generated by image matching due to direct acquisition of 3D coordinates (Baltsavias 1999b). While VHR satellite imagery provides a greater Area of Interest (AOI) than LiDAR, the imagery is compromised by lower data resolution, affecting final product accuracy.

There is a need then to explore methods that can reduce the requirement for detailed manual field inventory data acquisition. Unmanned aerial systems (UAS), referred to as ‘‘drones’’, have successfully introduced a smaller, cheaper-to-operate platform concept, with demonstrated capability for collecting spatially dense, accurate, and repeatable measurements for vegetation inventory applications on demand, by using SfM and image matching techniques (Colomina and Molina 2014; Tomaštík et al. 2017). Once UAS technology has proven to be sufficiently accurate and reliable, it can replace or complement manual data acquisition from field inventories.

Chapters 4 and 5 describe the procedures, methods, analyses, factors and principal issues used in the photogrammetric processing of stereo-pairs from commercially available VHR satellites and UAS imagery in Australian tropical savannas.

2.4 Spatial resolution of remote sensing data and scale factor

Australian savannas are heterogenous and highly dynamic in terms of woody cover change and carbon sequestration due to their vast spatial extent, high productivity, vulnerability to climatic effects and fires. To deal with research challenges and to guarantee the effective use of remotely sensed data required for assessing savanna landscapes, it is necessary to keep an understanding of scale as a fundamental concept (**Figure 2.2**). The scale determines the quality and type of information that can be extracted from data (Wulder 1998). Individual trees (herein defined, following the *Australian Soil and Land Survey Field Handbook* (2009), as a woody plant more than 2 m tall with a single stem or branches well above the base), can be considered as one principal unit of measurement and estimation; a primary scale. However, due to cost, effort, processing and storage issues, VHR data cannot cover the full area of interest (e.g. NT mesic savannas). Until now, most commonly used geo-data have spatial resolutions extending from 10 m to ~ 1 km. However, the information that can be extracted from these data is generally more useful for landscape-scale assessments, as individual trees cannot usually be discerned.

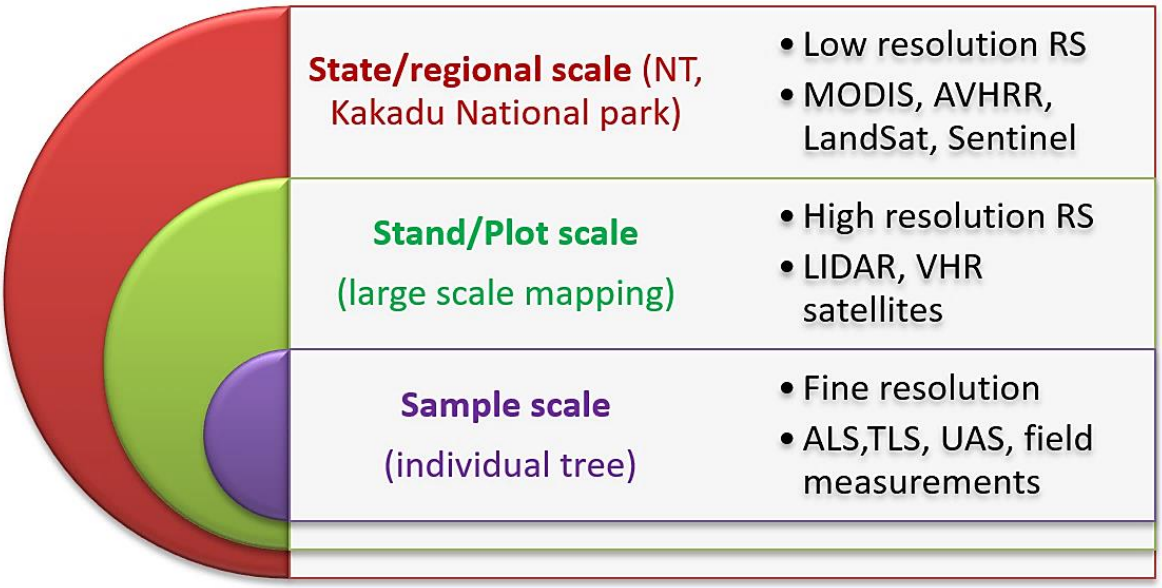

Figure 2.2: Relationships between different land mapping scales and remote sensing data.

The scale determines the amount of information that can be derived from the sensors and is critical to effective use of remotely sensed data for forestry applications (Hay et al. 2005). Each source of remote sensing data is provided with different acquisition parameters: spatial resolution (pixel size or pts m^{-2}), radiometric resolution (sensitivity to EMR), spectral resolution (EMR spectrum range), level of attribute detail, accuracy (spatial and attribute) and temporal resolution (Lee 2008). There is a direct relationship between the coverage of the area of interest on the ground and the image (pixel) spatial resolution **(Table 2.3)**. Spatial resolution defines the level of spatial detail depicted in an image. It defines the smallest feature that can be resolved by the instrument and, in this sense, is directly related to ground sample distance (GSD). Determining the optimum image spatial resolution could be critical for individual tree crown and canopy identification in Australian savannas. This requirement forms the basis of the research question that is addressed in this research.

Table 2.3: Most common RS tools with potential (grey filled boxes) to provide information of vegetation structure and inventory parameters for biomass estimation studies, including the measurable tree-canopy parameters. The spatial resolution and coverage data are given in categorical scale.

Sensors	Spatial resolution	Coverage	Tree component:	Tree crown height		Canopy height metrics	CHM	Ind. Tree crown	Canopy	NDVI
		km^2/hr	stem, branch	Midstory	Overstory			Delineation		
Active										
Terrestrial LiDAR	< 0.05 m	< 1								
Airborne LiDAR	< 1m	< 300								
RADAR sat. sensors	2.5 - 10 m	> 8000								
Passive										
UAS imagery	< 10 cm	< 1								
Airborne imagery	5 - 50 cm	< 300								
VHR satellite imagery	0.4 - 2.5 m	> 20000			stereo only		stereo only			
Hyperspectral satellite imagery	1 - 5 m	> 20000								
Sentinel, LandSAT, SPOT, Aster	10 - 30 m	Full, 5,16 days								
MODIS, AVHRR	250 -1100 m	Full, Daily								

To better ascertain the predictability of vegetation structure, it is necessary to provide an ability to discern broad-scale patterns and processes, and relate these to finer scales (Hay et al. 2001; Staver 2018). Consequently, and as a compromise, there is a need to make use of coarser scale remote sensing data to provide a representation of the landscape, but to use finer spatial resolution data to provide critical calibration and validation data, algorithms, data processing methodology and perspectives. Precisely exchanging data between scales is essential, as many environmental and resource management problems can only be dealt with effectively at broad scales (Wu and Qi 2000). This thesis therefore set out to use high spatial remote sensing data (Lidar and high-resolution stereo imagery) to derive precise and reliable models providing information to extrapolate biomass estimates from fine scale to broader landscapes.

Chapter 3

Hierarchical integration of individual tree and area-based approaches for savanna biomass uncertainty estimation from airborne LiDAR

Page intentionally left blank

This work has been published in peer reviewed international journal:

Goldbergs, G., Levick, S. R., Lawes, M., & Edwards, A. (2018). Hierarchical integration of individual tree and area-based approaches for savanna biomass uncertainty estimation from airborne LiDAR. *Remote Sensing of Environment*, *205*, 141-150. https://doi.org/10.1016/j.rse.2017.11.010

The following table detailing relative contribution by me and my co-authors refers to the published paper:

Contributing author	**Contribution**	**Tasks Performed**
Grigorijs Goldbergs	85 %	Study design, field data collection, RS data and field data analysis, manuscript writing
Shaun R Levick	15 %	Manuscript review and editing
Michael Lawes		Manuscript review and editing
Andrew Edwards		Manuscript review and editing

Page intentionally left blank

3.0 Abstract

Understanding the role that the vast north Australian savannas play in the continental carbon cycle requires reliable quantification of their carbon stock at landscape and regional scales. LiDAR remote sensing has proven efficient and accurate for the fine-scale estimation of above-ground tree biomass (AGB) and carbon stocks in many ecosystems, but tropical savanna remain under studied. We utilized a two-phase LiDAR analysis procedure which integrates both individual tree detection (ITC) and area-based approaches (ABA) to better understand how the uncertainty of biomass estimation varies with scale. We used estimations from individual tree LiDAR measurements as training/reference data, and then applied these data to develop allometric equations related to LIDAR metrics. We found that LiDAR individual tree heights were strongly correlated with field-estimated AGB (R^2=0.754, RMSE = 90 kg), and that 63% of individual trees crowns (ITC) could be accurately delineated with a *canopy maxima* approach. Area-based biomass estimation (ABA), which incorporated errors from the ITC steps, identified the quadratic mean of canopy height (QMCH) as the best single independent variable for different plot sample sizes (e.g. for 4 ha plots: R^2=0.86, RMSE = 3.4 Mg ha^{-1}; and 1 ha plots: R^2=0.83, RMSE = 4.0 Mg ha^{-1}). Our results show how ITC and ABA approached can be integrated to understand how biomass uncertainty varies with scale across broad landscapes. Understanding these scaling relationships is critical for operationalizing regional savanna inventories, monitoring and mapping.

3.1 Introduction

The savanna biome approaches 20% of total land cover and accounts for approximately 25% of total gross primary production (GPP), making them a globally important carbon sink (Saugier et al. 2001) and an important resource for carbon sequestration (Beringer et al. 2011; Lehmann et al. 2014). Despite increased interest in terrestrial carbon dynamics following implementation of the Kyoto Protocol, the distribution of terrestrial carbon stocks and flows in savanna ecosystems remains uncertain (Beringer et al. 2011; Grace et al. 2006). Australia's tropical savannas cover 1.9 million km^2, accounting for approximately 12% of the world's tropical savannas (Beringer et al. 2015), and it is estimated that they store 33% of Australia's terrestrial carbon (Williams et al. 2004). To fully understand the role that these extensive savannas play in the global carbon cycle it is necessary to refine carbon stock estimates at landscape and regional scales (Collins et al. 2009).

Current estimates of carbon stocks in Australian tropical savannas rely heavily upon field-based measures of woody vegetation structure which are used to calculated biomass through allometric equations derived from destructively sampled trees (**Table 3.1**). The extensive field measurements (species, DBH, height etc.) required for periodic biomass monitoring is time consuming and expensive. Remote sensing methods offer a rapid and cost-effective alternative method of estimating the local above-ground biomass (AGB) in many ecosystems (Lefsky et al. 2002; Lucas et al. 2008; Næsset and Økland 2002), and greater exploration of such approaches and their uncertainty is needed in tropical savannas (Asner and Mascaro 2014). Advances in airborne/satellite multispectral imagery (passive optical sensors), LiDAR (light

detection and ranging) and radar technologies (active sensors) are rapidly facilitating the uptake of remote sensing in AGB mapping.

Table 3.1: Examples of woodland biomass studies - Biomass estimation allometry by destructive sampling in Australian tropical savannas

Authors	Location	Species	Best allometric equations	Results, Notes
Williams et al. (2005b)	NT,QSL,NSW Australia	12 *Eucalyptus* species, plus *Terminalia ferdinandiana* and *Erythrophleum chlorost*.	$\ln(AGB)=\ln(D)+(\ln(H))^2$ $\ln(AGB) = a + b * \ln(D)$	General allometric relationship across 14 woodland species, from different regions of northern Australia. DBH alone accounts for > 97% of the AGB variation.
O'Grady et al. (2000)	Tropical savanna NT, Australia	*Eucalyptus miniata, E. bleeseri, E. tetrodonta, E. porrecta, Terminalia ferdinandiana, Erythrophleum chlorostachys.*	AGB comp.= $a * (DBH)^b$ AGB total = $a * (DBH)^b$	*Eucalyptus miniata* R^2=0.91 (total AGB) *Eucalyptus tetrodonta* R^2=0.96 (total AGB) Trees community R^2=0.95 (total AGB)
Werner and Murphy (2001)	Kakadu National Park NT, Australia	*Eucalyptus miniata, Eucalyptus tetrodonta, Eucalyptus papuana*	AGB = $a * (DBH)^b$	*Eucalyptus miniata* R^2=0.99 (total AGB) *Eucalyptus tetrodonta* R^2=0.97 (total AGB)
Chen (2002)	Tropical savanna NT, Australia	*Eucalyptus miniata, E. bleeseri, E. tetrodonta, E. porrecta, Terminalia ferdinandiana, Erythrophleum chlorostachys.*	AGB = $a * (DBH)^b$ AGB = $a * (DBH^2 * H)^b$ AGB = $a * (H)^b$	Trees community R^2=0.95 (total AGB by DBH alone) Trees community R^2=0.97 (total AGB by DBH+H) Trees community R^2=0.73 (total AGB by H alone)

In Australia, several successful studies investigating the combination airborne/satellite active and passive sensors data have explored biomass estimation in savannas. Lucas et al. (2008) illustrated the integration of LiDAR and Compact Airborne Spectrographic Imager (CASI) hyperspectral data for estimating AGB and component biomass at the individual tree or tree cluster level. Ediriweera et al. (2014) showed the efficacy of merging LiDAR and Landsat 5 TM methods to predict and improve plot-scale AGB estimates in subtropical rainforest and eucalypt-dominated forest in topographically complex landscapes in north-eastern Australia. Tickle et al. (2006) have shown that large-scale aerial photography and LiDAR can provide more comprehensive and precise estimates of stand level floristics and structure (e.g., canopy cover) compared to field measurements alone. Collins et al. (2009) investigated the use of polarimetric AirSAR (TopSAR) radar backscatter intensity for estimating biomass and carbon storage of *Eucalyptus miniata* and *E.tetrodonta* dominated open savanna in the Northern Territory, Australia. Optical sensors (except stereo imagery) are typically unable to detect stand characteristics (e.g. tree heights, DBH) that can be directly correlated to vegetation biomass (Harrell et al. 1997), and atmospheric interference from clouds and smoke haze limit their utility in tropical regions (Stibig et al. 2003). For these reasons, tree height and crown shape properties are most reliably obtained from active sensors, while species/stand health information may be better inferred from imagery, providing synergic capabilities for reliable data output (Valbuena et al. 2011).

Globally, airborne LiDAR sensing has proven to be efficient and accurate for the fine-scale estimation of above-ground tree biomass by indirect allometry (primarily tree height) (Maltamo et al. 2014). In Australia, airborne LiDAR surveying of ecosystems has increased over the last decade (Kandel et al. 2011; Lee and Lucas

2007; Miura and Jones 2010; Rombouts et al. 2010; Shendryk et al. 2016). However, the applications of LiDAR have not been fully tested for tropical savannas, and biomass uncertainty needs further attention. Depending on the sensor used and the accuracy required, two main approaches for deriving tree biomass information from LiDAR data have been applied to date: (1) the area-based approach - ABA (also known as the raster-based approach), based on statistical canopy property distributions; and (2) the single-tree approach (individual tree crown – ITC), relying on individual tree detection (ITC) (Barbati et al. 2009).

The ABA with low-point-density data (~ 1 pulse/m^2) is more efficient and cost-effective for both computation and laser data acquisitions (Jakubowski et al. 2013). Also, the calculation of cloud metrics is faster and technically easier compared to individual tree detection methods, which need more skilled and experienced operators. The ABA has become the most used method for biomass estimation in remote temperate forests and in ecosystems dominated by deciduous tree species. However, considerable field data are required to calibrate the relationship between laser-derived height metrics and tree characteristics (Yu et al. 2010). Chave et al. (2004) demonstrated that a minimum area of 5 ha of tropical forest is necessary to estimate the landscape-scale AGB by LiDAR metrics to within 10% of the ground-based estimates, and at least 100 weighted trees should be used for allometric equation creation. The individual tree-based LiDAR methods using high laser pulse densities of >5 pulses/m^2 can reduce amount of expensive fieldwork that is needed for the area-based approach, and provided that the data can be adequately calibrated against a stratified sample from ground-based assessments in the field (Ferraz et al. 2016a; Vastaranta et al. 2012).

The degree to which individual trees and their crowns are successfully detected is the efficiency criterion of ITC. The frequency of systematic omission (missed trees) and commission (over-segmentation) errors is affected by the crown detection algorithm and the tree structure (Vauhkonen et al. 2011). The efficient way to reduce or prevent the systematic errors and overcome extensive field work is the combination of ABA and ITC approaches (Lindberg et al. 2010; Maltamo et al. 2004; Vastaranta et al. 2012) and semi-ITC approach based on determining how many trees an extracted segment/cluster contains and use regression models to estimate the parameters of the associated trees (Breidenbach et al. 2010; Ferraz et al. 2016b; Kandare et al. 2016).

In this study, we integrate both individual tree and area-based LiDAR methods for estimating the AGB of tropical savanna in northern Australia, with the goal of understanding how uncertainty of estimates varies with spatial scale. We use estimations from individual tree LiDAR measurements as training/reference data for the area-based LiDAR approach estimators. To achieve this goal, we: (1) establish allometric relationships between field-derived individual tree AGB and LiDAR-derived crown area and tree height; (2) classify individual trees crown and quantify commission/omission errors; (3) integrate individual tree and area-based methods for savanna biomass and biomass uncertainty estimation; and (4) evaluate uncertainty in savanna biomass estimates at different plot scales.

3.2 Methods

3.2.1 Study area and existing field data

This study was undertaken in Litchfield National Park (13° 08’ S - 13° 14’ S, 130° 44’ E and 130° 51’ E), 100 km south-west of Darwin, in the Northern Territory, Australia. The Litchfield National Park Savanna Supersite (LSS; 12 km^2 with mean AGB 29.3 Mg ha^{-1}) is typical of high rainfall tropical savanna across north Australia (TERN 2012). Savanna distribution in the Northern Territory is determined by the seasonality of climate with most rain falling from November to March; mean annual rainfall is approximately 1600 mm. Compared to South America and Africa, Australian savannas have little topographic relief and are relatively intact (Beringer et al. 2011), due to low human population distribution and minimal infrastructure. Within the LSS the terrain elevation varies from 210 to 220 m, mean annual maximum temperature is 33°C. The savanna woodland vegetation is dominated by *Eucalyptus spp.* and mixed perennial/annual grasses (Landsberg et al. 2011). Above the 1200 mm isohyet, savannas are dominated by *Eucalyptus miniata* and *E. tetrodonta* open forest with a grass understorey (O'Grady et al. 2000).

Field data were previously collected from a 100 × 100 m (1 ha) plot in 2013. The corners of the plot were established with differential GPS. Then, the plot was divided into 25 subplots (20x20 m) and every tree with a height > 1.5 m and DBH > 2 cm was measured. The DBH, tree height (Suunto PM-5/360PC clinometer), and tree species were recorded in the inventory (**Table 3.2**).

AGB was estimated using previously fitted species-specific allometric models with tree DBH as independent variable based on the power model (Chen 2002; O'Grady et al. 2000; Werner and Murphy 2001; Williams et al. 2005b):

$$AGB = a*DBH^{b} \quad \textbf{(3.1)}$$

For other tree species, for which there was no existing biomass equation, the AGB was estimated from the general equation used in the Northern Territory, Queensland and New South Wales (Williams et al. 2005b) (**Table 3.2**).

The two dominant tree species *Eucalyptus miniata (82.3%)* and *E. tetrodonta (15.6%)* contributed 98% of plot live biomass (**Table 3.2**). The combined living AGB of the entire 1 ha field plot was estimated to be 26.1 Mg ha^{-1}. The dominant and co-dominant trees in the field plot with a height > 10 m (79 of 239 trees) comprised 85% of the living AGB.

Table 3.2: Summary of field inventory of 1 ha sample plot and reference AGB estimates

Tree species	No. Trees	No. Trees %	Max height (m)	Mean height (m)	Max DBH (cm)	Total AGB (Kg)	Total AGB %	Allometry used	Allometry equations
Eucalyptus miniata	179	74.9	22.5	10.47	40.0	21485.0	82.32	Chen (2002)	$AGB=0.0932*(DBH^{2.5064})$
Eucalyptus tetrodonta	21	8.8	19	8.5	40.0	4060.6	15.56	Chen (2002)	$AGB=0.0782*(DBH^{2.6815})$
Livistona humilis	12	5.0	6.5	3.7	13.0	148.6	0.57	Chen (2002)	$AGB=0.03*(DBH^2 * H)^{1.0575}$
Grevillea pteridifolia	14	5.9	5.5	3.7	9.8	91.0	0.35		
Corymbia latifolia	6	2.5	8.5	6.2	17.5	237.9	0.91	Williams et al. (2005b)	$ln(AGB)= -2.0596+2.1561*Ln(DBH)+0.1362*Ln(H)^2$
Pandanus_spiralis	1	0.4	6	6	15.0	67.8	0.26		
Other species	6	2.5	3.2	2.6	4.5	9.6	0.04		

3.2.2 Airborne LiDAR surveying and canopy height model generation

Airborne LiDAR data were acquired for the 12 km^2 study area by Airborne Research Australia (ARA) in June 2013. A Riegl LMS-Q560 full waveform time-of-flight LiDAR sensor operating at 240 kHz, average flying height 300 m AGL, swath width ~300 m, strip spacing 125 m., and flying speed ~ 40 m/s was used. The data were decomposed into discrete returns (20 cm footprint) to obtain an average point density of 15 returns m^{-2} (**Fig. 3.1**). All further point-cloud processing tasks (e.g. points classification, canopy height models (CHMs) creation) were performed with the *LAStools* software modules (rapidlasso GmbH2014).

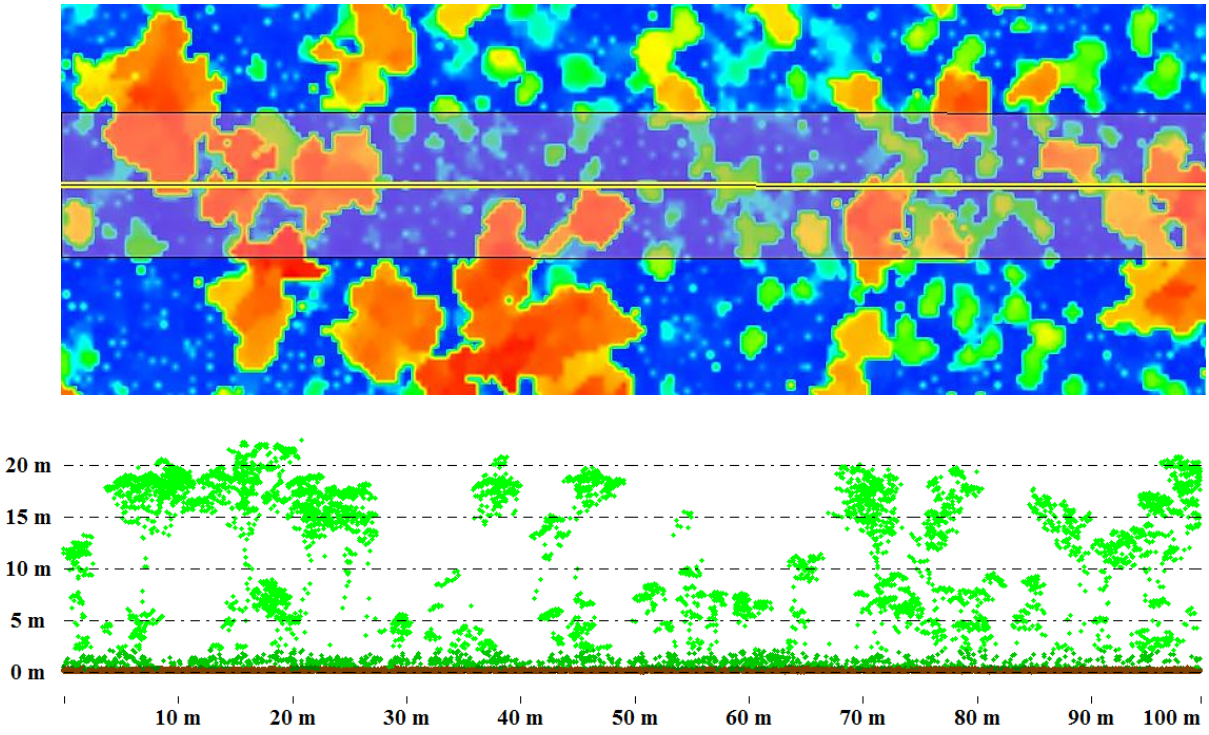

Figure 3.1: CHM (0.5m) and LiDAR point cloud profile (west to east) of 1ha reference plot dominated by *Eucalyptus* tree species.

3.2.3 Individual tree biomass estimation from airborne LiDAR

The local maxima approach was used to detect individual trees from the LiDAR point cloud. Local maxima were determined from the raster canopy height model (CHM), which was interpolated from the dense point data using the 'CanopyMaxima' routine in *Fusion* (McGaughey 2015). The local maxima approach uses an appropriately sized circular search window for identifying individual canopy peaks, rather than a crown delineation. If the search window size is too small, a higher number of false peaks will be detected (errors of commission or false positives); if too large, a greater number of true peaks will be missed (errors of omission or false negatives) (Popescu et al. 2002). The default search window diameter used in *Fusion* is based on conifer species in temperate forests, so we modified the search radius to use the height-crown diameter relationship more appropriate for our region. To obtain a relationship between the height of eucalypt trees and their crown size, 372 trees across the study site were selected in the *Fusion* LiDAR point cloud data viewer (LDV) and crown dimensions were digitized manually. Non-linear regressions were then performed to derive the best-fit equations for the crown diameter (Cd) based on the tree height (H) relationship.

The CHM rasters of the 1 ha field plot at spatial resolutions of 0.3, 0.5, and 1m were generated to determine the optimal spatial resolution for local maxima delineation of individual trees. We also tested the influence of the mean and median convolution smoothing filters on local maxima detection. Altogether three filter options (models) were tested: no filter, median 3 x 3 filter, and mean 3 x 3 filter. After

performing the local maxima detection on each CHM resolution and filter option, the most appropriate settings were determined by comparing the spatial off-set between automatically generated maxima and field-measured stem locations (n = 239 trees; **Table 3.2**) using GIS analysis.

Individual trees detected using the most appropriate local maxima settings were manually matched with field measured trees using GIS, 3D LiDAR data viewer and verification from field observations. We estimated the individual biomass from the 239 matched trees by applying existing allometric biomass equations based on field-measured DBH (**Table 3.2**), and established the power model relationship between individual tree biomass and LiDAR derived tree height, as well the relationship between field-measured DBH and LiDAR derived tree height.

The additional parameter of 'CanopyMaxima' routine related to '*crown size'* (radius) computed using average of 16 radial profiles extracted from CHM (McGaughey 2015) have been evaluated. The automatically extracted '*crown size'* radius of 372 trees across the study site were linearly regressed against manually extracted ones. Additionally, the individual tree AGB was estimated by combination a LiDAR height and 'crown size', as two independent variables by multiple nonlinear regression.

3.2.4 Accuracy validation and AGB uncertainty calculation of ITC approach

In our analysis, we assumed that both field measurements of DBH and LiDAR derived tree height measurements were robust. Since the ITC local maxima approach was used to acquire AGB training data for the ABA, the reliability of tree detection became the major error source for biased AGB estimation on plot level due to

omission/commission errors (Vastaranta et al. 2011). Thus, the errors of tree-level local maxima tree detection and individual tree AGB uncertainty were considered in the process of upscaling AGB from tree to plot levels.

We performed local maxima accuracy validation by digitally distributing 4 square plots of 1 ha each across the 12km^2 study site. All visible trees crowns (2015 trees) were manually measured inside these plots with *Fusion* LiDAR LDV. To evaluate the detection and precision rate uncertainty of manual tree measurement procedure in *Fusion* LDV and corresponding impact on AGB estimation, the field measured trees from the original 1 ha plot were compared with manually extracted ones. Then, the *Fusion* local maxima routine was evaluated by comparing the manually tree crown polygons (2015 trees in 4 ha of validation plots) with the automatically generated crown centres from local approach to establish the accuracy and omission/commission errors of trees detection. The tree detection rates were calculated by following equations (Goutte and Gaussier 2005; Li et al. 2012):

$$r = TP / (TP + FN) \quad (3.2)$$

$$p = TP / (TP + FP) \quad (3.3)$$

$$F_{score} = 2 * ((r * p) / (r + p)) \quad (3.4)$$

where, r is the tree detection rate, p is the correctness of the detected trees, F_{score} is overall accuracy, *TP* (true positive) is number of correctly detected trees, *FN* (false negative) is number of the trees which were not detected by local maxima (omission error), FP (false positive) is number of trees which do not exist in the field (commission error).

To propagate the AGB uncertainty from ITC to plot level, firstly, the AGB bias between all field measured (1 ha) and manually extracted trees was calculated, based on obtained tree detection rates and commission/omission errors ratio. Then, the obtained bias was introduced to the 4 ha of validation plots to calculate, in its turn, the AGB bias caused by local maxima tree detection commission/omission errors. Lastly, the total AGB of every plot across the study area (12km2) was corrected by AGB bias related to local maxima uncertainty obtained in the previous step.

3.2.5 Hierarchical integration of individual tree and area-based approaches

To determine the most appropriate metrics and scales for area-based estimations of AGB we digitally surveyed 300 rectangular 4ha sample plots, 1200 1ha plots, 4800 0.25ha plots and 19200 0.0625ha (25X25m) plots from throughout the entire 12km^2 study area covered by the normalized LiDAR data. Raster CHMs with a spatial resolution of 0.5m were calculated for each set of sample plots from the LiDAR 3D point cloud using *Fusion*. In each plot, individual trees with height >1.5m were identified using the *local maxima* method with a median 3 x 3-pixel kernel filter, due to the best settings identified in the previous step. The ITC results were used to acquire AGB training data for the ABA. The AGB of every detected individual tree was calculated inside each plot by using the power function Eq. (**3.6**), derived from the individual tree height-AGB correlation. The total AGB of each plot was calculated as the sum of the AGB of all detected trees in a plot and was used as the training reference biomass value. The obtained training AGB were calibrated based on uncertainty analysis of local maxima tree detection approach (previous paragraph).

LiDAR metrics were calculated using the *cloudmetrics* utility in *Fusion* for every plot and three different cloud metric sets were calculated with no cut-off, 0.5m and 1.5m point cloud ground cut-off thresholds. The training reference AGB of every sampled plot was included as the dependent variable, while laser height metrics were the independent variables for further multiple stepwise regression analysis. We used log-linear multiple stepwise regression with best model estimation implemented in the *XLSTAT* statistical software package. The best regression models were identified from the coefficient of determination (R^2) and the root mean square error (RMSE).

3.3 Results

3.3.1 Individual tree detection and biomass estimation

We found a strong correlation between LiDAR measured tree height (H) and crown diameter (Cd) (R^2 = 0.70, RMSE = 1.29 m (24% of Cd mean)) (**Fig. 3.2a**):

$$Cd = 1.22 + 0.019*(H)^2 \quad (3.5)$$

The inclusion of this relationship in our local maxima approach led to the efficient detection of overstorey trees. The most appropriate settings derived using the 'Canopy Maxima' routine in *Fusion* were the 0.5 m CHM and median 3 x 3-pixel kernel filter. The mean spatial offset between automatically generated crowns based on most appropriate 'CanopyMaxima' settings and field validated stem locations provided acceptable results (**Table 3.3**).

Table 3.3: Spatial offset between 239 LiDAR detected trees (canopy maxima) and field measured stem locations. (RMSE - root-mean-square error, SD - standard deviation).

Tree Heights	Mean (m)	RMSE (m)	SD
<5m	1.22	1.33	0.53
5-10m	1.37	1.59	0.81
10-15m	2.03	2.26	1.01
>15m	3.43	3.86	1.70

LiDAR tree heights were strongly correlated with field-estimated AGB (R^2=0.754, RMSE = 90 kg, **Fig. 3.2b**) based on the power function:

$$AGB = 0.0109*(H_{Lidar})^{3.58} \quad \textbf{(3.6)}$$

where, AGB is estimated AGB (kg), and H_{Lidar} is LiDAR tree height (m).

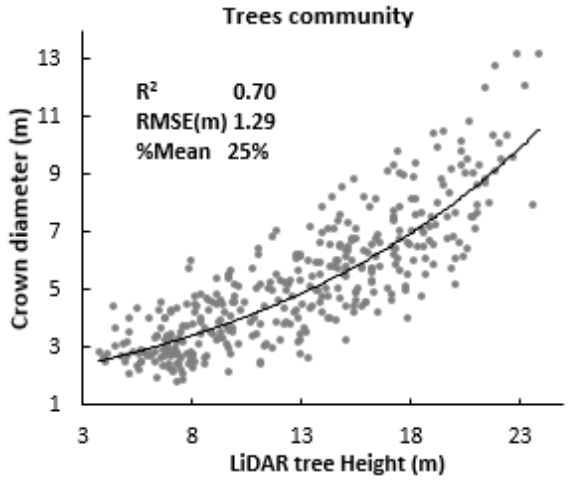

(a) Cd (m) = 1.22 + 0.019*(H)^2

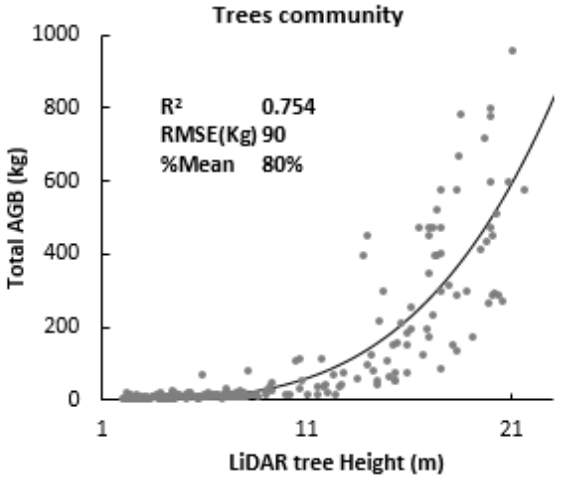

(b) AGB (kg) = 1.09E-02*(Lidar Height)$^{3.58}$

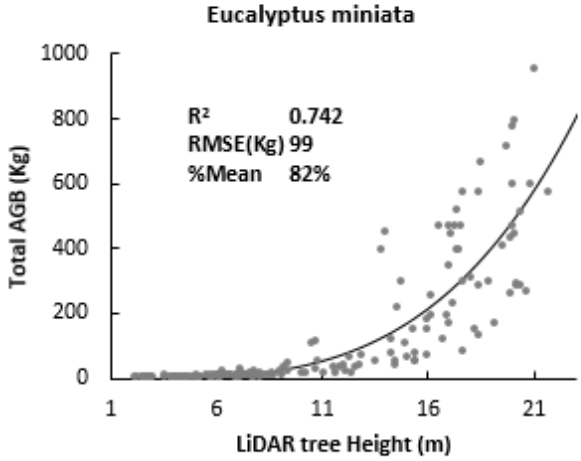

(c) AGB (kg) = 9.46E-03*(Lidar Height)$^{3.62}$

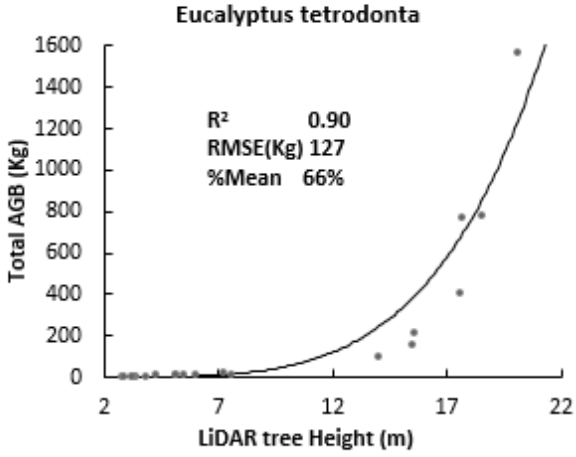

(d) AGB (kg) = 1.62E-03*(Lidar Height)$^{4.51}$

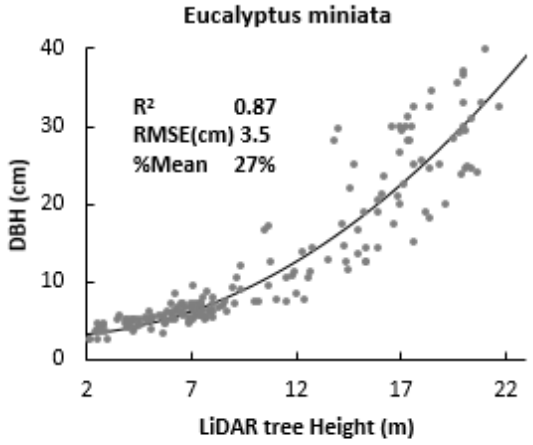

(e) DBH (cm) = 3.08 + 6.044E-02*(Lidar Height)$^{2.04}$

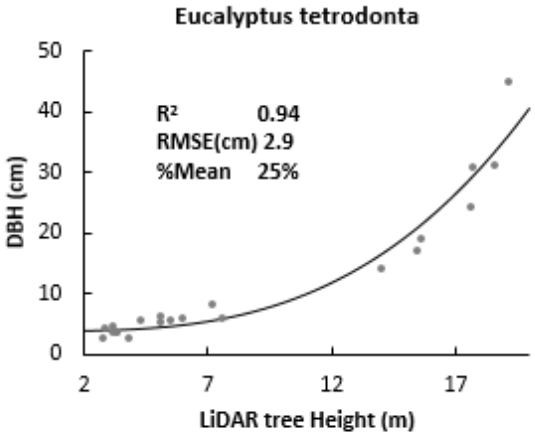

(f) DBH (cm) = 3.70 + 4.62E-03*(Lidar Height)^{3}

Figure 3.2: (a) LiDAR height vs. crown diameter (Cd). AGB (b,c,d) and DBH (e,f) regression equations with highest R^2 against LiDAR tree height. The %Mean is RMSE percentage of the mean.

Including '*crown size'* parameter of 'CanopyMaxima' routine in the regression models did not improve AGB estimation. The result of best regression model has shown same result (R^2 = 0.75, RMSE = 90 kg) with LiDAR height as one independent variable. The poor correlation between '*crown size'* parameter of 'CanopyMaxima' and manually extracted trees crown radius (n = 372 trees, R^2 = 0.18, RMSE = 0.94 m) shows insufficiency for AGB prediction. This implies that 'CanopyMaxima' cannot correctly extract '*crown size'* due to considerable variation of crown diameter of dominant and co-dominant *Eucalypt* trees.

3.3.2 Accuracy validation and AGB uncertainty calculation of ITC approach

The manually digitized trees distribution by heights (**Figure 3.3**) and the detailed results of the individual tree detection by local maxima approach in 4 ha of validation plots are listed in **Table 3.4**, based on most appropriate *canopy maxima* settings (0.5 m CHM and median 3 x 3 pixel kernel filter).

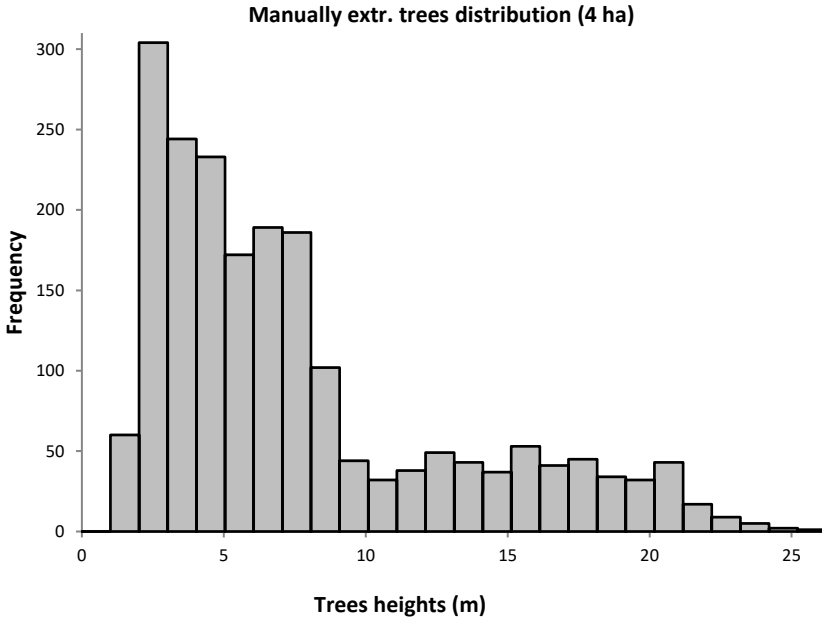

Figure 3.3: The height class distribution of manually extracted trees (n = 2015) in 4ha validation plots.

Table 3.4: Accuracy assessment of individual tree detection by local maxima (LM) approach in comparison with 2015 manually extracted trees within 4 ha validation plots.

	All trees	Trees mean H	Trees with H > 10m	Error type
	Nr	m	Nr	
Crowns without LM	736	6.3	136	omission
Correctly matched	1279	8.3	349	
LM inside crowns	125	11.2	43	commission
LM outside crowns	469	2.8	50	commission
Total crowns (trees)	2015	7.65	485	
Total LM in crowns	1404		392	
Total LM points	1873		442	

The overall tree detection rates (eq. 3.2-3.4) for manually extracted trees (1 ha field plot) and local maxima ITC validation (4 ha) plots are presented in **Table 3.5**:

Table 3.5: Accuracy assessment for individual tree detection procedures. The trees detection rates (r, p, F_{score}) of manually extracted trees by *Fusion* LDV and automatically detected by LM approach.

	Manually extracted trees 1ha field plot		Local maxima trees 4ha validation plots	
Rates	All trees	Trees H >10m	All trees	Trees H >10m
r (%)	82	94	63	72
p (%)	85	96	68	79
F score	84	95	66	75

The overall accuracy of the LiDAR local maxima points to validate our individual tree approach was 66 % for all trees, and 75 % for trees > 10m (which account for 91 % of the biomass in this system). Due to omission errors of manually

trees measurement procedure, the calculated predicted biomass showed biased AGB underestimation in 7 % in comparison with 1 ha field data. After introducing the given bias to validation 4 ha plots, the overall systematic error in AGB estimation related to ITC local maxima approach indicated the 10 % of AGB underestimation from reference data. Thus, for ABA regression analysis, the total AGB of every trained plot across study area (12km^2) was corrected by 10 %.

3.3.3 Hierarchical integration of individual tree and area-based biomass estimation approaches

The best estimates of plot-based biomass were obtained from including all LiDAR points in the analysis (no cut-off) (**Table 3.6**). Stepwise regression analyses identified the quadratic mean of canopy height (QMCH) (Lefsky et al. 1999) as the best single predictor variable of AGB in all cases (**Figure 3.4**).

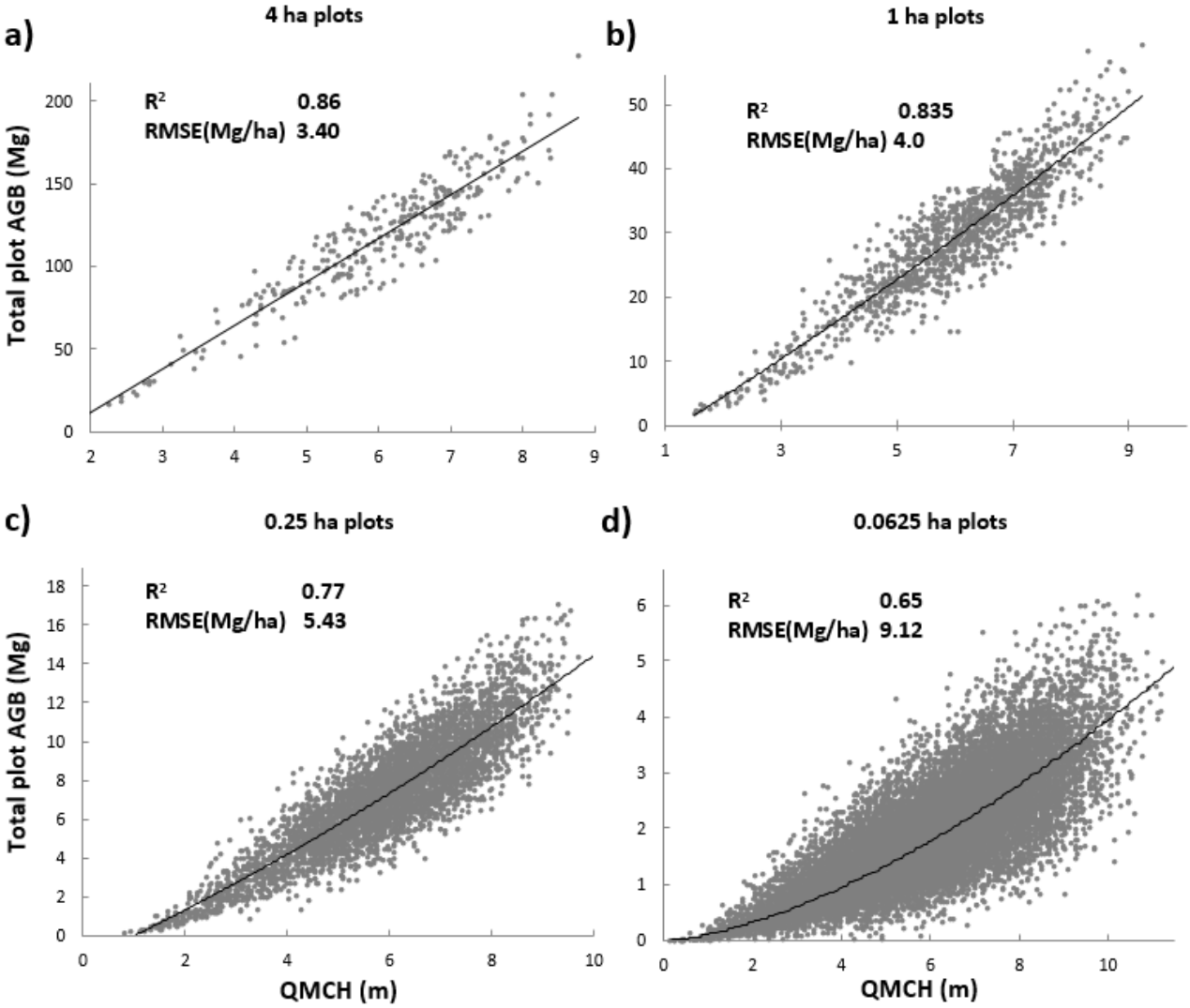

Figure 3.4: Plots of total AGB *versus* the best single predictor variable, QMCH (the quadratic means of canopy height), based on all echoes and all points (no cut-off) in (a) 4 ha, (b) 1 ha, (c) 0.25 ha and (d) 0.0625 ha sample polygons. The RMSE values are converted to Mg ha^{-1}.

Table 3.6: Best models of cloud metrics derived from multiple stepwise regression compared to AGB. (P80, P95… - percentiles of the laser canopy height distributions, Mean – mean of laser canopy heights, QMCH - quadratic mean of canopy height).

Plot size (ha)	Height cut-off (cm)	Independent variables	Regression Equation	R^2	RMSE (Mg/ha)	RMSE % of mean AGB
4	0	QMCH	AGB= EXP(9.17+1.39*ln(QMCH))	0.86	3.40	11.6
		P75, P95	AGB= EXP(7.13+0.093*ln(P75) +1.64*ln(P95))	0.90	2.93	10.0
4	50	QMCH	AGB= EXP(8.27+1.42*ln(QMCH))	0.76	4.47	15.2
		P50, QMCH	AGB= EXP(7.52-0.44*ln(P50) +2.16*ln(QMCH))	0.78	4.30	14.7
4	150	QMCH	AGB= EXP(7.94+1.51*ln(QMCH))	0.74	4.64	15.8
		P50, QMCH	AGB= EXP(7.21-0.70*ln(P50) +2.50*ln(QMCH))	0.76	4.50	15.4
1	0	QMCH	AGB= EXP(7.82+1.37*ln(QMCH))	0.835	4.0	13.6
		P80, P95	AGB= EXP(6.15+0.134*ln(P80) +1.44*ln(P95))	0.85	3.79	12.9
1	50	QMCH	AGB= EXP(6.84+1.44*ln(QMCH))	0.74	4.97	17.0
		P60, QMCH	AGB= EXP(6.60-0.41*ln(P60) +1.96*ln(QMCH))	0.75	4.91	16.7
1	150	QMCH	AGB= EXP(6.49+1.54*ln(QMCH))	0.72	5.17	17.6
		P40, Mean	AGB= EXP(6.21-0.70*ln(P40) +2.39*ln(Mean))	0.74	5.00	17.0
0.25	0	QMCH	AGB= EXP(6.47+1.36*ln(QMCH))	0.77	5.43	18.5
		QMCH, P95	AGB= EXP(5.72+1.04*ln(QMCH) +0.48*ln(P95))	0.78	5.35	18.2
0.25	50	QMCH	AGB= EXP(5.37+1.48*ln(QMCH))	0.68	6.39	21.8
		P60, QMCH	AGB= EXP(5.23-0.22*ln(P60) +1.77*ln(QMCH))	0.69	6.36	21.7
0.25	150	QMCH	AGB= EXP(5.01+1.58*ln(QMCH))	0.66	6.62	22.6
		P40, Mean	AGB= EXP(5.00-0.50*ln(P40) +2.13*ln(Mean))	0.67	6.53	22.3
0.0625	0	QMCH	AGB= EXP(5.08+1.37*ln(QMCH))	0.65	9.12	31.1
		Mean, QMCH	AGB= EXP(4.74-0.25*ln(Mean) +1.71*ln(QMCH))	0.65	9.09	31.0
0.0625	50	QMCH	AGB= EXP(3.75+1.59*ln(QMCH))	0.57	10.06	34.3
		P70, QMCH	AGB= EXP(3.79-0.23*ln(P70) +1.82*ln(QMCH))	0.58	10.05	34.3
0.0625	150	QMCH	AGB= EXP(3.40+1.68*ln(QMCH))	0.55	10.40	35.5

The simple split-sample or hold-out method of cross-validation was performed to assess the accuracy of the predictive models of total AGB based on QMCH. We used 70% of data plots for the training set and 30% for the test set. For AGB, the R^2 values in the cross-validation procedure increased from 0.72 to 0.92, when comparing the 0.0625 ha and the 1 ha plots (**Table 3.7**). Results of the cross-validation procedure, as well as AGB quantitative assessment of the 1 ha measured field data, indicate that the models have reasonable predictive power in the study area.

Table 3.7: Cross-validation procedure: AGB training set (based on QMCH metric) regressed *against* the AGB data obtained from the Individual tree approach (Eq. 3.3). No height cut-off was applied.

Plot size (ha)	No. Obs Train/Test	R^2	RMSE (Mg/ha)
4	210/90	0.95	2.51
1	840/360	0.92	3.34
0.25	3360/1440	0.78	5.40
0.0625	13440/5760	0.72	8.28

3.4 Discussion

3.4.1 The effect of individual tree detection on the accuracy of biomass estimation

The accuracy of individual tree detection has a direct effect on the accuracy of the final AGB estimation and is affected by the detection algorithm and its parameterization (Kaartinen et al. 2012). In our case, it was related to: (1) the spatial resolution of the chosen raster CHMs; (2) an appropriately sized circular height-crown

diameter relationship search window for identifying individual canopies; (3) the choice of smoothing filters; and (4) vegetation structure.

The CHM spatial resolution has large impact on detection of small trees < 10 m (omission error) and duplicated local maxima detections (commission error) of tall trees crowns. We found that small, understorey and intermediate trees could not be reliably identified with the local maxima approach at all resolutions (omission error from 40%, 0.3m-0.5m CHM resolution, to 60% at 1 m CHM resolution). Similarly, depending of ITC approach, many other studies (Duncanson et al. 2014; Edson and Wing 2011; Ferraz et al. 2012; Reitberger et al. 2009), shown low detection rates (<40 %) in supressed and small trees due to poor representativeness in point clouds and overstore obscuration. However, the error of omission for trees < 10m tall had minor influence on final biomass calculations as these small trees account for less than 10% of total AGB across the entire study area (12 km^2).

The occurrence of false tree peaks (errors of commission, false positives) added further challenges. Only 21% of commission errors related to multi LMs in corresponding tree crowns, while the remaining proportion represent falsely detected trees (**Table 3.4**). We found that using the 0.3 m CHM significantly increased (by ~30%) the number of extra LM in corresponding tree crown of dominant trees (H > 10 m). In turn, this leads to lower detection rate of dominant trees and to substantial AGB overestimation. The detection of dominant and co-dominant trees remained stable by using the 0.5 and 1 m CHMs resolutions, providing a high tree detection rate (>70%) for subtropical *Eucalyptus spp.* savanna.

The obtained overall tree detection rate (63%) match those observed in recent Shendryk et al. (2016) study for *Eucalyptus spp.* forest in south Australia. In their

study, the tree detection rates (r) varied from 55% to 67% depend on LiDAR point density by using LiDAR full-waveform information based on tree trunk detection using conditional Euclidean distance clustering and post-processing of detected tree trunks. Also, our findings is consistent with Duncanson et al. (2014) research related to deciduous species in western USA which algorithm correctly identified 70% of dominant trees, 58% of co-dominant trees, 35% of intermediate trees and 21% of suppressed trees by watershed delineation. Ferraz et al. (2012) demonstrated higher detection rates for dominant (> 90%) and dominated (65%) *Eucalypt* trees by using 3D segmentation.

In our study, the above described omission and commission errors do not compensate for each other which obviously leads to systematic and biased estimation of AGB. After introducing the AGB correction (7% underestimation) related to manually extracted trees procedure, we got the overall underestimation of AGB based on chosen local maxima ITC approach equal to 10%. As the individual tree heights were aggregated to the plot level, the introduced AGB bias correction is scale-invariant and independent from plot sampling.

One of the issues related to tree detection accuracy was the significant effect of the local maxima search window size relative to the tree crown size. Therefore, appropriate filter dimensions require careful selection (Popescu et al. (2002); Turner (2006)). As a result, the individual tree detection accuracy can be improved by clarification of height-crown diameter relationships before each project when undertaking the canopy *maxima* approach.

Our results of correlation between individual tree AGB and corresponding LiDAR height (eq. **3.6**) are in agreement with Chen (2002) who found a similar correlation

(R^2=0.73) by using tree height as a single parameter in biomass prediction based on a destruction approach in *Eucalypt* tropical savanna of northern Australia.

3.4.2 Hierarchical integration of individual tree and area-based approaches for improved savanna biomass estimation

Our area-based biomass estimation approach identified the QMCH as the best single variable independently from plot sample sizes. This finding was expected as QMCH places a greater weighting on the upper canopy LiDAR points, thus emphasizing the role of dominant and co-dominant trees in LiDAR metrics (Lefsky et al. 1999). Although other independent variables (percentile heights: P60, P75, P90; Mean of Laser canopy heights) provide good estimates of total AGB (**Table 3.6**), we propose to use the QMCH in most cases and this is consistent with other studies (Asner et al. 2008; Kandel et al. 2011; Rombouts et al. 2010).

In our study, we demonstrated that where field-plot data are spatially limited, it is possible to use a hierarchical integration approach based on AGB uncertainty calculation and calibration to upscale AGB estimates from individual trees to broader landscapes. The main limitation of this study related to fact that presented values of AGB uncertainties can be applied only in local areas with similar *Eucalyptus spp.* vegetation and LiDAR acquisition parameters. Positively, the presented approach can be relatively easily performed by using the computationally fastest and simplest local maxima technique (Kaartinen et al. 2012) and digitally delineated tree crowns as trained "true" reference data. It can thus be suggested that ITC rates can be improved by implementation into framework the semi-ITC algorithms to prevent the systematic errors on the tree segment level (Maltamo et al. 2014). Due to lack of independent field

data across the whole study site for our ABA output results validation, a further study with more focus on AGB estimation accuracy assessment of is therefore suggested.

A key limitation of the monitoring and mapping of vegetation in large remote areas with LiDAR is that whether high-density data are necessary to obtain accurate results at the plot-scale (Jakubowski et al. 2013). If airborne LiDAR were to become standard for monitoring large areas of northern Australia, it is likely that only low densities of 1-2 pulses m^{-2} could be achieved. Many studies have reported that reducing plot pulse densities (1 pulse m^{-2}) has no adverse effects on the quality of the fit of volume or biomass models when using statistical height metrics as predictor variables (Næsset and Gobakken 2008; Thomas et al. 2006). In our case, to perform the individual tree detection approach and AGB calibration based on manually digitized trees, high-density LiDAR data (>10 pulses m^{-2}) still are necessary. Our results demonstrate that only a small area (5 ha in our case) of high-density data need to be used to estimate and update regression equations that relate laser data to field observations, and then generalise the calibrated prediction of AGB for the whole area using low-density LiDAR metrics.

3.4.3 The effect of plot size on LiDAR area-based approach model performance

Plot size strongly influenced the accuracy of AGB estimates obtained from LiDAR metrics. We found that regression model fits and estimated accuracy improved noticeably as plot size increased from 0.0625 ha to 4 ha (**Table 3.6; Fig. 3.5**). Similarly, Frazer et al. (2011) showed that predictions of total AGB improved markedly as plot size increased from 0.0314 ha (10 m radius) to 0.1964 ha (25 m radius). Gobakken and Næsset (2009) argued that the accuracy of sample plot positions

and the size of the sample plots are the important factors affecting the precision of AGB calculations based on LiDAR data. Asner and Mascaro (2014) point out that the difference between LiDAR-predicted and field-estimated aboveground carbon density, declines towards 10% at 1 ha sample plot size.

There are several reasons why increasing the field plot size should be considered when estimating ABG from airborne LiDAR data. Plot edge effects decrease with larger plot size and this improves the accuracy of AGB estimates (Mascaro et al. 2011). Edge effects arise because trees located just outside the plot boundary still have some portion of their crowns falling within the plot (Levick et al. 2016; Mascaro et al. 2011).

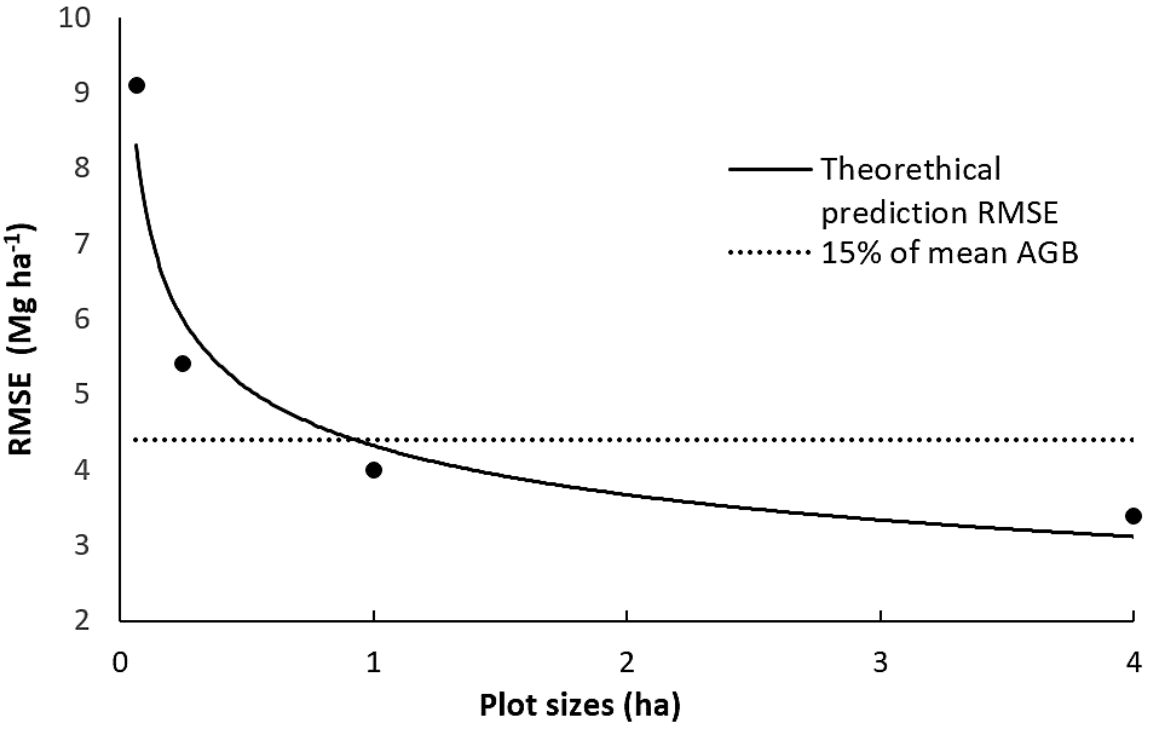

Figure 3.5: Observed stem localized AGB estimates RMSE for plot sample sizes from 0.0625 to 4 ha, based on QMCH regression analysis against AGB with no cut-off point cloud threshold in 12 km^2 study area.

A larger plot has a lower perimeter-to-area ratio, resulting in fewer potential edge-effects. Also, the plot edge-effect may cause over- or under-estimates due to large trees in small plots and an increase in co-registration errors between field and predicted data, whether or not the LiDAR area-based or individual tree procedures are applied. In our study, the use of 1 and 4 ha plots for the LiDAR ABA provided the best estimation of total AGB. Thus, larger 1-4 ha grid sizes reduce the error caused by edge effects and are more appropriate suitable for large area biomass estimations across north Australia with airborne LiDAR.

3.5 Conclusions

The two-phase ITC-ABA procedure adopted here can be applied in northern Australia and other remote areas, where road networks are non-existent or sparse and field access if limited and costly. We found that the sparse crown distribution and relatively low stand density of trees in this tropical savanna enables sufficient (> 70%) detection accuracy of dominant and co-dominant trees. The method we applied here is most effective for trees that are relatively isolated and for a CHM with 0.5 -1 m resolution. Above ground biomass and the uncertainty of estimation can be quantified from LiDAR data in tropical savanna by integrating both individual tree detection and area-based approaches, facilitating regional savanna inventories, monitoring and mapping.

Acknowledgements

This work was supported by Charles Darwin University and Darwin Centre for Bushfires Research, whose staff are gratefully thanked for their cooperation and research funding. Jorg Hacker and Airborne Research Australia (ARA) are thanked for having provided LiDAR data. For the field data collection we thank the M.Bradford, L.Hutley, C.Walker and M.Valencia. We acknowledge the valuable long-term infrastructure at the Litchfield Savanna Super Site, which is part of the Australian Super Site Network (www.supersites.net.au), funded by Australia's Terrestrial Ecosystem Research Network (TERN).

Chapter 4

Efficiency of Individual Tree Detection approaches based on light-weight and low-cost UAS imagery in Australian Savannas

Page intentionally left blank

This work has been published in peer reviewed international journal:

Goldbergs, G., Maier, S. W., Levick, S. R., & Edwards, A. (2018). Efficiency of Individual Tree Detection Approaches Based on Light-Weight and Low-Cost UAS Imagery in Australian Savannas. *Remote Sensing*, *10*(2), 161. https://doi.org/10.3390/rs10020161

The following table detailing relative contribution by me and my co-authors refers to the published paper:

Contributing author	Contribution	Tasks Performed
Grigorijs Goldbergs	85 %	Study design, field data collection, RS data and field data analysis, manuscript writing
Stefan W Maier	15 %	Study design, RS data collection, Manuscript review and editing
Shaun R Levick		Manuscript review and editing
Andrew Edwards		Manuscript review and editing

Page intentionally left blank

4.0 Abstract

The reliability of airborne LiDAR for delineating individual trees and estimating aboveground biomass (AGB) has been proven in a diverse range of ecosystems, but can be difficult and costly to commission. Point clouds derived from structure from motion (SfM) matching techniques obtained from unmanned aerial systems (UAS), could be a feasible low-cost alternative to airborne LiDAR scanning for canopy parameter retrieval. This study assesses the extent to which SfM 3D point clouds, obtained from a light-weight mini-UAS quadcopter with an inexpensive consumer action GoPro camera, can efficiently and effectively detect individual trees, measure tree heights, and provide AGB estimates in Australian tropical savannas. Two well-established canopy maxima and watershed segmentation tree detection algorithms were tested on canopy height models (CHM) derived from SfM imagery. The influence of CHM spatial resolution on tree detection accuracy was analysed, and results were validated against existing high-resolution airborne LiDAR data. We found that the canopy maxima and watershed segmentation routines produced similar tree detection rates (~70%) for dominant and co-dominant trees, but yielded low detection rates (<35 %) for suppressed and small trees due to poor representativeness in point clouds and overstory occlusion. Although airborne LiDAR provides higher tree detection rates and more accurate estimates of tree heights, we found SfM image matching to be an adequate low-cost alternative for detection of dominant and co-dominant tree stands.

4.1 Introduction

Accurate and reliable information about forest structure and composition is critical for forest management, biomass estimation, and monitoring of health status (Trumbore et al. 2015). Canopy structural parameters can be extracted directly or indirectly by ground-based, airborne or spaceborne remote sensing techniques. Advances in airborne/satellite multispectral imagery (passive optical sensors), LiDAR (light detection and ranging) and radar technologies (active sensors) over varying spectral, spatial and temporal scales are rapidly facilitating the benefits of remote sensing use in measurements and monitoring of forest structure. Globally, airborne LiDAR sensing has proven to be efficient and accurate for the fine-scale estimation of forest structure parameters by indirect allometry (primarily tree height (H)) based on high-density 3D point cloud canopy height models (CHM) (Asner and Mascaro 2014; Goldbergs et al. 2018a; Lefsky et al. 2002; Maltamo et al. 2014). Accurate estimation of canopy height is a key parameter for remote quantification of forest structure, for both individual tree crown and plot-based canopy metrics.

Innovations in computer vision and digital photogrammetry have led to development of the structure from motion (SfM) technique for generating 3D point clouds from stereo imagery that is similar in many aspects to LiDAR point clouds (Colomina and Molina 2014). SfM relies on algorithms that reconstruct the 3D geometry and detect 3D object coordinates by simultaneous matching of the same 2D object points in every possible image throughout the multiple overlapping set of imagery. Camera positions and image geometry are reconstructed simultaneously using automatically measured tie points by a multi-view matching technique (Westoby

et al. 2012). Image blocks are geo-referenced through a combination of global navigation satellite systems (GNSS) and inertial navigation systems (INS) with or without ground control points (GCP). In the last decade, due to advances in high performance computing, hardware miniaturization, cost reduction of GPS and INS, lightweight Unmanned Aerial Systems (UAS) have developed into an alternative field-portable remote sensing platform that enables low-cost collection of very high-resolution image data when and where it is needed. The combination of UAS and modern SfM matching techniques has a wide range of applications for forest management and inventory needs with low cost, high performance and flexibility (Paneque-Gálvez et al. 2014; Tang and Shao 2015; Torresan et al. 2017).

These advances have potential to change the way we obtain tree parameters - such as location, height and canopy cover, for estimation and monitoring of aboveground biomass (AGB). Australia's tropical savannas cover 1.9 million km^2, accounting for approximately 12% of the world's tropical savannas (Beringer et al. 2015). It is estimated that they store 33% of Australia's terrestrial carbon (Williams et al. 2004). Estimation of greenhouse gas emissions due to extensive and annual burning in north Australia and changes in standing carbon stocks rely upon pre-and post-fire calculations of biomass (Russell-Smith et al. 2009). Commonly, monitoring of vegetation and measurement of biomass change relies on extensive field measurements (species, diameter at breast height (DBH), height etc.) (Russell-Smith et al. 2009). However, over much of the landscape, field data collection is limited by accessibility, especially during the wet season. Our working hypothesis is that incorporating low-cost UAS image data into the existing field data collection framework can enhance performance and flexibility and improve final product outputs.

To date, there have been several successful studies investigating the potential of UAS to measure and monitor structural properties of different types of Australian forest (Hung et al. 2012; Wallace et al. 2016; Wallace et al. 2012; Whiteside and Bartolo 2016). Wallace et al. (2016) compared airborne LiDAR and imagery SfM point clouds for assessing absolute terrain height, and the horizontal and vertical distribution of *Eucalyptus* tree canopy elements. While they found that airborne laser scanning (ALS) provides more accurate estimates of the vertical structure of forests across the larger range of canopy densities, SfM was found to be an adequate standalone low-cost alternative for surveying forest stands, estimating 50% of canopy cover and 82% of tree top locations (H > 5m). Hung et al. (2012) assessed a technique for the automatic segmentation and object detection of tree crowns in Australian open savanna based on UAS imagery spectral classification and object shadow information, detecting >75% of the trees. However, the application of low-cost UAS image data for characterising vegetation structure and estimation of the plot/individual tree AGB has not been fully tested for Australian tropical savannas.

The main aim of this study is to evaluate the potential for imagery from consumer-grade light-weight and low-cost UAS (< $2000) for estimating tree structural parameters and quantifying biomass in Australian tropical savannas. To achieve this goal, we: (1) analyse the effect of gimbal/non-gimbal use on SfM performance and tree detection accuracy; (2) analyse the influence of SfM CHM spatial resolution on tree detection accuracy; (3) assess the applicability and accuracy of canopy maxima and watershed segmentation tree detection algorithms; and (4) compare the reliability of CHMs derived from LiDAR and UAS SfM 3D point clouds for individual tree detection and biomass estimation.

The main advantage of small and low-cost UAS is their ability to collect imagery with high spatial and temporal resolution. Stable and correct alignment of the images can be achieved by camera platform-stabilizing (gimbal use) during data acquisition. The base kit of many low-cost UAS do not contain a gimbal due to additional weight and cost. Therefore, we analyse the effect of gimbal/non-gimbal use on SfM performance and tree detection accuracy.

4.2 Methods

4.2.1 Study area

This study was undertaken in Litchfield National Park (13° 10’ S, 130° 47’ E), 100 km south of Darwin, in the Northern Territory, Australia. The study area (2.2 ha, flat terrain with elevation 215 m, mean AGB 29.3 Mg ha^{-1}) is representative of high rainfall tropical savanna across north Australia (TERN 2012). Savanna structural distribution in the Northern Territory is determined primarily by the seasonality of climate with most rain falling from November to March; mean annual rainfall is approximately 1600 mm. Compared to South America and Africa, Australian savannas have little topographic relief and are relatively intact (Beringer et al. 2011), due to low human population and minimal infrastructure. Within the study area, the vegetation is dominated by *Eucalyptus miniata* and *E. tetrodonta* open forest (>30% canopy cover) contributing more than 70% of the total tree basal area (O'Grady et al. 2000).

4.2.2 Airborne LiDAR and reference trees extraction

Existing airborne LiDAR data were used as reference data for this study. LiDAR data were acquired for a 25 km^2 area of Litchfield National Park, including the

study area, by Airborne Research Australia (ARA) in June 2013 and made available by the AusCover facility of the Terrestrial Ecosystem Research Network (TERN). A Riegl LMS-Q560 full waveform time-of-flight LiDAR sensor operating at 240 kHz, average flying height 300 m AGL, swath width ~300 m, strip spacing 125 m, and flying speed ~ 40 m/s was used. The data were decomposed into discrete returns (20 cm footprint) to obtain an average point density of 15 returns m^{-2}. All further point-cloud pre-processing tasks (e.g. point cloud classification, CHMs creation) were performed with the *LAStools* software modules (Isenburg 2014). In our further analysis, we assumed that LiDAR point cloud classification and LiDAR derived ground surface needed for CHM generation were accurate and correct.

To extract the reference data from LiDAR data, all visible trees with a height > 1.5 m across the study area (2.2 ha) were selected in the *Fusion* LiDAR point cloud data viewer (LDV) (McGaughey 2015) and circular crown dimensions with tree top heights were digitized manually. To update the extracted information to the UAS imagery acquisition date (2016), fieldwork was undertaken to assess and correct for structural changes.

A total of 1277 trees were extracted in Fusion LDV as reference data for individual tree detection (ITD) and plot biomass estimation. The selected trees spanned a broad range of height classes, with a mean of 7.45 m and a maximum height of 25 m (**Figure 4.1**). 258 individuals were taller than 10 m and were considered overstory trees. The trees in the field plot with a height > 10 m comprised 87% of the living AGB (**Figure 4.1**).

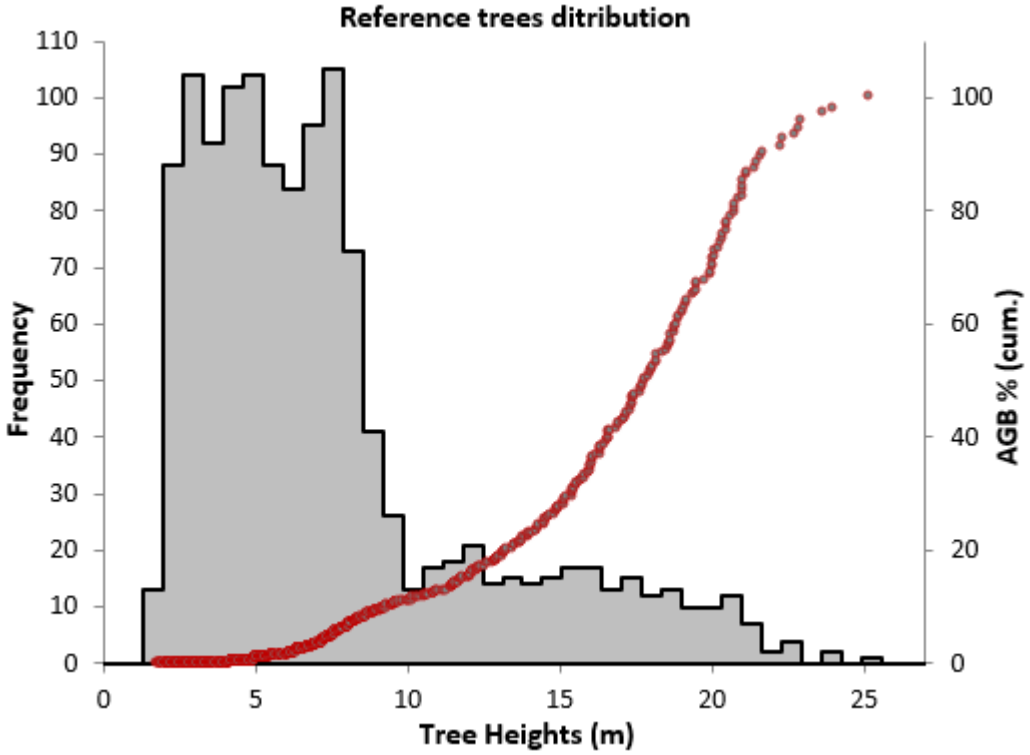

Figure 4.1: The height class and cumulative AGB (red line) distribution of reference trees (n = 1277) in the 2.2 ha study area.

The AGB of every reference tree was estimated using a previously fitted general allometric model for *Eucalyptus spp.* (RMSE 90 kg with plot level accuracy of 10%) with tree height as independent variable based on the power model (Goldbergs et al. 2018a):

$$AGB = 0.0109*(H)^{3.58} \quad (4.1)$$

where, AGB is estimated AGB (kg), and H is tree height (m).

4.2.3 UAS platform and image data acquisition

The commercially available mini-UAS quadcopter Solo (3D Robotics) was used for this study. The maximum payload of this platform is 700 g. The camera was a GoPro HERO4 Silver (GoPro, Inc, USA) with a 4000 × 3000 pixel CMOS detector

(1.55 μm pixel size, 4.35 mm fixed focal length) that captured images in automatic exposure mode. The standard fish-eye lens was replaced with a 4.35mm lens to reduce image distortions and adjust the field of view for this application with the infrared blocking filter removed.

The two UAS airborne flights of the study area were conducted on 4 and 19 July 2016 with the same acquisition settings (f/2.8, 1/929 - 1/2732 sec, ISO 100, 2.5 – 3 m/s wind speed) but with a different gimbal and lens filter setup. During the first flight (12:00 AM local time), the gimbal-mounted platform was used with a 600nm long pass lens filter (Hoya R60) providing the Red+NIR/NIR/NIR spectral channels. During the second flight (11:00 AM local time), the gimbal-mounted platform was not used, but with a BG3 (Schott) lens filter, providing NIR/NIR/Blue+NIR spectral channels. Use of the NIR bands provided improved discrimination between vegetation and non-vegetation. For both flights, the flying height was ~120m above ground level providing ~4.4 cm ground sample distance (GSD). Each image was geotagged, using the GPS, and the triggering time recorded. In both cases, the imagery was collected with high forward and side overlaps of at least 80%, in continuous shoot mode (1 image per second), at a flight speed of 10m/s.

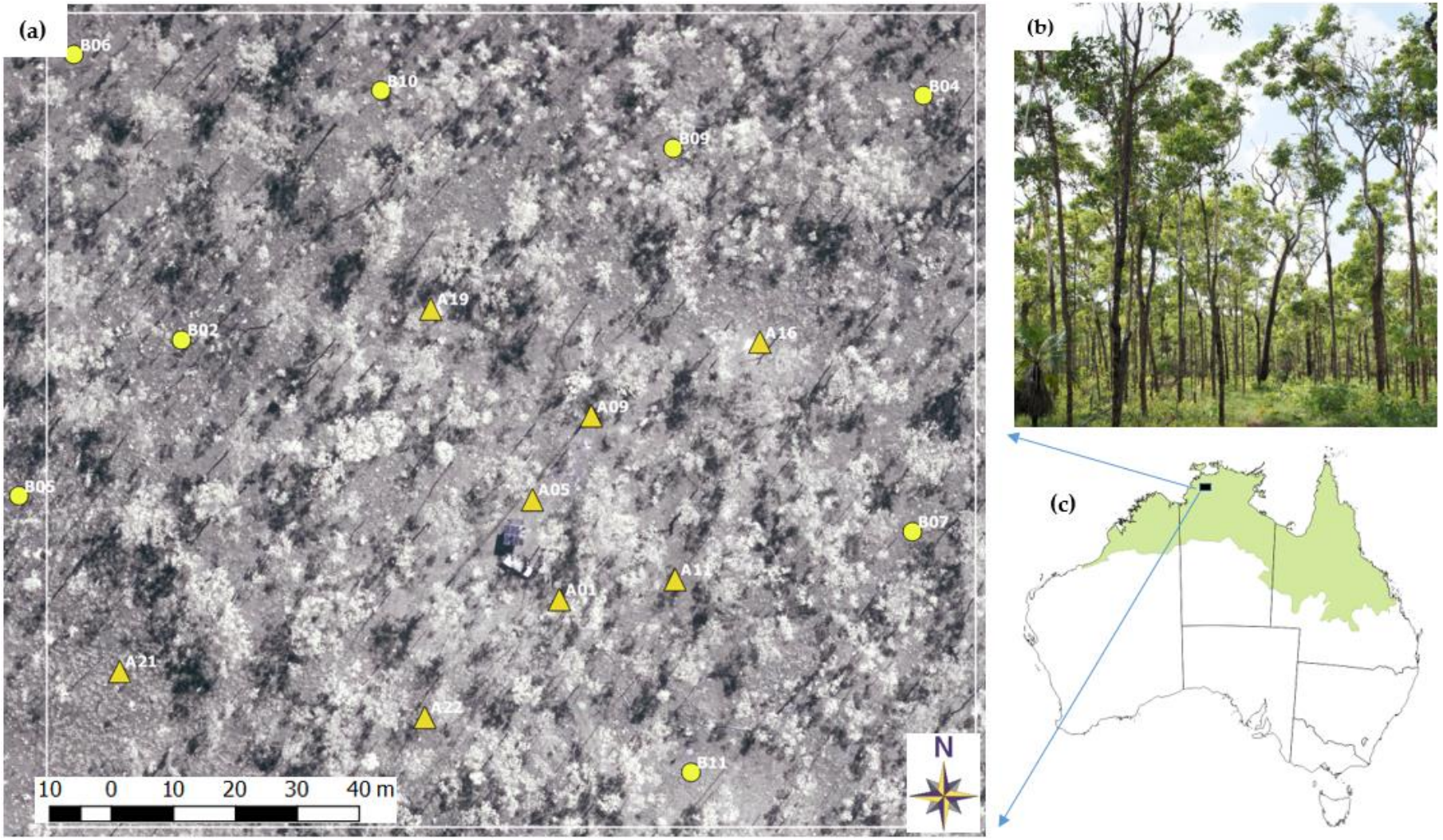

Figure 4.2: The 2.2ha study area: **(a)** with GCPs locations (Δ - full GCP (XYZ), O – height GCP (Z)); **(b)** dominated by *Eucalyptus spp.*; **(c)** in the north Australian tropical savanna (in green).

The collected imagery was not initially considered for the current study, so we were restricted to measuring well identified man-made (poles, concrete slab corners) and natural (tree stumps) objects as ground control points (GCPs), 11 weeks later. Eight full (XYZ) and eight height (Z) GCPs were established across the study area to perform image block geo-referencing (**Figure 4.2**). The GCPs were surveyed using a ProMark3 (Magellan Navigation, Inc, USA) differential GPS. As no permanent GPS base station was available within a 100 km radius, the temporal base and rover setup were used with a final absolute point accuracy < 1 m.

4.2.4 Image data processing and point cloud generation

Corrupted and low-quality UAS images were removed preserving 80-90% forward overlap. Seventy-seven (77) gimbal and ninety-two (92) non-gimbal flight images were chosen for further processing (**Figure 4.3**). Two photogrammetric software packages *Photomod* and *PhotoScan*, with different implemented matching algorithms, were used in parallel conventional photogrammetric image data processing to fulfil the given study tasks, based on automated workflows. *Photomod* has been chosen for processing, as one of the authors is commonly using it. *PhotoScan* was added due to its low cost and high popularity among UAS users and researchers.

Photomod 6.2 (Racurs, Russia) allows for the extraction of geometrically accurate spatial information from almost all commercial imagery, whether obtained from film, digital cameras, UAS, or high-resolution satellite scanners. For 3D point cloud generation, *Photomod* uses semi-global matching (SGM), an SfM global matching technique performed at the pixel level with pathwise aggregation of a global cost function (Hirschmüller 2011). The second software *PhotoScan 1.3.1* (Agisoft

LLC, Russia) has a user-friendly processing workflow with its own image-matching algorithm, similar to the scale invariant feature transform (SIFT) object recognition algorithm and pair-wise depth map computation for dense surface reconstruction (Agisoft 2011).

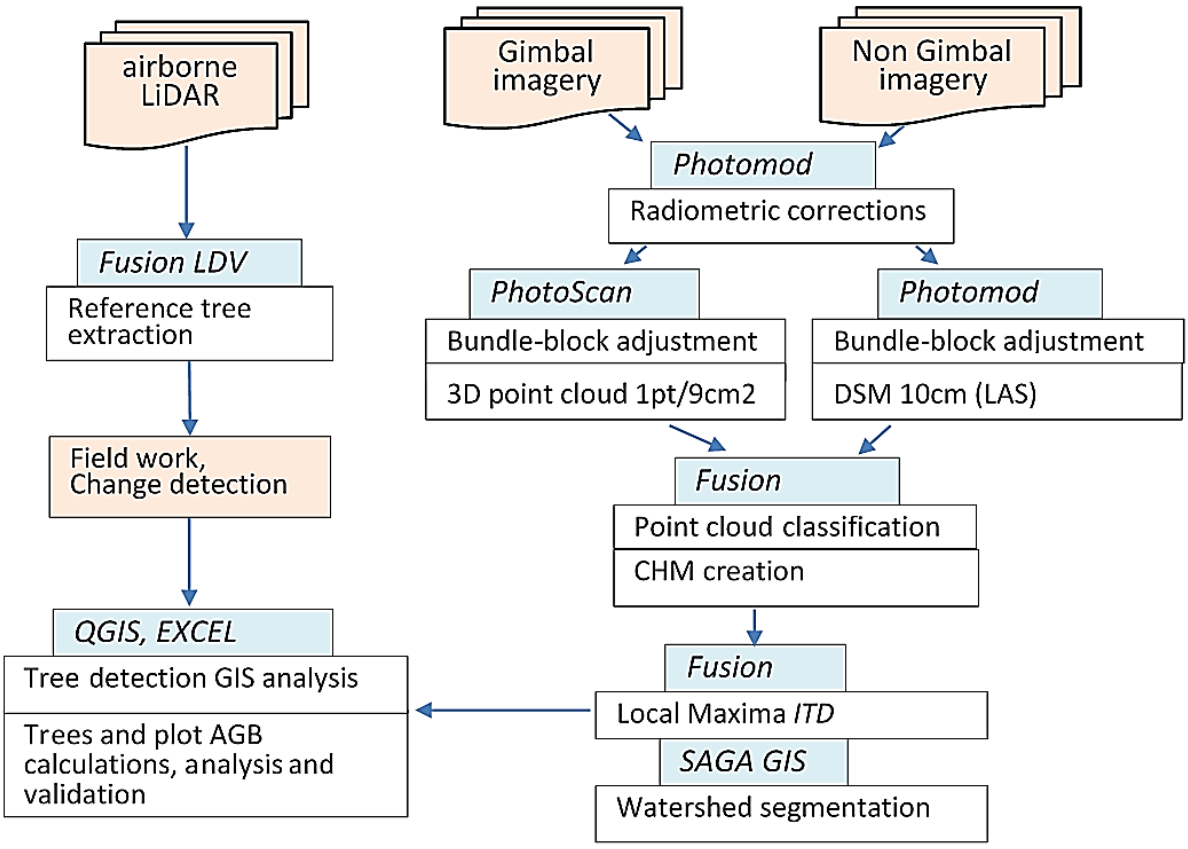

Figure 4.3: Workflow outline for this case. The two UAS imagery sets with and without gimbal setup, and LiDAR reference data were used to perform individual tree detection and AGB estimation. The software used are shown in blue boxes.

Image post-processing commenced with radiometric corrections, applied to both flights' imagery data, by using only *Photomod* tools. The same radiometrically corrected images were used for further processing in both software packages. Then, automatic tie point calculation and bundle-block adjustment with the camera self-calibration algorithm was applied in both software to obtain camera orientation

parameters (**Figure 4.3**). The stereo mode for manual measurements of GCPs was used in *Photomod,* as only a semi-automatic mono approach was available in *PhotoScan*.

We extracted 3D dense point clouds for both flights in *Photomod* with the default settings based on the census transform (CT) matching cost function. Due to insufficient quality (high noise level) of the generated raw 3D point cloud, a gridded digital surface model (DSM) with 10 cm defined cell size was used. Then, after a DSM null cell fill interpolation, the DSM was transformed to the LAS point cloud format for further processing.

The 3D dense point clouds were generated for both flights in *PhotoScan* in 'High resolution' mode (~ 9cm GSD) with 'mild' depth filtering and exported to LAS format for subsequent processing.

All point-cloud processing tasks (e.g. point classification, CHMs creation) were performed with the *Fusion* software modules (McGaughey 2015). The digital terrain models (DTM) of SfM acquired point clouds, needed for CHM generation, were identified using the *GroundFilter* and *GridSurfaceCreate* tools of the *Fusion* software. The vertical accuracy evaluation of the SfM based DTMs were performed by their comparison with the LiDAR based terrain model.

4.2.5 Local maxima tree detection approach and CHM resolution choice

The local maxima approach, computationally the fastest and simplest algorithm (Kaartinen et al. 2012), was used to detect individual trees from the image derived CHMs, interpolated from the 3D dense point data using the 'CanopyMaxima' routine in *Fusion* (McGaughey 2015). The local maxima approach uses an appropriately sized circular search window for identifying individual canopy peaks,

rather than crown delineation. If the search window size is too small, a higher number of false peaks will be detected (errors of commission; false positives); if too large, a greater number of true peaks will be missed (errors of omission; false negatives) (Popescu et al. 2002). The default search window diameter used in *Fusion* is based on conifer species in temperate forests, so we modified the search radius to use the height-crown diameter relationship more appropriate for the study area. To obtain a relationship between the height of eucalypt trees and their crown size, the 1277 manually digitized reference trees were selected by performing non-linear regression.

To determine the optimal spatial resolution for local maxima detection of individual trees, we used only *Photomod* processed gimbal flight CHMs with the assumption that local maxima efficiency is mostly dependent on vegetation structure rather than SfM algorithms and software choice. The raster CHMs were generated in *Fusion* at spatial resolutions of 0.3, 0.4, 0.5, and 1m, based on previous results showing 0.5m CHM resolution as optimal for LiDAR based local maxima models in *Eucalyptus spp.* tropical savanna (Goldbergs et al. 2018a). The median convolution smoothing filter was applied to all CHMs for local maxima detection with preserved local peaks in the final CHMs. Every two maxima with closest location distance 0.60 m (tree height < 10 m) and 2.30 m (tree height > 10 m) were merged based on the minimum distance between the reference trees. After performing the local maxima detection on each CHM resolution, the most appropriate CHM resolution was determined by comparing detection rates for trees > 10 m using GIS analysis and field observation validation.

Tree detection rates were calculated using the following equations (Goutte and Gaussier 2005; Li et al. 2012):

$$r = TP / (TP + FN) \quad (4.2)$$

$$p = TP / (TP + FP) \quad (4.3)$$

$$F_{score} = 2 * ((r * p) / (r + p)) \quad (4.4)$$

where, r is the tree detection rate or recall, p is the correctness of the detected trees or precision, F_{score} is overall accuracy, *TP* (true positive) is number of correctly detected trees, *FN* (false negative) is number of trees which were not detected (omission error), FP (false positive) is number of extra trees which do not exist in the field (commission error).

4.2.6 Individual tree detection processing

After determination of the most appropriate spatial resolution of the CHM for local maxima routine, eight models were chosen for the final individual tree detection (ITD) processing. These models include four (gimbal and non-gimbal) canopy maxima and four watershed segmentation models based on *Photomod* and *PhotoScan* 3D data raster CHMs. For all models, we only identified individual trees with height > 1.5 m. Additionally, the individual tree detection routines were applied on dominant and co-dominant trees with heights > 10 m.

The watershed segmentation workflow was performed in *SAGA* GIS freeware (Conrad et al. 2015). The CHMs (ASCII raster format) were imported from *Fusion* into SAGA. A Gaussian filter with kernel radius 2 pixels and standard deviation of 30 were applied. To preserve the local peaks for the smoothing filter, the maximal height

values of maxima seeds from the non-smoothed surface were assigned to the final segments. A 1.5 m height break limit threshold was applied to CHMs before segmentation. During watershed segmentation, the segments were joined based on 0.5 m seed to saddle difference threshold. Finally, the extracted segments were exported to *Quantum GIS* freeware (QGIS 2017) for further analysis. All segments smaller than 0.32 m^2 (tree height < 10 m) and 2 m^2 (tree heights > 10 m) were deleted based on the minimum values of the reference trees.

4.2.7 AGB estimation and data validation

The ITD results were used to calculate plot AGB for every model. The AGB of every estimated individual tree was calculated by using Eq. (4.1). The total plot AGB of each model was calculated as the sum of the AGB of all trees in a plot and was compared to the reference biomass value. Non-linear regression was also performed to check the correlation between reference tree AGB and the corresponding crown area segment obtained in the watershed segmentation process. To perform the ITD validation and comparison, the canopy maxima and watershed segmentation routines were applied to the LiDAR based 0.5 m resolution CHM. The tree height difference analysis was performed for every model, based on every matched tree height compared with reference tree height.

4.3 Results

4.3.1 Bundle-block adjustments

Table 4.1 shows the accuracies of the bundle-block adjustments based on quality statistics (root mean square errors (RMSE) in the X, Y and Z coordinates of ground control points and means of rotation angles (pitch, roll and yaw) provided by corresponding software. The bundle-block adjustment of the non-gimbal flight was the least accurate, as expected due to the instability of the platform, leading to non-systematic errors of object recognition, and of pair-wise depth map computation during tie point matching (**Figure 4.4**).

Table 4.1: Results of bundle-block adjustments of two flights, where: $б_o$ – the overall accuracy of the photogrammetric measurements; RMSE – root mean square errors based on GCP measurements; pitch, roll and yaw – mean sensor orientation angles.

		$б_o$ (pix)	RMSE (X) (m)	RMSE (Y) (m)	RMSE (Z) (m)	Pitch (deg)	Roll (deg)	Yaw (deg)
Gimbal	Photomod	0.38	0.17	0.13	0.31	0.02	0.04	2.8
	PhotoScan	n/a	0.19	0.16	0.36	-0.05	0.28	2.8
Non-Gimbal	Photomod	0.97	0.33	0.29	0.33	-12.5	10.6	-37
	PhotoScan	n/a	0.25	0.28	0.44	-12.7	8.2	-37

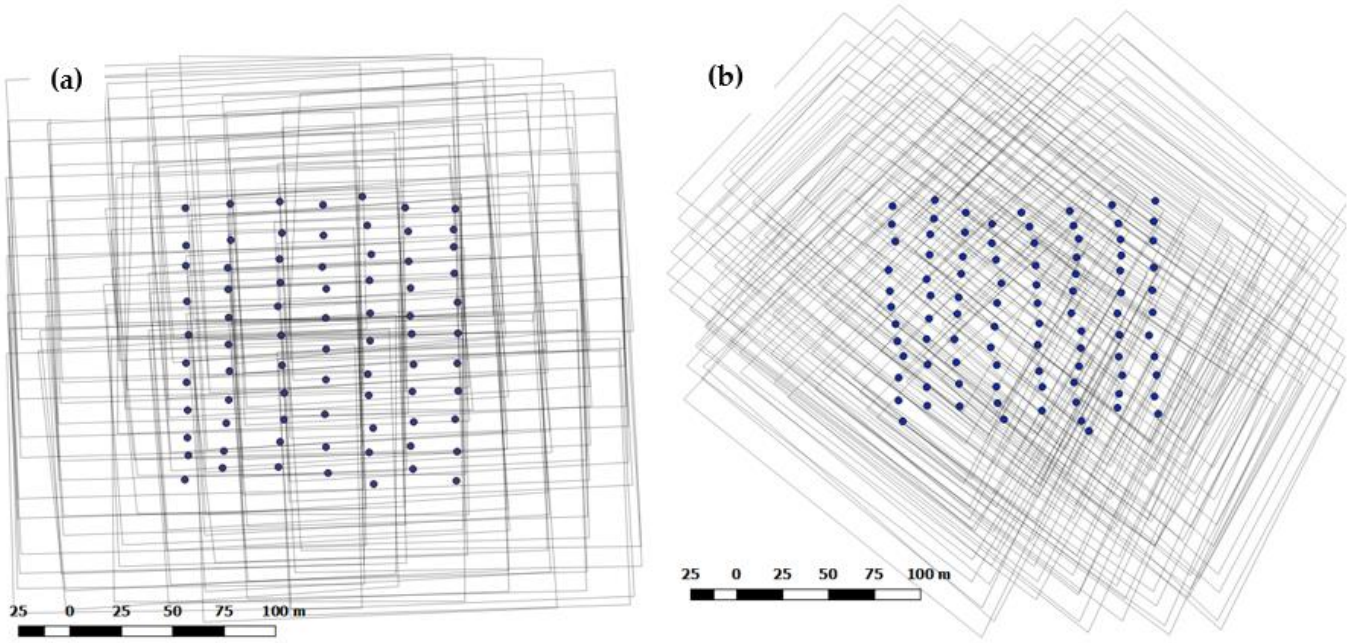

Figure 4.4: The block schemes (imagery footprints and projection centers) of two UAS flights based on block adjustment results (*Photomod*) **(a)** with gimbal and **(b)** without gimbal.

4.3.2 Accuracy of the SfM based ground surfaces

The vertical accuracy evaluation of the SfM based ground surfaces were based on comparison of the raster DTMs cells (0.40 m) with the corresponding LiDAR reference data and are shown in **Table 4.2**. It is apparent that all SfM based DTM models show ground overestimation in comparison with LiDAR ground surface data. The largest differences in the terrain representation are provided by models based on non-gimbal flight data.

Table 4.2: The results of the comparison the SfM based (DTM_{SfM}) and LiDAR (DTM_{LiDAR}) raster ground surfaces, based on corresponding elevation cell difference statistics: mean error, root mean square error (RMSE) and standard deviation (SD).

$DTM_{SfM} - DTM_{LiDAR}$	Photomod		PhotoScan	
	Gimbal	Non-gimbal	Gimbal	Non-gimbal
Mean Error (m)	0.12	0.27	0.08	0.41
RMSE (m)	0.22	0.43	0.19	0.54
SD (m)	0.19	0.34	0.17	0.35

4.3.3 Optimal CHMs resolution choice

We found a strong relationship between LiDAR measured *Eucalyptus spp.* tree heights (H) and crown diameters (Cd) ($R^2 = 0.84$, RMSE = 0.81 m (30% of Cd mean)), according to the following relationship:

$$Cd = 1.22 + 0.018*(H)^2 \quad (4.5)$$

The inclusion of this relationship in the local maxima routine led to the efficient detection of overstory trees. **Table 4.3** lists the tree detection rates for different image-derived CHM resolutions (**Figure 4.5**), which were used for optimal spatial resolution determination for the local maxima tree detection routine. The 40 cm resolution CHM provided the highest rate of detected trees (r) and overall accuracy (F_{score}). We found that using the 30 cm CHM markedly increased, by 100%, the number of extra local maxima (false tree peaks) in the tree crowns of dominant trees. This led to lower precision (59%) of dominant tree detection and to substantial AGB overestimation.

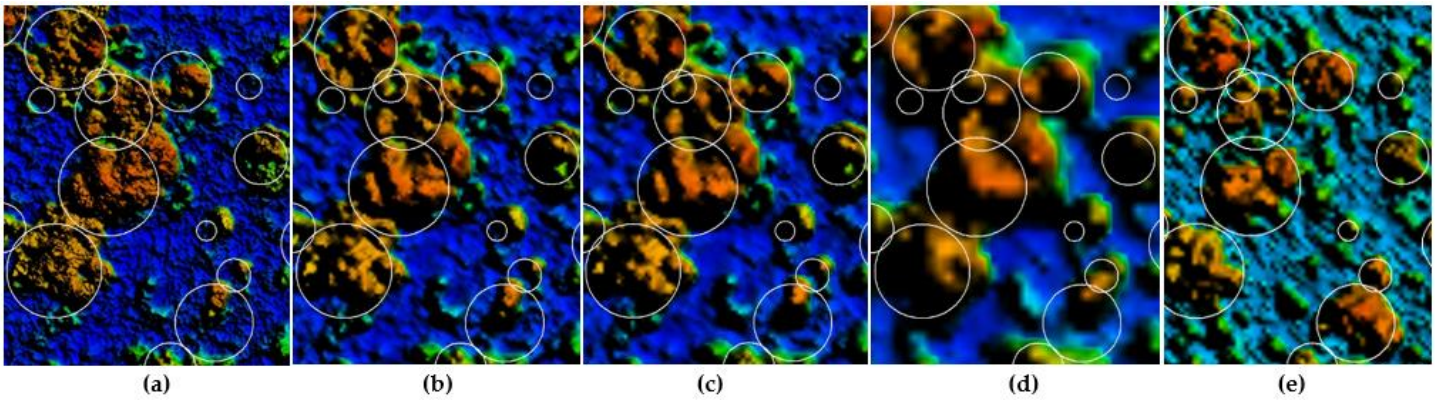

Figure 4.5: Study area subset (35 x 42 m) of *Photomod* processed raster CHMs with different GSD resolutions and applied 3x3 smoothing kernel filter. **(a)** Original 10 cm GSD, **(b)** 30 cm, **(c)** 40 cm, **(d)** 1 m and **(e)** LiDAR 50cm CHM. White circles represent the crowns of reference trees (> 10 m).

Table 4.3: *Eucalyptus spp.* tree (height > 10m) detection rates (r), using eq. 4.2-4.4, correctness of the detected trees (*p*), and overall accuracy (*F score*) based on local maxima for 30, 40, 50 and 100 cm CHM resolutions derived from the *Photomod* gimbal flight data.

	CHM resolutions			
Rates	**30cm**	**40cm**	**50cm**	**100cm**
r	69%	70%	66%	64.%
p	59%	71%	72%	77%
F score	64%	71%	69%	69%

4.3.4 Local Maxima Individual tree detection and watershed segmentation results

The 40cm resolution CHM was used for further *local maxima* processing and watershed segmentation as the optimal spatial resolution, **Table 4.3**. Overall, the

canopy maxima and watershed segmentation routines were not able to perform sufficiently reliable tree detections of all trees in the study plot (**Table 4.4**).

Table 4.4: *Eucalyptus spp.* tree (n = 1277) detection rates (r), using eq. 4.2-4.4, correctness of the detected trees (*p*), and overall accuracy (*F score*) based on local maxima and watershed segmentation results using raster 40 cm CHMs.

	Local Maxima					Watershed Segmentation				
	Photomod		PhotoScan		LiDAR	Photomod		PhotoScan		LiDAR
Rates	Gimbal	Non-gimbal	Gimbal	Non-gimbal		Gimbal	Non-gimbal	Gimbal	Non-gimbal	
r	42%	43%	41%	43%	61%	32%	34%	35%	36%	43%
p	74%	68%	76%	60%	69%	76%	79%	81%	71%	83%
F score	53%	53%	54%	50%	65%	45%	48%	49%	48%	57%

The canopy maxima and watershed segmentation routines achieved adequate tree detection rates for trees with heights > 10 m (**Figure 4.6; Table 4.5**), except in the case of the non-gimbal *PhotoScan* model. The low precision rate (*p*) is explained by a higher number of false tree detections and the high commission/omission trees ratio (1.9).

Table 4.5: *Eucalyptus spp.* tree (H >10 m; n = 258) detection rates (r), using eq. 4.2-4.4, correctness of the detected trees (*p*), and overall accuracy (*F score*) based on local maxima and watershed segmentation results using raster 40 cm CHMs.

	Local Maxima					Watershed Segmentation				
	Photomod		PhotoScan		LiDAR	Photomod		PhotoScan		LiDAR
Rates	Gimbal	Non-gimbal	Gimbal	Non-gimbal		Gimbal	Non-gimbal	Gimbal	Non-gimbal	
r	70%	71%	71%	70%	80%	67%	68%	69%	71%	81%
p	71%	72%	72%	57%	78%	68%	69%	72%	56%	72%
F score	71%	71%	71%	63%	79%	68%	69%	71%	63%	76%

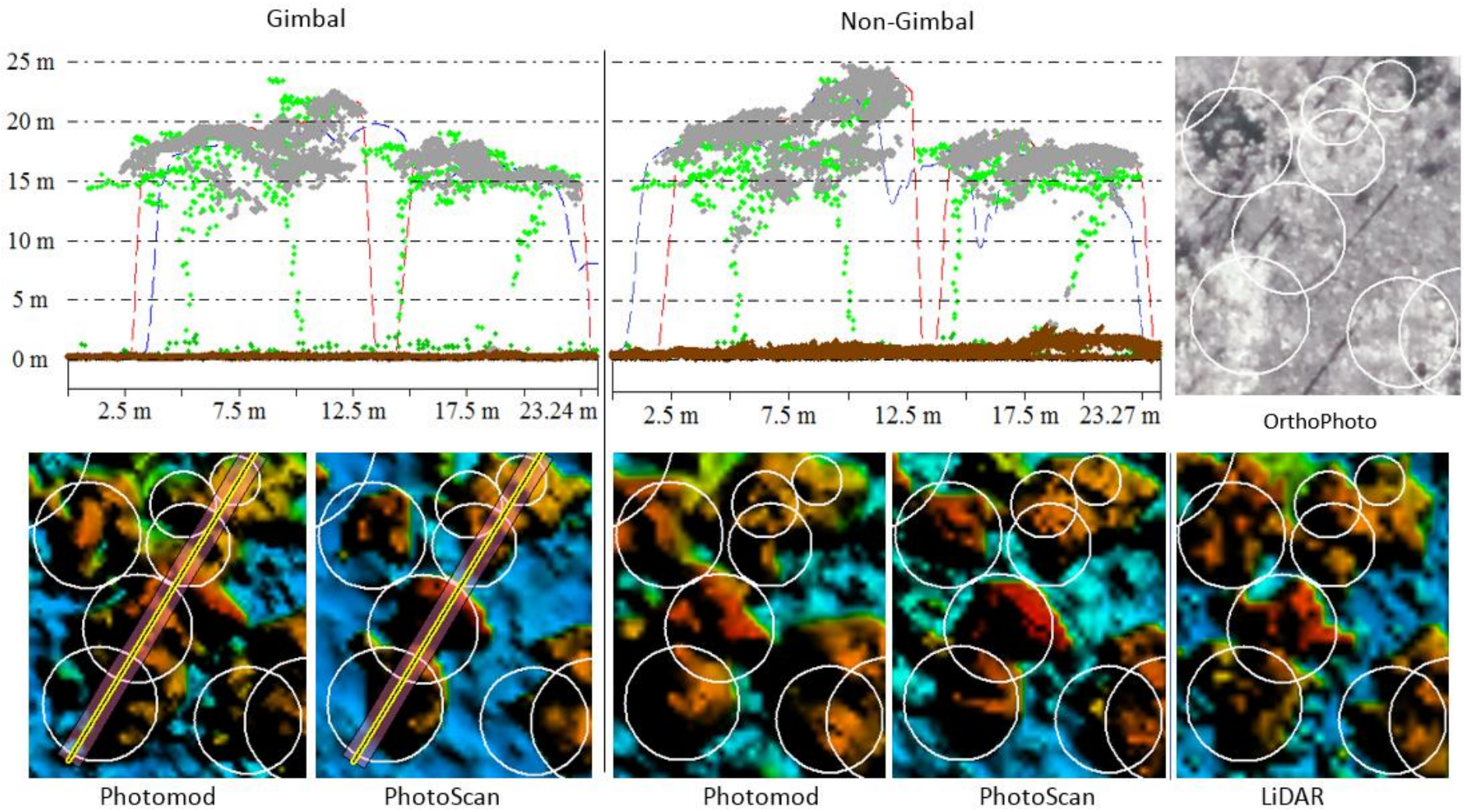

Figure 4.6: Horizontal transect (1.6m wide) of study area subset. Reference LiDAR 3D point cloud (green dots), *PhotoScan* extracted point cloud (grey dots – vegetation; brown dots – classified terrain), *Photomod* DSM (blue line), *PhotoScan* DSM (red line) and their corresponding 0.4 m raster DSMs used for local maxima and watershed segmentation.

4.3.5 AGB estimation

Given the limitations of the local maxima and watershed segmentation results for the detection of all trees, only trees with heights > 10 m were chosen for further AGB estimation/comparison and tree height difference analysis (**Table 4.6**). The dominant and co-dominant trees in the field plot with a height > 10 m (258 of 1277 trees) comprised 87% of the living AGB.

Table 4.6: Matched tree height differences (mean error values and standard deviation (SD)) and total plot AGB differences based on local maxima and watershed segmentation results (trees height > 10m). Negative values represent an underestimation.

	Local Maxima				**Watershed Segmentation**			
	Photomod		**PhotoScan**		**Photomod**		**PhotoScan**	
	Gimbal	Non-gimbal	Gimbal	Non-gimbal	Gimbal	Non-gimbal	Gimbal	Non-gimbal
Mean Error (m)	-0.28	-0.04	0.09	0.55	-0.25	-0.08	0.12	0.68
SD (m)	1.22	1.36	1.18	1.42	1.27	1.39	1.21	1.50
AGB plot diff (%)	-11%	7%	12%	46%	-4%	14%	15%	57%

The high commission/omission tree ratio (1.9) and average 55 cm tree height overestimation resulted in significant total plot AGB overestimation (+46%) in the non-gimbal *PhotoScan* model. *Photomod* based models underestimated H, and the corresponding AGB, compared to the *PhotoScan* and LiDAR based models.

The non-linear regressions of the tree reference AGB and the corresponding crown area segments obtained in the watershed segmentation process were poorly correlated (for H > 10m; *PhotoScan*: $R^2 = 0.12$, RMSE = 191 kg/tree, 77% of mean;

Photomod: R^2 = 0.15, RMSE = 160 kg/tree, 65% of mean). These results can be explained by the poor correlation between the reference 'tree crown area' (calculated as, $Pi*r^2$) and extracted tree segments from the watershed segmentation (for H > 10m; *PhotoScan*: R^2 = 0.25, RMSE = 21 m^2, 64 % of mean; *Photomod*: R^2 = 0.28, RMSE = 20 m^2, 60% of mean).

4.4 Discussion

4.3.1 Accuracy of individual tree detection based on canopy maxima and watershed segmentation approaches

The accuracy and completeness of CHMs generated from 3D dense point clouds have a direct effect on individual tree detection performance. CHM generation is affected by the SfM matching algorithm and accuracy of 3D scene geometry reconstruction from 2D images. In our study, it was primarily related to: (1) accuracy of the bundle-block adjustment; (2) vegetation structure; (3) the spatial resolution of the raster CHMs; (4) an appropriately sized circular height-crown diameter relationship search window for identifying individual canopies by the *local maxima* routine; and (5) the effectiveness of the chosen SfM matching algorithm.

Important factors in the consideration of bundle-block adjustment accuracy are the number of GCPs needed for image geo-referencing, their distribution, and camera self-calibration calculations. Agüera-Vega et al. (2017) and Goldstein et al. (2015) showed that optimal results for UAS image bundle-block adjustment and SfM can be reached with 10 - 15 signalized GCPs. In our case, the GCP measurements were performed after the image data acquisition, so we were restricted to measuring well

identified man-made (poles, concrete slab corners) and natural (tree stumps) objects. Due to the limited number of such GCPs across the study area, the height (Z) GCPs were added to preserve the block homogenous accuracy. As vertical accuracy of bundle-block adjustment is extremely influential on tree heights measurements, we suggest measuring additional non-signalized or even signalized height (Z) GCPs across the study area, based on regular locational pattern. In this study, the *Photomod* package produced better results related to the enhanced vertical accuracy of the bundle-block adjustment, attributable to the stereo-mode for GCP manual measurements, which is not available in *PhotoScan*.

The accurate representation of the terrain is crucial for characterizing the 3D structure of vegetation which is necessary for CHM calculations (Wallace et al. 2016). The current study found that *Eucalyptus spp* savanna vegetation structure is sufficiently transparent for accurate terrain reconstruction by SfM matching techniques. Based on our results, ~ 50% of all 3D point cloud extracted points related to the ground surface, which negates the need to use an external digital terrain model for CHM generation (**Figure 4.6**). On the other hand, crown transparency had direct impact on tree detection rates using SfM matching. These findings suggest that the optimal image data acquisition time is between the end of the wet and start of the dry seasons, when canopy cover of Australian tropical savanna is at maximum (Russell-Smith et al. 2015). Overall SfM based ground surfaces provided accurate and applicable representation of the terrain across the study plot (Table 2). The largest differences in the non-gimbal SfM based models likely originates from the poor reconstructed image geometry during image block relative orientation (tie point matching) and 3D point cloud SfM calculations (high noise; **Figure 4.6**).

The spatial resolution of the CHM greatly impacts the detectability of small trees < 10 m (omission error), whilst simultaneously impacting the local maxima detection of tall tree crowns (commission error). We found that small, understorey and intermediate trees could not be reliably identified with the local maxima approach at all resolutions, where the detection rate was 35 % at 0.3 m - 0.4 m CHM resolution, reduced to 25 % at 1 m CHM resolution. Similarly, depending on the ITD approach, many other LiDAR studies (Duncanson et al. 2014; Edson and Wing 2011; Ferraz et al. 2012; Reitberger et al. 2009), demonstrate similarly low detection rates of small trees (< 40 %), describing poor representativeness in point clouds due to overstory obscuration. However, the omission error for trees < 10 m, in our study had a minor influence on the final biomass estimates, since all small trees account for 13 % of total AGB only.

The occurrence of false tree peaks (H > 10 m) added further challenges. The ~ 40% commission error is related to multi-local maxima in corresponding tree crowns, while the remaining proportion represent falsely detected trees. We found that using the 0.3 m CHM significantly increased (by ~100%) the number of extra local maxima in corresponding tree crowns. In turn, this led to greater commission errors and to substantial AGB overestimation. The detection of dominant and co-dominant trees remained stable for the 0.5 and 1 m CHMs resolutions, providing a reliable tree detection rate (65% - 70%) for tropical *Eucalyptus spp.* savanna (**Table 4.3**).

Despite the fact that all models (**Tables 4.4** and **4.5**) showed similar tree detection rates, our findings demonstrate slightly better results related to models based on the *PhotoScan* 3D point cloud, especially with watershed segmentation. This variance could be attributed to different matching algorithms used in the two software

packages. Although all SfM based models showed generally adequate tree detection rates, LiDAR based measurements were better by 17% for all trees and by 9% for dominant and co-dominant trees. Comparison of the LiDAR and SfM point cloud vertical profiles (**Figure 4.6**) show that SfM does not capture the foliage distribution of the midstory and understory canopy layers. Same time, the SfM point cloud provide a greater point density than LiDAR data and depend on image resolution and used matching algorithms. It is likely, that the discrepancy in detection rates between LiDAR and SfM could be partly ameliorated by using a camera with a larger sensor and oblique imagery, which is an important consideration for future research.

Another issue related to tree detection accuracy was the significant effect of the local maxima search window size relative to the tree crown size. Therefore, filter dimensions require careful selection (Popescu et al. 2002; Turner 2006). As a result, individual tree detection accuracy can be improved by clarification of height-crown diameter relationships before each project when undertaking the canopy maxima approach. Therefore, it may be the case that watershed segmentation can be used as a key tree detection approach as it does not need the height-crown diameter relationship calculation. To minimize tree detection commission errors, the watershed segmentation needs definition of the threshold value for segments join. Another advantage of watershed segmentation use over a *local maxima* approach is that it provides additional tree attributes, such as crown delineation and canopy area data. Similarly, the watershed segmentation approach cannot correctly extract tree segment areas due to considerable variation in crown diameter and the crown transparency of dominant and co-dominant Eucalypt trees. Thus, the crown area segments extracted

by the watershed segmentation cannot improve the AGB estimation of Eucalypt trees in Australian tropical savannas.

4.3.2 The effect of camera calibration precision on the accuracy of tree height and biomass estimation

In this study, the accuracy of the CHM had a direct effect on final AGB estimation given indirect allometry based only on tree height. Under/overestimation of tree heights (**Table 4.6**) led to corresponding variation in plot AGB estimation, from -11% to +15% for trees (H > 10 m), depending on the model (except in the case of the non-gimbal *PhotoScan* model). The *Photomod* gimbal-based CHMs tended to underestimate tree height (~ -25 cm), while the *PhotoScan* models overestimated (~ +10 cm). The tree height underestimation in the *Photomod* models can be partly explained by smoothing filters and interpolation process applied during DSM creation from the 3D point cloud. As well, the results from *Photomod* and *PhotoScan* are likely to be related to volatility and errors in the camera's self-calibration process during the independent block-bundle adjustments (**Figure 4.7**), which therefore affected the vertical accuracy of the extracted digital surface model (James and Robson 2014).

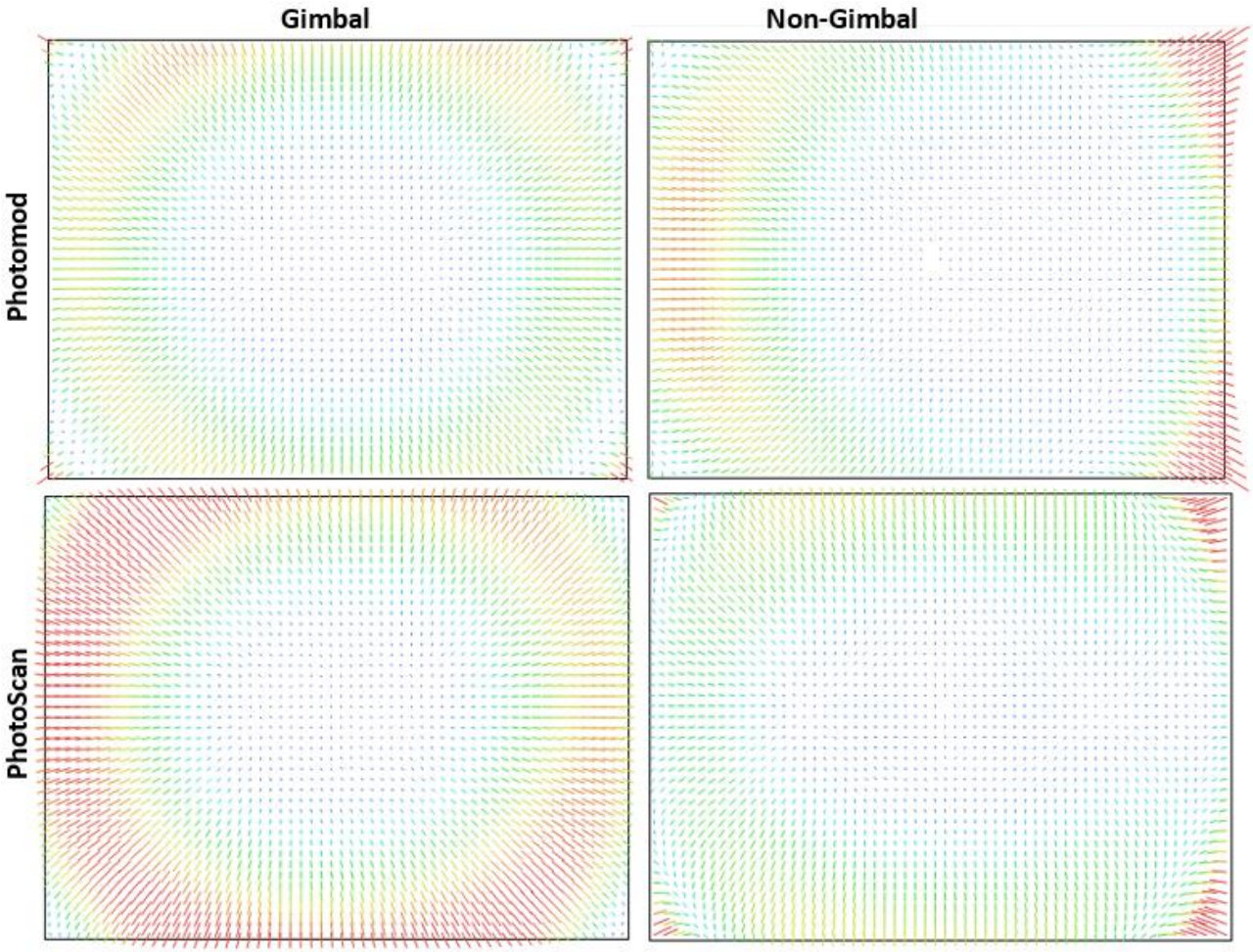

Figure 4.7: GoPro camera lens distortion plots based on camera self-calibration results in *Photomod* and *PhotoScan*. The estimated camera distortions are presented at the same scale (x161) across all figures.

The differences in the self-calibration results may be explained, firstly, by the fact that all GCPs are located on flat terrain (< 0.5 m height range) which is disadvantageous in terms of accuracy and correlation between camera parameters; it is a non-optimal approach to producing metrically corrected and scene-independent calibration (Luhmann et al. 2016). Based on James and Robson (2014), another possible explanation for this discrepancy is that the self-calibrating bundle adjustment of non-metric cameras may not be able to derive lens radial distortion accurately so that a systematic vertical error may remain even with sufficient numbers of GCPs. We

anticipate that a camera with a larger sensor and detector pixel size can provide better accuracy in tree height estimation due to its more stable internal sensor geometry and better radiometry.

The *Photomod* based model of the non-gimbal flight provided slightly better results in comparison with the gimbal flight, especially in the case of several tall tree detections (**Figure 4.8**). These results are likely to be related to noticeable changes of camera orientation angles and the fact that the camera was not angled at nadir, during the non-gimbal flight. Besides self-calibration issues, the tree detection omission and commission errors do not compensate for each other which obviously leads to systematic under/overestimation of AGB in each corresponding model.

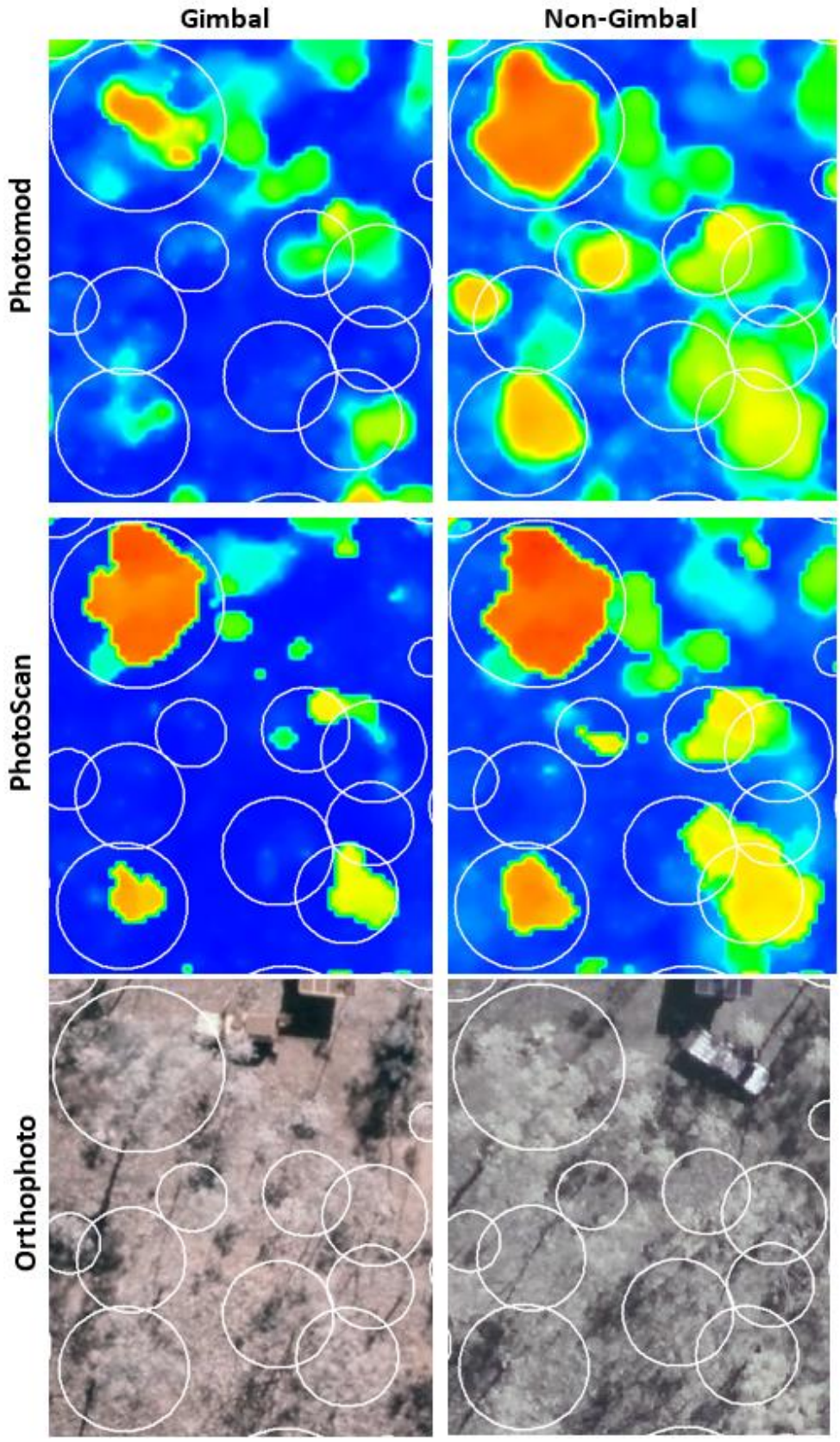

Figure 4.8: Study area subsets (28 x 24 m) demonstrating the better results of the non-gimbal over the gimbal derived raster CHMs. CHM resolution is 40cm GSD. White circles represent the crowns of reference trees (> 10 m).

4.3.3 Aspects and limitations of data acquisition by GoPro HERO4 camera

The main limitation of the GoPro camera is that the very small sensor (1.55 μm detector pixel size) in combination with a small lens aperture has low sensitivity to light (low signal to noise ratio and low dynamic range). Additionally, the operations of the camera are limited by the availability only of automatic shooting and continuous data acquisition modes (1 second in our case). As a result, to provide sufficient shutter speed (< 1/1000 sec) for image acquisition, the camera must be operated in sunny conditions with a sun angle >50°. Hence, we do not recommend using the acquired GoPro imagery without basic radiometry pre-processing (contrast, sharpness etc.).

Direct geo-referencing, based only on on-board GoPro GPS data, cannot be used for accurate forestry applications due to the low accuracy of the mobile GPS (5 - 20 m absolute error, in our case). The GCPs must be measured for indirect image geo-referencing and camera self-calibration. This study, and our experience in UAS data processing, has demonstrated that on-board GPS precision is not a major factor defining successful UAS imagery processing results. More important is ability to deliver radiometrically corrected and undistorted images with high overlap and stable camera orientation angles, which is in agreement with Bosak (2011). This can be achieved by camera platform-stabilizing (gimbal use) during data acquisition. Despite the fact that the non-gimbal acquisition reduces the cost and weight of the equipment and sometimes can provide better results in the tree detection (**Figure 4.8**), we recommend using a gimbal for accurate UAS mapping. The gimbal can help prevent unexpected problems related to image block relative orientation (tie point matching) and 3D point cloud matching (high noise, which has impact on point classification accuracy (**Table 4.2; Figure 4.6**)). In most cases, the problems we've mentioned

cannot be solved by an inexperienced user and require highly skilled photogrammetric ability and experience, and comprehensive software tools (stereo mode, pair-wise error deep analysis etc.). Taking all these factors together, we conclude that a GoPro camera with gimbal can be used for AGB estimation of the dominant and co-dominant trees in Australian tropical savannas with a plot accuracy +/- 15% (without counting both small and understory tress). Furthermore, the limitation of this study related to fact that presented individual tree detection results can be applied only in local areas with similar *Eucalyptus spp*. vegetation.

4.5 Conclusions

The main aim of this study was to evaluate the efficiency of consumer light-weight and low-cost UAS imagery (< $2,000) for estimating tree structural parameters and quantifying biomass in Australian tropical savannas based on well-known canopy maxima and watershed segmentation tree detection algorithms. We found that the canopy maxima and watershed segmentation routines could achieve similar tree detection rates (~70%) for dominant and co-dominant trees, but low detection rates (<35 %) for small trees due to poor representativeness in the point clouds and overstory obscuration. The GoPro camera, with gimbal setup and sufficient number of GCPs, can be used for acceptable (+/- 1.2 m) height estimation of dominant and co-dominant trees. We conclude that this low-cost UAS option currently cannot be used for reliable AGB estimation due to unstable sensor internal geometry, which affected the vertical accuracy of extracted CHMs. Although LiDAR provides higher tree detection rates and more accurate estimates of tree heights, image matching was found to be an adequate low-cost alternative for detection of dominant and co-dominant tree stands in Australian tropical savannas.

Acknowledgments: This work was supported by Charles Darwin University and Darwin Centre for Bushfire Research, whose staff are gratefully thanked for their cooperation and research funding. The authors wish to acknowledge the financial support from the Bushfire and Natural Hazards Cooperative Research Centre, made available by the Commonwealth of Australia through the Cooperative Research Centre program. Jorg Hacker, AusCover facility of the Terrestrial Ecosystem Research Network (TERN) and Airborne Research Australia (ARA) are thanked for having collected and provided LiDAR data. The authors wish to express their thanks to Dr. V.Adrov (Racurs company) and Agisoft LCC for the technical support. The authors also would like to thank Prof. J. Russell-Smith (Darwin Centre for Bushfire Research) for providing valuable comments. We acknowledge the valuable long-term infrastructure at the Litchfield Savanna Super Site, which is part of the Australian Super Site Network (www.supersites.net.au), funded by TERN.

Chapter 5

Limitations of high resolution satellite stereo imagery for estimating canopy height in Australian tropical savannas

Page intentionally left blank

This work has been published in peer reviewed international journal:

Goldbergs, G., Maier, S. W., Levick, S. R., & Edwards, A. (2019). Limitations of high resolution satellite stereo imagery for estimating canopy height in Australian tropical savannas. *International Journal of Applied Earth Observation and Geoinformation*, 75, 83-95.

https://doi.org/10.1016/j.jag.2018.10.021

The following table detailing relative contribution by me and my co-authors refers to the published paper:

Contributing author	**Contribution**	**Tasks Performed**
Grigorijs Goldbergs	85 %	Study design, field data collection, RS data and field data analysis, manuscript writing
Stefan W Maier	15 %	Study design, Manuscript review and editing
Shaun R Levick		Manuscript review and editing
Andrew Edwards		Manuscript review and editing

Page intentionally left blank

5.0 Abstract

Obtaining reliable measures of tree canopy height across large areas is a central element of forest inventory and carbon accounting. Recent years have seen an increased emphasis on the use of active sensors like Radar and airborne LiDAR (light detection and scanning) systems to estimate various 3D characteristics of canopy and crown structure that can be used as predictors of biomass. However, airborne LiDAR data are expensive to acquire, and not often readily available across large remote landscapes. In this study, we evaluated the potential of stereo imagery from commercially available Very High Resolution (VHR) satellites as an alternative for estimating canopy height variables in Australian tropical savannas, using a semi-global dense matching (SGM) image-based technique. We assessed and compared the completeness and vertical accuracy of extracted canopy height models (CHMs) from GeoEye 1 and WorldView 2 VHR satellite stereo pairs and summarised the factors influencing image matching effectiveness and quality.

Our results showed that stereo dense matching using the SGM technique severely underestimates tree presence and canopy height. The highest tree detection rates were achieved by using the near-infrared (NIR) band of GE1 (8 – 9 %). WV1-GE1 cross-satellite (mixed) models did not improve the quality of extracted canopy heights. We consider these poor detection rates and height retrievals to result from: i) the clumping crown structure of the dominant *Eucalyptus* spp.; ii) their vertically oriented leaves (affecting the bidirectional reflectance distribution function); iii) image

band radiometry and iv) wind induced crown movement affecting stereo-pair point matching. Our detailed analyses suggest that current commercially available VHR satellite data (0.5 m resolution) are not well suited to estimating canopy height variables, and therefore above ground biomass (AGB), in Eucalyptus dominated north Australian tropical savanna woodlands.

5.1 Introduction

Mapping of forests to assess their status and productivity is of increasing importance given their role in the global carbon cycle and the wide range of ecosystem services they can provide (Franklin 2001; Rogers et al. 2012). The collection of accurate and precise data related to forest structure, biomass and species composition has become an important part of forest management, inventories and monitoring (Trumbore et al. 2015). Different remote sensing methods have been used to address these issues, with varying levels of success. During the past 20 years, there has been an increasing emphasis in the use of active sensors like Radar and airborne laser scanning light detection and ranging (LiDAR) systems and stereo passive optical sensors (airborne and satellite imagery) to estimate various 3D characteristics of canopy and crown forest structure (Fatoyinbo 2012; Lu et al. 2016; Newton 2007). Results obtained differ between studies, depending on the sensor type, tree species and site conditions. Worldwide, LiDAR data, combined with up-to-date advanced data processing methods, have proven to be efficient and precise tools for indirect fine-scale estimation of forest 3D structure parameters (primarily tree height) derived from high-density 3D point clouds (Asner and Mascaro 2014; Goldbergs et al. 2018a; Lefsky et al. 2002; Maltamo et al. 2014).

However, relatively high acquisition costs prevent airborne LiDAR from being used across vast territories, and for regularly updating maps of forest structural state and dynamics. Australia's tropical savannas cover 1.9 million km^2, accounting for approximately 12% of the world's tropical savannas (Beringer et al. 2015). When considering alternatives to airborne LiDAR for continuous wide-area surveys, more cost-effective approaches utilising satellite data need to be considered. The main

advantages of satellite data over airborne remote sensing data include higher temporal resolution, lower cost, wider area coverage and spatially more homogeneous image content with multispectral information (Immitzer et al. 2016). Recently, there has been growing interest in the use of Very High Resolution (VHR) satellite-derived stereo imagery to generate dense digital surface models (DSM) analogous to LiDAR data to support forest inventory and monitoring (White et al. 2013). Structure from motion (SfM) and photogrammetric stereo matching techniques (Ahmadabadian et al. 2013; Hirschmuller 2008) for generating dense DSM from stereo satellite and aerial imagery rely on algorithms that restore the 3D geometry and calculate 3D object coordinates by simultaneous pixel-based matching of the same 2D object points in every possible image.

To date, several studies have effectively evaluated the combination of modern SfM image matching techniques and unmanned aerial systems (UAS) to extract tree biophysical and vertical structural parameters in different types of Australian forest (Hung et al. 2012; Wallace et al. 2016; Wallace et al. 2012; Whiteside and Bartolo 2016). Goldbergs et al. (2018b) evaluated the efficiency of consumer light-weight and low-cost UAS aerial imagery (< $2,000) for estimating tree structural parameters and quantifying biomass in Australian tropical savannas. The study found that the canopy maxima and watershed segmentation routines could achieve tree detection rates for dominant and co-dominant trees of ~70%, which is similar to results from airborne LiDAR.

However, the performance of image matching applied to VHR satellite stereo imagery for the retrieval of forest inventory attributes has not been studied intensively. The most successful studies are related to boreal and coniferous forests with dense

canopy cover and planophile foliage. St-Onge et al. (2008) assessed the accuracy of boreal forest canopy height metrics estimations based on canopy height models (CHM) comparison of an IKONOS stereo pair (1m resolution) and LiDAR data in the study area located in Quebec, Canada (bias -0.38m and RMS 4.24m). Neigh et al. (2014) found IKONOS Geo stereo data to be a useful low-cost LiDAR alternative for CHM generation (R^2 0.71 and RMSE 2.6m) in dense coniferous forests, where high-quality digital terrain models (DTMs) were available. d'Angelo and Reinartz (2011) evaluated WorldView-1 stereo imagery DSMs models against LiDAR data in Spanish steep mountain forests (carob, Aleppo pine trees) and obtained 4.86m standard deviation (SD) error. Immitzer et al. (2016) demonstrated the potential of WorldView-2 (WV2) stereo data together with Germany National Forest Inventory field plots (beech, oak) to generate maps of the growing stock with explained 56% of the variability. Persson and Perko (2016) indicated that stereo matching of WV2 satellite images is suitable for forest height mapping in boreal (spruce, pine) forests, where a Lorey's mean height could be estimated with a RMSE of 1.5 m (8.3%). For similar tree species, Yu et al. (2015) achieved similar results for plot (1024m^2) Lorey's mean height estimation with a RMSE of 1.4 m (6.63%). Straub et al. (2013) reported an RMSE of 44.4% for estimating timber volume at plot level and 19.6% at stand level in a complex mixed forest (Germany) using solely height data derived from stereo WV2. Aguilar et al. (2014c) confirmed that the quality of the extracted DSMs largely depended on the target land cover, being better for DSMs covering flat areas and best accuracy was attained for the case of pure along-track same-date stereo pairs.

However, there is currently little experience of how accurately forest attributes can be estimated using VHR satellite stereo dense image matching, particularly in open

and heterogeneous forests and savannas with a complex vertical and horizontal structure. In this research, we have filled this knowledge gap through the assessment of both GeoEye-1 (GE1) and WorldView-1 (WV1) stereo imagery for woodland structure parameter extraction and biomass estimation in Australian mesic savannas.

The main aim of this study was to evaluate the potential for stereo imagery, from commercially available VHR satellites, for estimating canopy height variables in open canopy Australian tropical savannas. To achieve this goal, we: (1) evaluated and compared the completeness and vertical accuracy of extracted canopy height models (CHMs) from GE1 and WV2 VHR satellite stereo pairs, in the same area and conditions, by using a LiDAR-derived CHM as reference; (2) analysed the effect of acquisition imagery geometry on stereo matching performance and canopy detection accuracy; (3) analysed the influence of stereo satellite spectral band radiometric characteristics on canopy detection accuracy and completeness; and (4) considered the influence of vegetation structure and the environmental conditions on CHM extraction.

5.2 Methods

5.2.1 Study Area

Litchfield National Park is located 100 km south of Darwin (13°10′S, 130°47′E), in the Northern Territory (NT), Australia (**Figure 5.1**). Our study area was located on the Tableland Plateu in a research "SuperSite", covering approximately 25 km^2. The area is representative of high rainfall tropical savanna (mean annual rainfall 1600 mm). The terrain is flat, elevation range is 203-228 m, and represents the dominant ecosystem type across northern Australia (TERN 2012). The rainfall is highly seasonal with most rain falling from October to April. During the fire season

(May to September), the understorey progressively cures with increasing biomass flammability (Maier and Russell-Smith 2012b). The study area is predominantly composed of savanna woodlands dominated by evergreen *Eucalyptus miniata* and *E. tetrodonta*, contributing more than 80% of the total above-ground tree biomass (Goldbergs et al. 2018a; O'Grady et al. 2000).

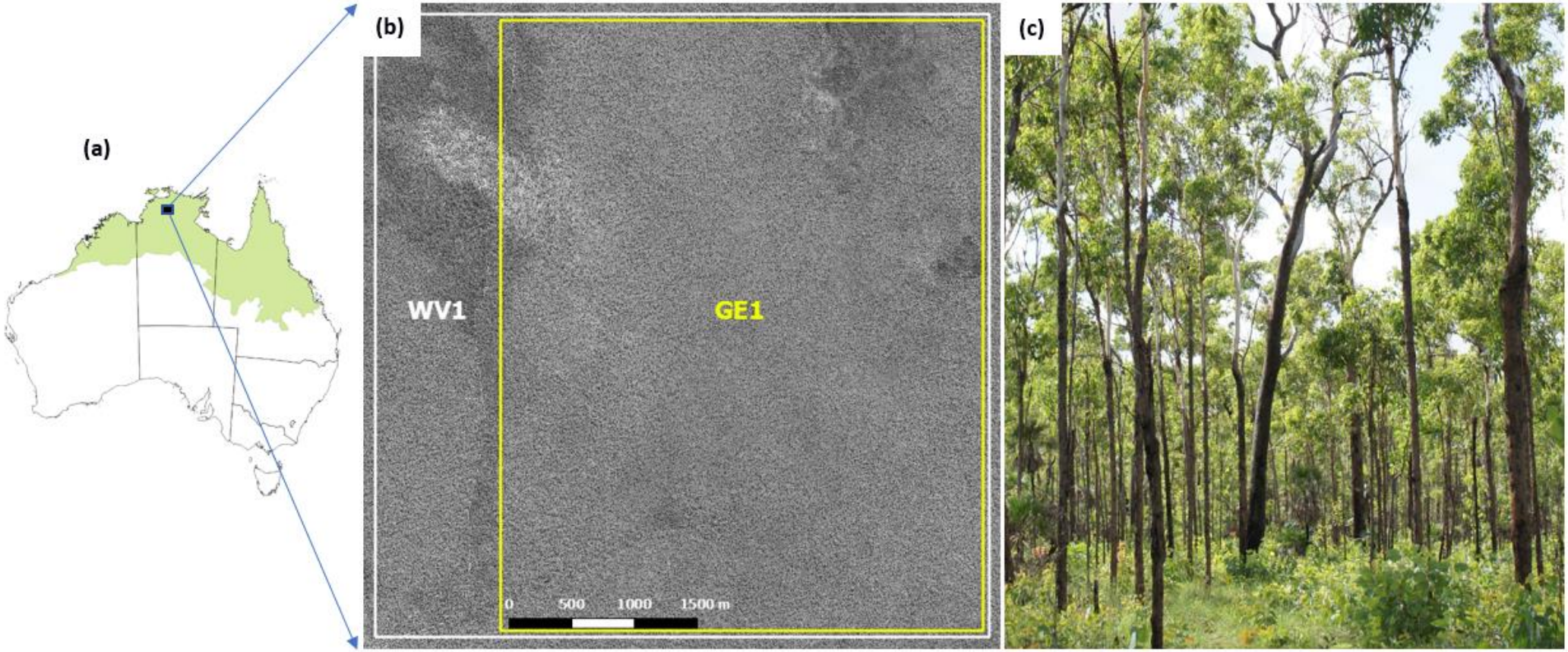

Figure 5.1: The 25 km^2 study area with elevation range 203-228 m: (a) in the north Australian tropical savanna (in green); (b) fully covered by WV1 (white box outline) and partly by GE1 (yellow box outlie); (c) photograph of the study area, dominated by Eucalyptus spp.

5.2.2 Airborne LiDAR data

Available LiDAR data were collected over the study area by Airborne Research Australia (ARA) in June 2013 and made available by the AusCover facility of the Terrestrial Ecosystem Research Network (TERN). The LiDAR data were collected with a Riegl LMS-Q560 full waveform sensor operating at 240 kHz, swath width of ~250 m, strip spacing of 125 m, with an average flying height above ground level (AGL) of 300 m, and flying speed of ~40 ms^{-1}. Although this study utilised the full waveform LiDAR system, the data were decomposed into 5 discrete returns with 20 cm footprints. The average LiDAR point density was 15 returns per m^2. Analyses related to the LiDAR data pre-processing, such as point cloud classification and CHM calculation, were carried out with the *LAStools* processing scripts (Isenburg 2014). The derived LiDAR-based CHM was used as reference data for this study.

5.2.3 Satellite data

Two pairs of along-track stereo GeoEye-1 (GE1) and WorldView-1 (WV1) imagery were obtained. No other imagery was available for the study area. The main characteristics of the imagery are given in **Table 5.1** and **Figure 5.2**. The images were 100 km^2 OrthoReady Stereo (OR2A) tiles, i.e. radiometrically (16 bit) and sensor corrected, projected to a plane using a Universal Transverse Mercator (UTM) map projection and had no topographic relief applied with respect to the reference ellipsoid, making them suitable for photogrammetric processing. While the WV1 imagery fully covered the study area, the GE1 stereo pair had 80% (20 km^2) coverage (**Figure 5.1**).

Table 5.1: Characteristics of stereo satellite imagery pairs (WV1 and GE1) acquired at the study site, where: PAN – panchromatic, R – red, G – green, B - blue, NIR – near-infrared sensor bands. All angles are given in degrees.

Spacecraft	Image ID	Acquisition date/time	Bands	Resolution GSD(m)	Convergence angle	Bisector angle	Asymmetry angle	Sun elevation
WV01	102001004098A300, 1020010041D67000	20 Jun 15 00:37 PM	PAN	0.5	42.5	73.9	3.83	52.6
GE01	1050410012C94300, 1050410012C94400	02 Jun 15 11:14 AM	PAN, R,G,B,NIR	0.5 2	34.6	82.3	3.95	48.1

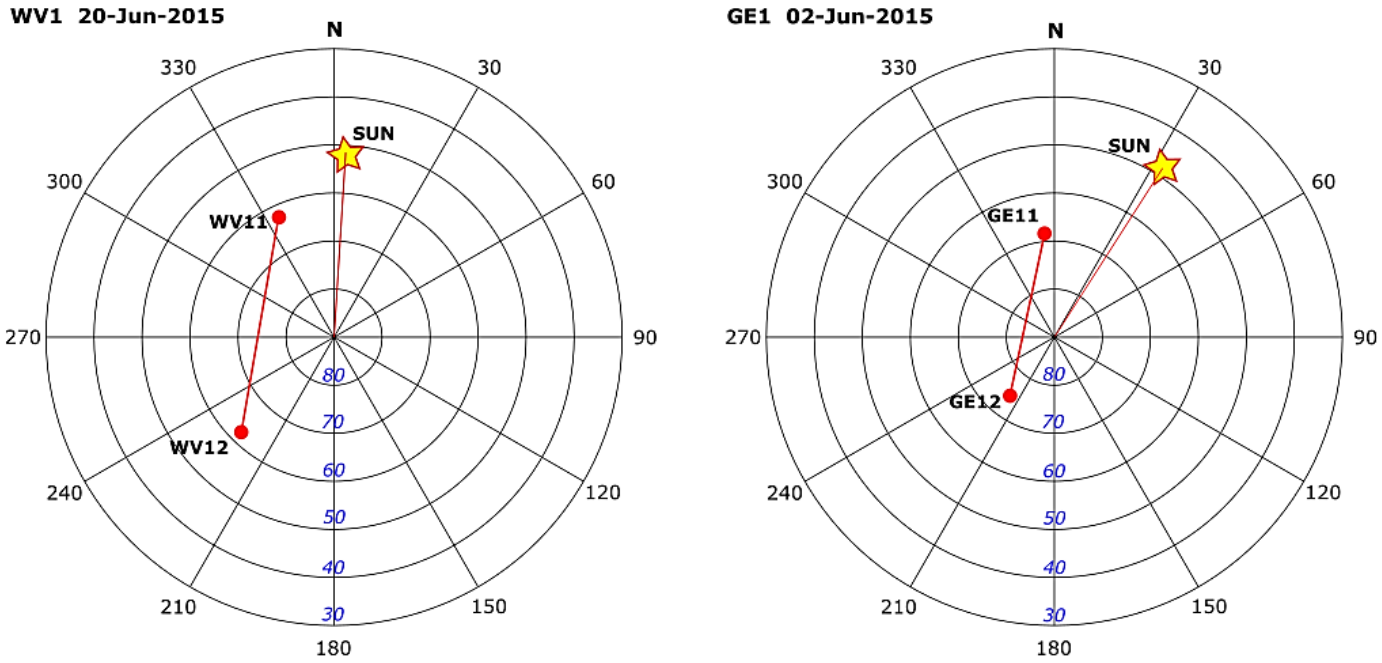

Figure 5.2: Polar diagrams of satellite stereo pairs: acquisition geometry describing the relative positions (elevation and azimuth angles) of the sun (yellow stars) and the sensors (red dots) to the target (circle centre). The given numbers of sensor positions (WV11, WV12, GE11, GE12), in each stereo pair, correspond to acquisition time and catalogue order. All angles are given in degrees.

5.2.4 Image data processing and sensor orientation

Two photogrammetric software packages, *Photomod* and *PCI Geomatica*, were used for regular parallel photogrammetric image data processing, related to image orientation, dense point DSM extraction and DTM creation. *Photomod V6.3* (Racurs, Moscow, Russia) and *PCI Geomatica V2017* (PCI Geomatics, Richmond Hill, Ontario, Canada), are complete and integrated desktop software packages that features tools for remote sensing, digital photogrammetry, geospatial analysis and map production. *PCI Geomatica* was included due to its high popularity among VHR satellite stereo imagery users and researchers, and to perform an independent parallel assessment of the processing results.

For dense DSM generation, both software packages use semi-global image matching (SGM) carried out at the pixel level (Hirschmüller 2011). In contrast to global matching approach, which seek to match every pixel in 2D image space, the SGM aggregate the matching (disparity) costs along several (8,16,32) symmetrical paths (1D constraints). As result, the SGM still achieves similar accuracy as global matching but makes process of matching more efficient and significantly faster (Hirschmuller 2008).

Image pre-processing commenced with pan-sharpening, which was applied to the GE1 imagery. While *PCI Geomatica* provides only one default pan-sharpening algorithm, we chose the most robust enhanced principal component analysis pan-sharpening method (from 3 others) in *Photomod*, as it does not require radiometric correction.

External sensor orientation was performed with an empirical model based on rational functions with rapid positioning capability (RPC) data, refined by a zero-order polynomial adjustment that required just one ground control point (GCP) (Grodecki and Dial 2003). To meet our research aims, image geo-referencing accuracy was improved by automatically measured tie points and ten manually positioned GCPs. Four out of the ten GCPs were surveyed using a *ProMark3* (Magellan Navigation, Inc., San Dimas, CA, USA) differential GPS. As no permanent GPS base station was available within a 100 km radius, a temporal base and rover setup were used with a final absolute point accuracy of ~1 m. Due to a limited number of well-identified man-made GCPs (poles, concrete slab corners) across the study area (4 of 10) and to achieve the best co-registration, the coordinates of six well-identified natural (tree stumps) objects were transferred from the LiDAR data. The GCPs were manually measured in stereo mode in *Photomod*. Only a semi-automatic mono approach was available in *PCI Geomatica*. Fewer GCPs were used for geo-registration of the GE1 imagery due to its partial coverage of the study area.

5.2.5 DSM, DTM and CHM extraction from VHR stereo satellite imagery

Altogether, six along-track models per program (WV1: PAN; GE1: PAN, R, G, B, NIR) were chosen for 0.5 m resolution grid DSM generation by using an SGM matching algorithm. Additionally, four cross-satellite grid DSM models were extracted, which comprised mixed stereo pairs combining single across-track images from both WV1 and GE1 sensors.

We extracted a DSM for each model in *PCI Geomatica* with default SGM settings, (not readily changeable), and applied a low pass smoothing filter (average

filter using a small filter size). In contrast to *PCI Geomatica*, *Photomod* allows the user to interact with all SGM settings starting from the number of calculation directions (paths) through to the disparity map interpolation distance and smoothing filter radius. After testing various SGM settings, we used slightly modified *Photomod* SGM default settings based on the census transform (CT) matching cost function with increased pixel cost calculation radius (5) and calculation paths (16); and a decreased penalty value (50) for parallax change by more than one pixel.

In total, four DTMs (0.5 m) were created, by using both programs' DSM editing tools, from PAN-based DSM models. The DSM filtering performance and the vertical accuracy evaluation of the DTMs were performed by comparison with the LiDAR-based gridded (1 m) DTM. The DTMs were then used for further CHM creation for all models.

The 0.5 m resolution grid CHM creation per model and comparison workflow was performed in *SAGA* GIS (Conrad et al. 2015) by subtracting the DTM from the corresponding gridded DSM. In every extracted along-track CHM model, we identified (selected) only grid values which represented a canopy height > 2 m. Thus, as no man-made objects (buildings etc.) existed, the height break threshold 2 m was applied automatically on all grid CHMs. The void values were assigned to the cells of all models < 2 m.

5.2.6 Accuracy assessment of CHMs

The LiDAR-derived CHM dense point cloud was gridded to 0.5 m by assigning the elevation of the highest return within each grid cell to the grid cell centre and used as reference data. The accuracy and quality of the image-derived along-track CHMs was assessed in two ways: completeness and vertical accuracy. The completeness of the image and LiDAR-derived CHMs was assessed as the proportion of grid cells representing "canopy" (H > 2m) of the total number of cells.

The vertical accuracy of the image and LiDAR-derived grid CHMs was assessed by matched cell (pixels) value comparison. The grid cell of any image-based model considered as matched in case of existence of corresponding valid (non-void) cell from LiDAR derived reference CHM. Descriptive statistics were calculated for all matched CHM grid cells in every model. The vertical accuracy of the matched cells was assessed by using robust accuracy measures suited for non-normal error distributions, as proposed for the accuracy assessment of digital elevation models (DEM) by Höhle and Höhle (2009). We modified the measures in relation to bias estimation between the reference data and the extracted CHMs. The set of accuracy measures (**Table 5.2**) are: mean bias difference between reference and modelled cells, median (50%) and 75% difference quantiles, median bias (%) - relation between the median of differences and reference (LiDAR) median vegetation matched cell heights; and the normalized median absolute deviation (NMAD). The NMAD is more resilient to outliers in comparison to standard deviation, as it is proportional to the median of the absolute differences between errors and median error.

Table 5.2: Accuracy metrics for extracted CHMs, where: Δh_j = difference between reference (LiDAR) and extracted CHM cell (j) values, and m = median quantile.

Accuracy measure	Notational expression
Mean	$\overline{\Delta h} = \frac{1}{n}\sum_{i=1}^{n} \Delta h_j$
Median (50%) quantile	$\hat{Q}_{\Delta h}(0.5) = m_{\Delta h}$
75% quantile	$\hat{Q}_{\Delta h}(0.75)$
Normalized median absolute deviation	$NMAD = 1.4826 * median_j(\lvert \Delta h_j - m_{\Delta h} \rvert)$
Median bias (%)	$m_{bias} = \frac{m_{\Delta h}}{m_{ref.}} * 100$

The accuracy and quality of the image-derived four cross-satellite models was assessed by visual comparison of the extracted DSMs, and all image-based CHMs (without height threshold cut) in comparison with the LiDAR, and presented in *Tukey* box plots (McGill et al. 1978).

5.3 Results

5.3.1 Accuracy of stereopair orientation

Table 5.3 shows the accuracies of the stereopairs orientation, based on quality statistics, root mean square errors (RMSE), of the X, Y and Z coordinates of the GCPs. The geo-positioning adjustment of the GE1 imagery was the least accurate, due to fewer GCPs. Another explanation for this is that identification of the same natural GCPs differed in the WV1 and GE1 pairs due to radiometric and geometric differences. The orientation of the *Photomod*-based models was better in comparison

with the *PCI Geomatica* ones, due to the manual GCP measurements in stereo mode. The use of stereo mode was especially important for the correct identification of the less accurate natural GCPs extracted from the LiDAR data.

Table 5.3: Root mean square errors (RMSE, based on GCP measurements) of orientation of three stereo pairs for Photomod and PCI Geomatica, where: WV1 – WorldView1, GE1 PAN – panchromatic GeoEye1, GE1 MS – pansharpened multispectral GeoEye1.

Stereo pair	Software	Nr. GCP	RMSE X (m)	RMSE Y (m)	RMSE Z (m)
WV1	Photomod	10	0.27	0.41	0.48
	PCI Geomatica		0.38	0.53	0.62
GE1 PAN	Photomod	7	0.71	0.82	0.60
	PCI Geomatica		0.76	0.93	0.87
GE1 MS	Photomod	7	0.61	0.66	0.57
	PCI Geomatica		0.78	0.82	0.78

5.3.2 Accuracy of the stereo imagery SGM based ground surfaces

The vertical accuracy evaluations of the DTMs, obtained from the panchromatic imagery, were based on a comparison of the grid DTM cells with the corresponding LiDAR DTM grid reference data, **Table 5.4**. Most SGM-based DTM models overestimated in comparison with the LiDAR DTM, except the *PCI Geomatica* GE1 model. The largest differences in the terrain representation are provided by models based on GE1 image data and can be explained by its less accurate sensor orientation in comparison with WV1 data. Despite the better sensor orientation results of the *Photomod*-based models over the *PCI Geomatica* (**Table 5.3**), the results were worse in the DTM comparison. This discrepancy is related to the efficiency of

PCI Geomatica which provided a more robust, comprehensive, simple to use DSM filtering and editing tool set.

Table 5.4: Comparison of the SGM-based (DTM_{SGM}) and LiDAR (DTM_{LiDAR}) - ground surfaces, based on corresponding elevation cell difference statistics: mean error and standard deviation (SD) (in metres). Negative values represent an underestimation.

$DTM_{SGM} - DTM_{LiDAR}$	WV1 20-06-15		GE1 02-06-2015	
	PCI Geomatica	***Photomod***	***PCI Geomatica***	***Photomod***
Mean (Bias)	0.10	0.23	-0.33	0.37
SD	0.28	0.39	0.62	0.71

5.3.3 Completeness and vertical accuracy of SGM based CHMs

The completeness of the image-derived CHMs was assessed by comparison with the LiDAR-derived CHMs, **Table 5.5**. Three *Photomod*-based CHMs derived from GE1 blue, green and red bands are not presented due to their similarity with the *PCI Geomatica* models. The most striking result to emerge from the data is that stereo-dense matching using the SGM technique failed in all models. No significant differences were found between models except for the model based on the NIR band of the GE1 stereo pair. The next discussion chapter, therefore, moves on to discuss the reasons of that outcome.

Table 5.5: The completeness of image-derived CHMs compared with LiDAR-derived CHMs, where: first row - the ratio between the number of grid CHM cells representing canopy (H > 2m) and total number of cells; second row - the percentage of image-derived CHMs matched cells (H > 2m) with LiDAR CHM. PCI = models extracted from PCI Geomatica, PH = Photomod; Pan, Blue, Green, Red and NIR = are sensor bands used for corresponding CHM extraction. All values are given in percentages.

	LiDAR	**WorldView 1**		**LiDAR**	**GeoEye 1**					
	25 km2	PCI *Pan*	PH *Pan*	20 km2	PCI *Pan*	PH *Pan*	PCI *Blue*	PCI *Green*	PCI *Red*	PCI *NIR*	PH *NIR*
Canopy cover (%)	36.7	0.82	1.6	35.2	0.4	0.7	0.05	0.32	0.03	4.3	5.4
LiDAR matched completeness (%)	100	1.46	2.9	100	0.74	1.3	0.09	0.42	0.05	7.6	9.1

Descriptive statistics were calculated for all matched LiDAR and image-based CHM grid cells (0.5 m, H > 2 m), in every model (second row, **Table 5.5**), and presented in *Tukey* box plots (McGill et al. 1978), **Figure 5.3**.

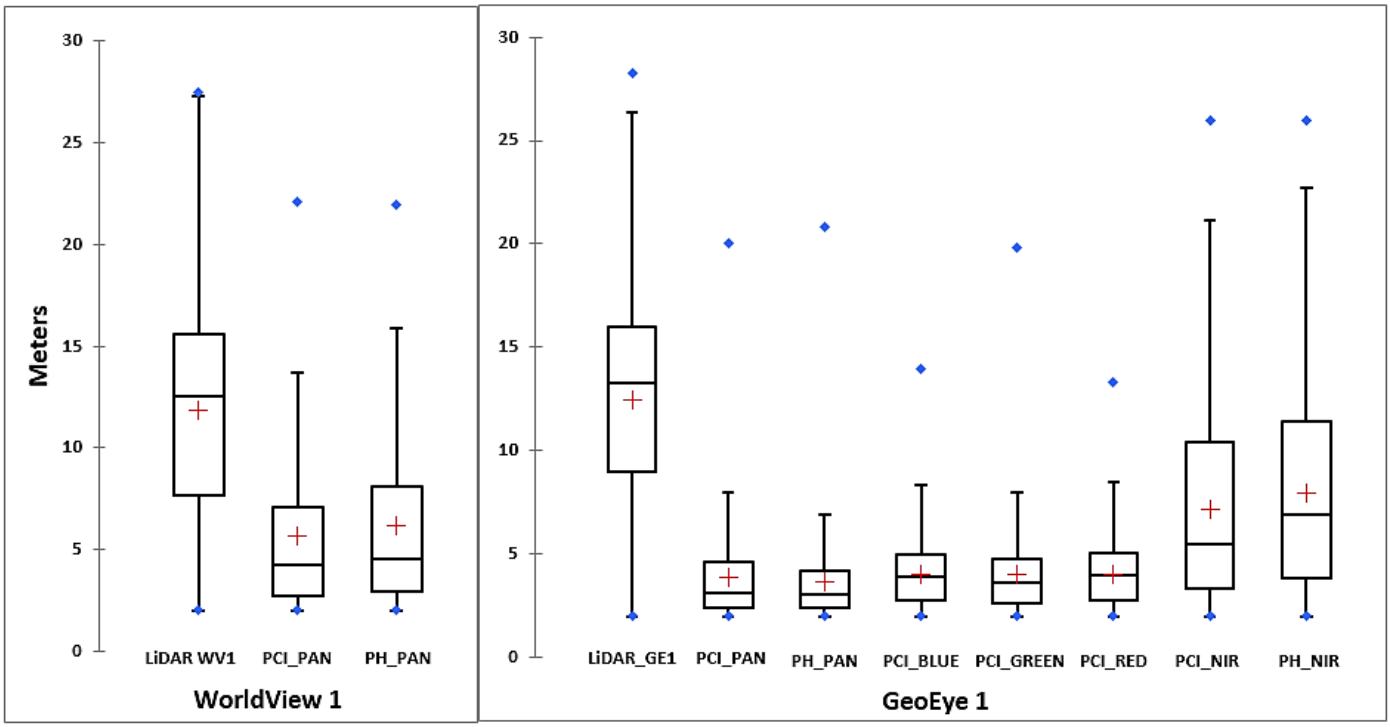

Figure 5.3: All matched LiDAR and corresponding image-based CHM grid cells in corresponding models (X axis), where: the vertical boxes represent the data range (Y axis, meters) between the lower (Q_1 = 25%) and higher (Q_3 = 75%) quartiles; the whisker length is within 1.5 times the interquartile range of Q_1 and Q_3; the red cross represents the mean value of the data; the horizontal line in the box is the statistical median; the blue point represents the maximum value of the dataset. PCi = *PCI Geomatica;* PH = *Photomod* based models with sensor band accordance.

The vertical accuracy assessments of the CHMs (matched cells, H > 2 m), **Table 5.6**, are based on the accuracy measurements given in **Table 5.2**. Due to a negligible number of matched cells, the GE1 DSM models related to blue, green and red bands were not analysed. All models, except for the NIR-based, have high underestimation bias with respect to the reference LiDAR data.

Table 5.6: Vertical accuracy assessment (**Table 5.2**) of extracted image-based CHMs, compared to the LiDAR (matched cells, H > 2 m), where PCI – *PCI Geomatica* and PH – *Photomod* based models, PAN – panchromatic and NIR – near-infrared. Values in metres, except median bias (%). Negative values represent an underestimation.

Accuracy measure	WorldView 1		GeoEye 1			
	PCI PAN	*PH PAN*	*PCI PAN*	*PH PAN*	*PCI NIR*	*PH NIR*
Mean (bias) (m)	-4.6	-5.6	-4.9	-5.7	-4.2	-4.5
Median (50%) (m)	-3.7	-4.6	-3.8	-5.1	-2.9	-3.4
75% quantile (m)	-0.7	-1.5	-0.8	-1.6	-0.4	-0.7
NMAD	4.6	5.9	4.4	5.8	4.5	5.3
Median bias (%)	37%	37%	53%	52%	25%	26%

5.3.4 The accuracy of the cross-satellite CHMs

The descriptive statistics of the cross-satellite CHMs (all grid cells, no height threshold) are presented in **Figure 5.4**, comparing with the reference LiDAR data and the best NIR band image-based model. All cross-satellite models demonstrated negligible correlation with the reference data, with extremely high overestimation and high variance. Relatively, reasonable results were obtained only for open terrain areas without canopy cover and in a few areas of the WV12-GE12 model where images were acquired opposite the sun direction (forward scattering).

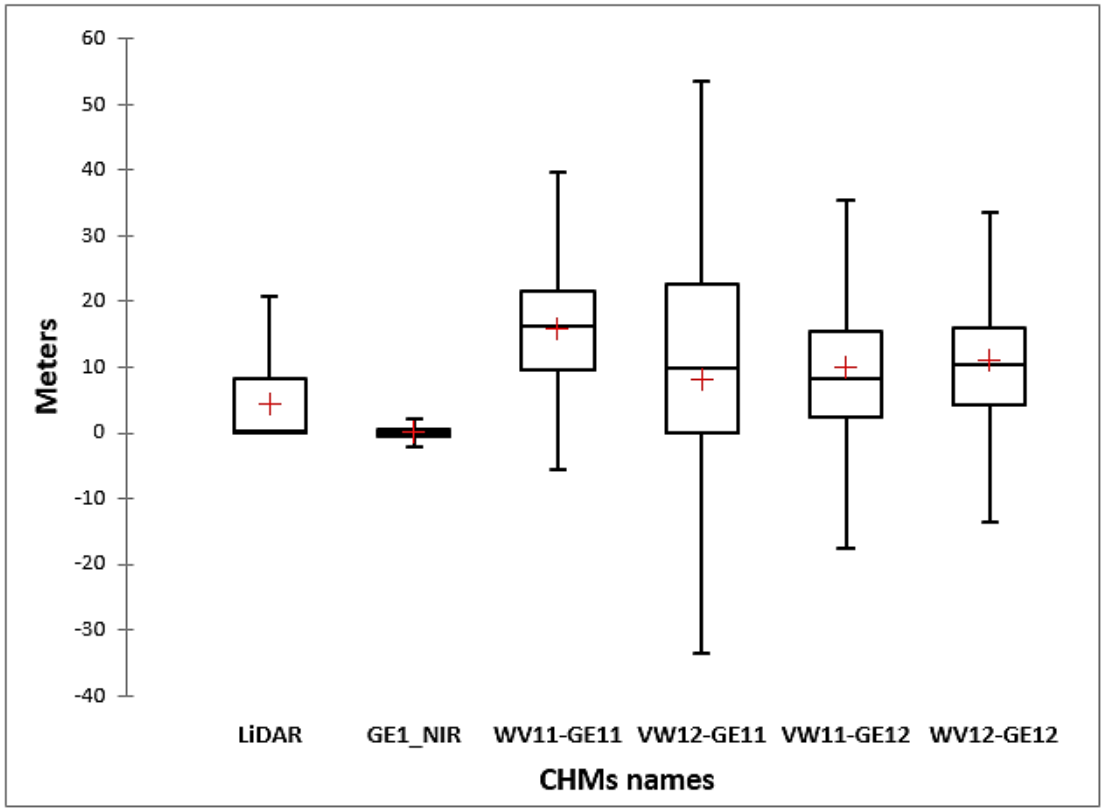

Figure 5.4: Box plots of LiDAR and corresponding *PCI Geomatica* image-based CHMs (X axis), where cross-satellite model names correspond to image locations in Figure 5.2. Each box represents the data range (Y axis, metres) between the lower (Q_1 = 25%) and higher (Q_3 = 75%) quartiles; the whisker length is within 1.5 times the interquartile range of Q1 and Q3; red cross – mean value of data, statistical median as a horizontal line in the box.

5.4 Discussion

DSM generation from VHR stereo satellite imagery is unreliable in the tropical savanna ecosystem that we studied. There were no significant differences among the DSM models, except for the NIR-derived model, which only provided an 8-9 % canopy detection rate. If the proportion of detected trees is as low as it was in this study, it is clear that there would be considerable underestimation of canopy heights (**Table 5.6**). However, these results provide important insights into the factors and

causes driving this negative outcome. The accuracy and completeness of DSMs generated by the SGM matching algorithm had a direct effect on canopy detection performance. In our study, it was related to a complex of interdependent factors, including: (1) vegetation structure and species composition; (2) observation geometry dependent reflectance (bi-directional reflectance factor, BRDF); (3) wind induced crown movement; (4) accuracy of image orientation and extracted CHMs and; (5) image band radiometry.

5.4.1 Eucalyptus miniata/tetrodonta structure

Canopy detection in savannas with low canopy cover and an open canopy structure is more difficult than in a forest with a closed canopy, since open canopies allow more sunlight to penetrate the forest canopy and result in the return of a mixed signal to the sensor. *Eucalyptus miniata* and *E. tetrodonta* are characterised by the presence of rigid and narrow leaves, vertically orientated (erectophile) in response to the high sun intensity (similar to needle leaves), making their canopies relatively more transparent when viewed from above (Goodwin et al. 2005; Jacobs 1955), **Figure 5.5a,5.5b**. The reflectance of canopies is also influenced by tree-crown density and canopy cover, represented by the Leaf Area Index (LAI), and understorey reflectance. Hutley et al. (2011) describe LAI along a rainfall gradient starting at a value of ~1, in the region encompassing our study site, down to 0.4, compared to a range of 0.5 to 5.5 in Eastern Australian Eucalypt dominated habitats (Woodgate et al. 2015).

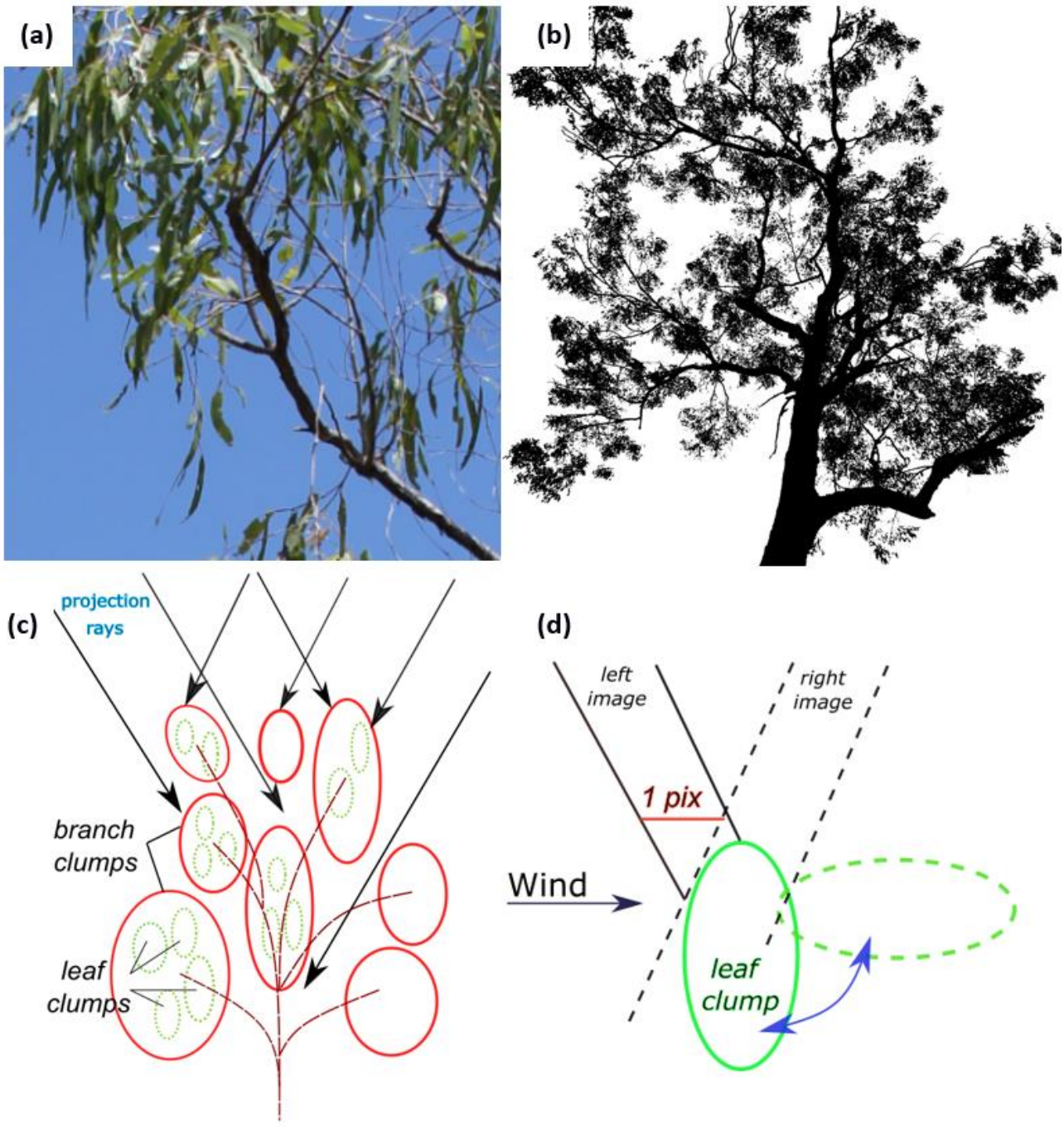

Figure 5.5: Eucalypt tree crown with clumped-leaf-grain structure, random vertical/horizontal clump organization and gaps, where: (a) a photograph of *E.miniata* vertically oriented and narrow leaves; (b) sparse, clump structure of *E.miniata* crown; (c) scheme of tree crown structure representing two-level clump hierarchy and transparency during image acquisition; (d) example of tree object (leaf clump) missing (moving) on one of the images due to wind effect.

Eucalypt tree crown structure is represented by a two-level clump hierarchy. Every big branch forms a clump (normally 3 - 7 m in diameter) which constitutes the first level of the crown hierarchy. Each branch clump consists of a group of smaller objects (leaf clumps, 0.5 - 2 m in diameter) that form a second level of the tree crown structural hierarchy and are arranged around small branches interspersed with large crown gaps (Jacobs 1955). Additionally, the tight leaf concentration around branches and large intra crown gaps result in low foliage cover with a variety of crown shapes (Culvenor 2000), where mean foliage projective cover in the study area is 20%.

Because leaf arrangement is tightly clumped, every Eucalypt tree crown has a clumped-leaf-grain structure with a random vertical/horizontal clump and gap organization (**Figure 5.5c**). Such a heterogeneous structure exhibits a small cross section when seen from above the canopy. As a result, the canopy is transparent and shows little contrast with the background. The sunlight, scattered by a clump, when colliding with another clump within the same crown, is more likely to escape through the mid crown lateral surface, resulting in relatively low upward reflection (Schull et al. 2011). As result in most cases, due to the clumped and transparent pattern of Eucalypt canopy structure, the fewer number of SGM image-matched points are unable to derive the upper canopy surface.

Our tests in the field confirmed that *Eucalyptus miniata* and *E. tetrodonta* are strongly affected by wind. We undertook continuous zenith photography of the tree crowns with time intervals 5 and 20 sec. from a fixed ground position, under similar conditions (5 - 6 $m^{-1}s$) as for the dates of image acquisition. The images demonstrated the tree crown and leaf clump movement, and deflections of up to several meters, (**Figure 5.5d**). As a result, within the time interval between the image pair (up to one

minute), tree crowns or parts thereof, are in vastly different locations violating the fundamental assumption of the SfM technique that both images capture exactly the same scene from two different locations. Thus, image objects disappear, in this instance the trees, from the CHM, and therefore account for a substantial error in the detection rates.

5.4.2 Vegetation reflectance and contrast effects

Reflectance of vegetation strongly varies with sun-sensor viewing geometry and is affected by a complex mixture of variables, including canopy, understorey and ground layer structure, species composition, soil type and soil moisture. These can be accounted for by the bidirectional reflectance distribution function (BRDF) (Gerard and North 1997). In our case, due to the leaf clumping, consequent crown transparency, proportionally low canopy cover and wind effect, the digital photogrammetric and computer vision techniques had to deal with complex mixed pixels, which included information related to the ground layer, foliage, crown woody parts, understorey components and shadows (**Figure 5.6a,5.6b**).

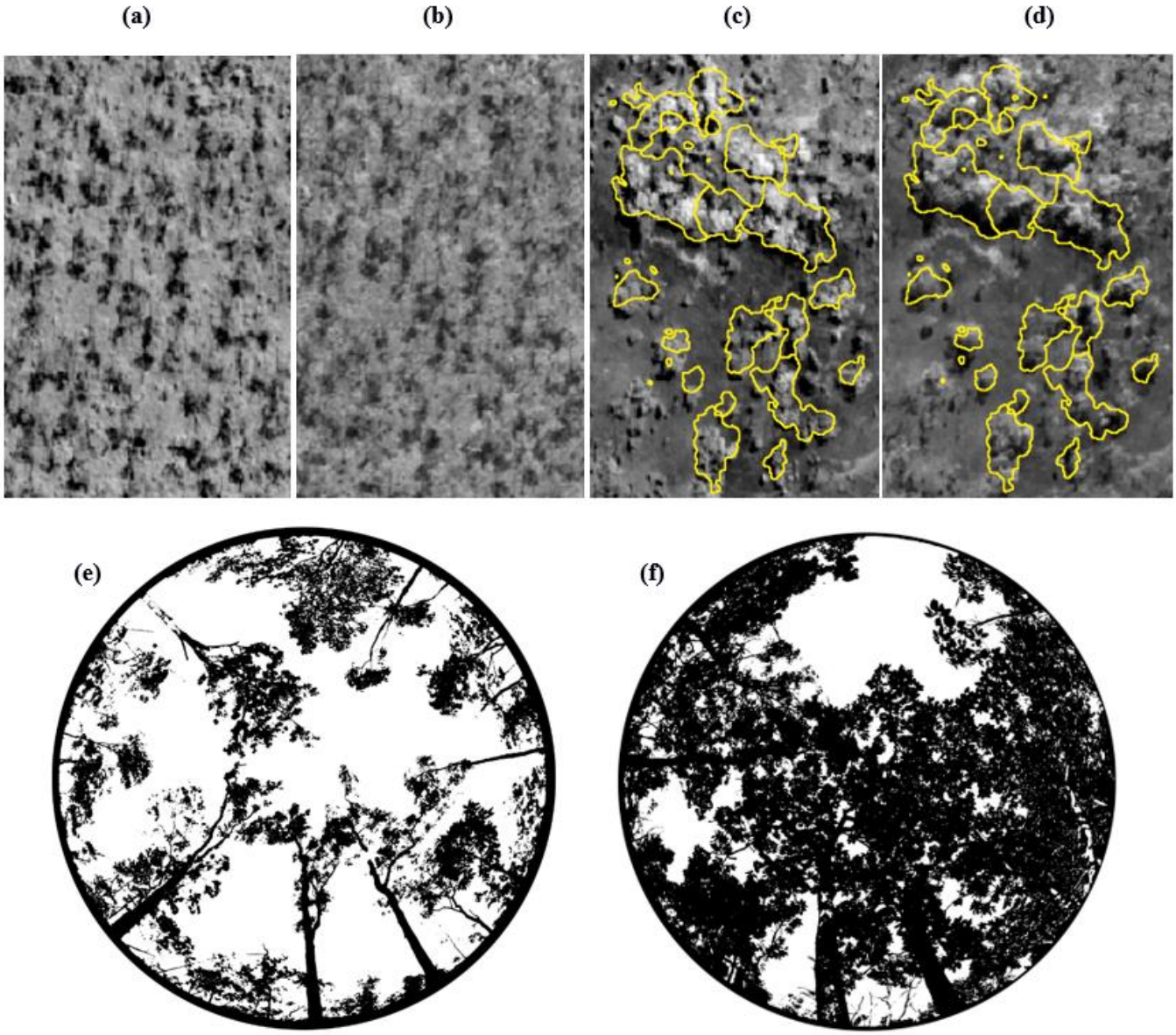

Figure 5.6: WV1 stereo imagery fragments (110 x 170 m) of the study area with extracted canopies (yellow polygons, H > 2 m), where: (a) left and corresponding (b) right image (toward sun) of the first stereo pair fragment, *E.miniata/terodonta spp*. dominant, with failed SGM technique; (c) left and corresponding (d) right image (toward sun) of the second stereo pair fragment with grouped broad leaf Ironwood (*Erythropleum cholorostachys)* trees and successful SGM-based CHM extraction; and corresponding *hemispherical* photographs of *E.miniata/tetrodonta (e)* and; Ironwood tree copses (f).

The sparse canopy pattern, highly scattered reflectance, and the relatively small brightness range between the shadows and sunlit areas, such as at the top of the canopy, resulted in insufficient image contrast for tree canopy separation (detection). This can be seen in images acquired opposite the sun direction (forward scattering) and creating a blurred effect (**Figure 5.6b**). In most cases, it was then impossible to detect tree crowns correctly during dense DSM extraction by SfM matching. SGM matching was more successful in dense groups of *planophile* leaf species, such as Ironwood (*Erythropleum cholorostachys)* (**Figures 5.6c, 5.6d**). Coexisting broad leaf species fill in the canopy gaps and reduce crown transparency, smoothing the roughness of the top of canopy shape thus increasing the reflectance, as crown shape topology has been found to have a significant influence on overall reflectance (Gerard and North 1997).

To increase the canopy detection rate, there must be sufficient image contrast between the canopy and the understorey. If the understorey and canopy have similar spectral properties, like *Eucalyptus spp.*, the matching technique is less likely to identify the top of the canopy, and thus the surface elevation measurement at the feature's location would be more representative of the ground (background) elevation. This finding is in agreement with Montesano et al. (2017) who showed that contrast and brightness between vegetation and the ground surface primarily determines whether elevations from SfM are derived from somewhere at the top or within the canopy, or from the ground. These findings were further supported in areas with burned understorey (**Figure 5.7**), which provided a darker background. In most such areas, the SGM canopy detection shows positive results in comparison to surroundings areas, which can be explained by the higher brightness/contrast between vegetation

and the darker ground surface (charred material). These findings also could partly explain the differences in completeness (**Table 5.5**) between WV1 (200% higher rate) and GE1 PAN imagery, as the areas with burned understorey were only covered by the WV1 images.

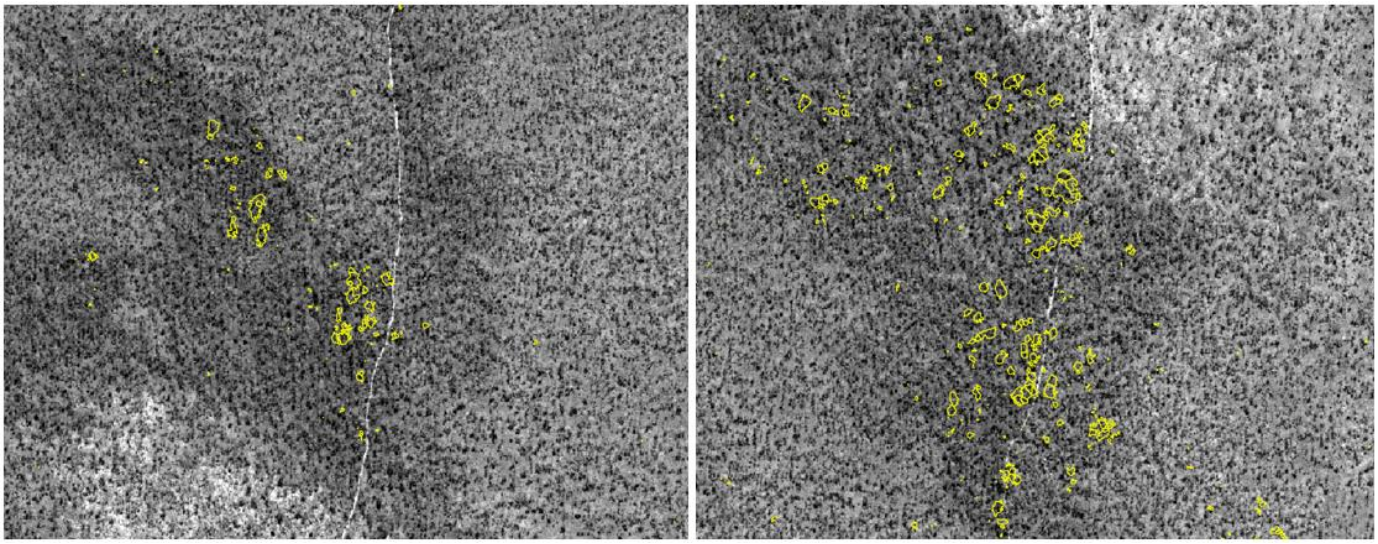

Figure 5.7: Two WV1 imagery fragments (1600 x 1200 m each) of the study area covering sites with burned understorey. Extracted canopy segments are depicted as yellow polygons. The burned understorey areas appear darker grey.

The highest tree detection rates were achieved by using the NIR band of GE1 imagery (**Figures 5.8, 5.9**), ~20 times higher than the green band results (**Table 5.5**). This is understandable, as photosynthetic Eucalypt vegetation spectra generally have the same shape and magnitude as other vegetation spectra dominated by chlorophyll and have the highest reflection in the NIR (Kumar et al. 2010), providing higher contrast between canopy and the bare ground surface. As in most cases, the ground is also covered in vegetation, it seems possible that these results are due to the high reflectance and transmittance of leaves with less pronounced shadow components and NIR BRDF effects in the spectral signature of the scene. However, the overall tree

detection rate is still unsatisfactorily low. Again, this likely arises because the reflected radiation received by the sensor integrates the reflectance from leaves, branches, stems of the trees, as well from the ground cover, dry leaves and soil. The final spectral signature consists of a greater combination of all these surface components in such open Eucalypt savanna.

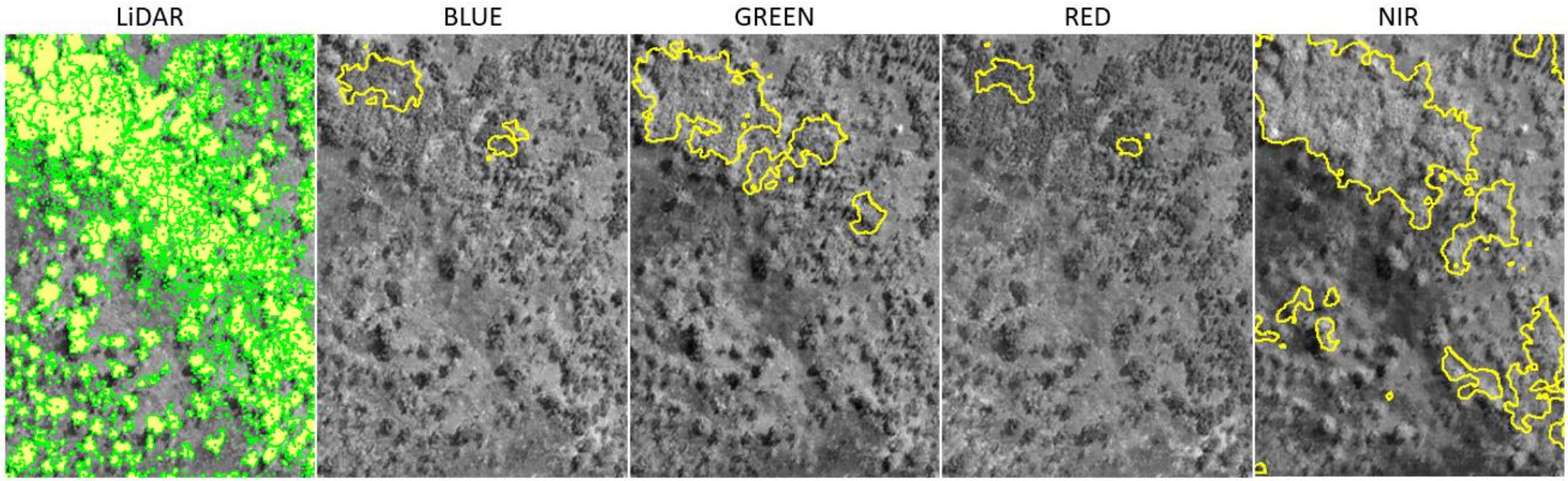

Figure 5.8: GE1 imagery fragment (170 x 120 m) of the study area with extracted image-based CHMs (yellow polygons; H > 2m) related to corresponding image bands (background) in comparison with reference LiDAR data (green polygons with yellow fill; H > 2m). All images are in the sun direction (backward scattering).

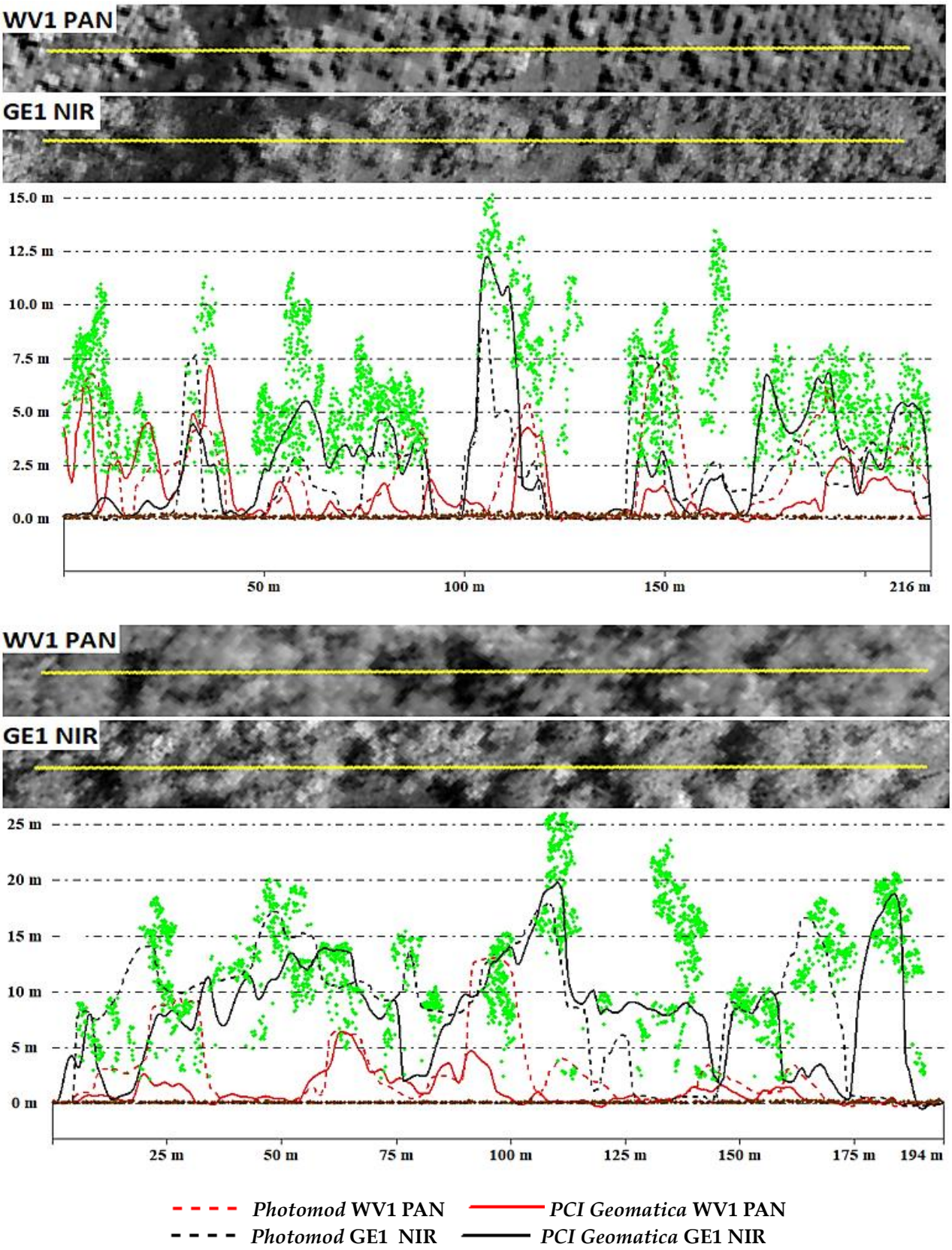

Figure 5.9: Two horizontal transect examples of successful CHM SGM matching based on WV1 PAN and GE1 NIR imagery in comparison with reference LiDAR 3D point cloud (green dots), where: *PCI Geomatica* 0.5 grid CHMs are solid lines and corresponding *Photomod* CHMs are dashed lines. Images are in the sun direction (backward scattering).

This study has been unable to demonstrate that cross-satellite (mixed) models could improve the quality of extracted DSM (**Figure 5.4**). This result could be attributed to radiometric differences between images, which are related to differences in acquisition dates, image geometry and different sensors. After stereo visual inspection of image DSM outliers, we found that a significant contributing factor was the effect of the movement of the shadows of single trees (displacement) between images due to different sun positions and sun-to-sensor geometry. Surprisingly, in most cases, the shadow displacement was insufficient to adversely affect cell matching along the clearly expressed shadow edges. Contrary to the radiometric differences, many DSM outliers were still correctly matched (mostly along shadow edges of single trees) and lead to incorrect height calculations (mostly overestimation). As a result, we cannot recommend using cross-satellite (mixed) imagery for DSM extraction in areas with clearly identifiable individual tree shadow patterns (**Fig. 5.6a**).

5.4.3 Ground estimation and DTM quality analysis

Accurate modelling of the terrain (DTM) is critical for CHM calculation. The results of this study indicate that Eucalypt-dominated savanna vegetation structure is sufficiently transparent to undertake accurate terrain reconstruction by SfM matching techniques. The present findings are consistent with our previous research (Goldbergs et al. 2018b) which found that the overwhelming majority of all 3D DSM point extractions related to the ground surface, negating the need to use an external digital terrain model for CHM generation. No significant differences were found between DTM_{SfM} and DTM_{LiDAR}, both providing similar representation of the terrain across the study plot. In our case, the default and automatic filtering procedures of the DSM

editing tools were acceptable for DTM extraction across the flat (20 m terrain height range) study area.

In addition, we assessed the efficiency of filtering procedures applied on rough terrain (150 m vertical range) using the same NIR band extracted DSM (with high tree detection rates) in an area outside of our available reference LiDAR data (**Figure 5.10**). Our results indicate that rough terrain DSM filtering, using LiDAR-based or photogrammetric techniques, requires an operator for the DSM manual editing process to achieve acceptable results in DTM creation. This is mostly due to limited visibility of the ground to successfully extract vegetated areas from the SfM based models, resulting in large gaps of ground area in the DSM. The removal of non-ground elevation values from the steep and vegetated rough terrain DSM, based only on automatic filtering tools, can lead to the elimination of good surrounding ground elements/cells, that otherwise contain artefacts related to above ground features. These results match those observed in DeWitt et al. (2017), who showed that subsequent filtering may reduce the effect of above-ground features, but at the cost of fine-scale terrain details. We should note, that depending on the terrain roughness and proportion of vegetation in the area, the DSM semi-automatic filtering process can take significant time.

Another important finding was that SGM-based canopy detection was more successful in rough terrain compared to flat areas. This may be explained by the fact that the rough terrain contains many creeks and therefore a lot of riparian vegetation, which has mostly *planophile* leaf orientation and much less transparency with higher canopy cover.

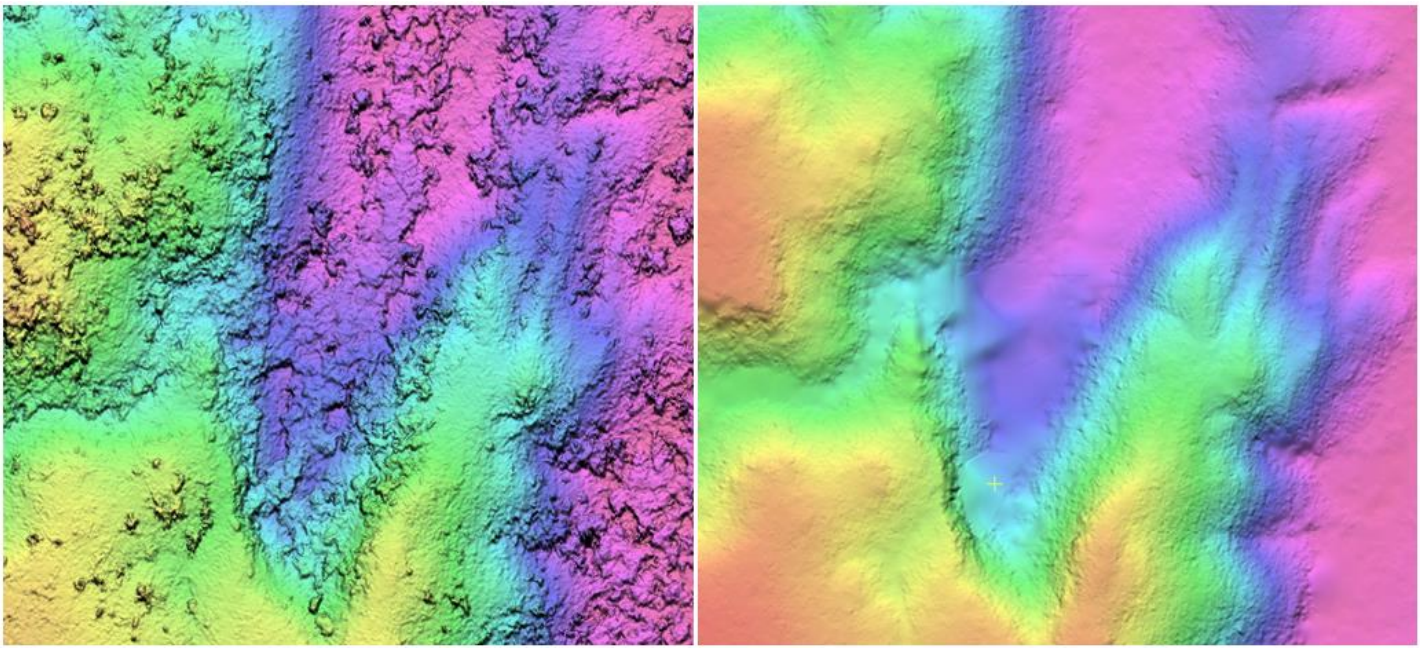

Figure 5.10: Visual comparison of DSM and corresponding DTM (800 x 700 m): (a) DSM (0.5m) extracted by SGM using NIR band of GE1 imagery; (b) corresponding DTM (150 m elevation range) after applying automatic and semi-automatic DSM filtering and editing techniques (*PCI Geomatica*).

5.4.4 Considerations, limitations and recommendations for data processing by stereo WV1 and GE1 satellites

It is reasonable to expect that the uncertainty in the canopy detection by SfM based techniques will vary from area to area depending upon many interrelated factors (**Table 5.7**). However, determining how much information (reflected energy, vegetation detail etc.) is needed from the tree crown for an acceptable result by SfM, is still unknown. In our recent research (Goldbergs et al. 2018b) the SfM based techniques achieved high tree detection rates (~70%) for dominant and co-dominant trees by using low-cost unmanned aerial systems (UAS) imagery (5 cm resolution). Taken together, these results suggest that there is an association between SfM efficiency and spatial resolution. The fine spatial resolution of the data can help to

reduce such factors like clumping vegetation structure and crown transparency. It is unlikely that an SfM technique based on single stereo pair measurements will allow accurate tropical savanna canopy extraction. The successful UAS-based results, image-to-sun geometry and object reflectance rules suggest multiple view angle image measurements are required. Further research should be done to investigate the source imagery resolution dependency and along-track multiple view image satellite measurements (e.g. triple stereo Pleiades) influence on SfM efficiency in tropical savannas.

Research is also needed to analyse satellite images acquired in different seasons, that is, to investigate the effect of tree leaf deciduousness and background (grass and litter) conditions on the quality of extracted DSMs. Unfortunately, in this research, stereo satellite imagery had very similar sensor-to-target and sun-to-sensor geometry (**Table 5.1; Figure 5.2**), acquired under similar seasonal and climatic conditions. This fact did not allow us to perform a comprehensive analysis of the effect of the image geometry differences (e.g. convergence, bisector and sun angles) and their influence on the quality of the extracted DSMs. This is an important issue for future research, especially in the extreme case, sun elevation angle 90^{o}, (February and October); and possible along-track stereo satellite image acquisition or multiple satellite constellation, where the path direction and/or image-to-target is perpendicular to the sun-to-target direction (principal plane).

Table 5.7: Summary of factors influencing SGM-based DSM quality and accuracy. (Derived from analyses in north Australian tropical savannas).

Factor	Level of influence	Affected by	Affected on	Possible solutions, comments
Vegetation clumped-leaf-grain structure and leaf vertical orientation	Highest	Type of vegetation (species etc.)	Amount of scattering and reflection energy; on canopy transparency; canopy separation from the ground; BRDF	Data acquisition with maximal leaf-on conditions (January to June) and highest contrast/brightness differences between canopies and ground: NIR band use, after understorey fire; optimal image-to-target geometry (further research needed); Multiple (more than two) along-track imagery acquisition (e.g. satellite triple stereo imagery) or multiple satellite constellation, where the path direction and/or image-to-target is perpendicular to the sun-to-target direction.
Stem density, tree canopy formation, canopy cover	High	Vegetation spp. and structure, terrain relief.	Crown/canopy shadowing; individual tree and ground surface detectability.	
Canopy/crown shadows	High	Sun position, sun-to-image geometry; vegetation structure and transparency.	Efficiency and quality of image matching, individual tree and ground surface detectability.	
Wind	High (if speed > 5m/s)	Wind speed	Leaf clump displacement due to wind	Data acquisition under low wind conditions (3 m/s)
Terrain, steep relief	Depend on terrain geomorphology		Ground surface detectability and quality of extracted DSM and DTM needed for CHM generation	DTM creation by semi-automatic DSM editing and filtering program tools with operator interaction. External high quality DTM use
Stereo imagery (image-to-target) geometry	Depend on image acquisition parameters	Sensor and acquisition parameters (e.g. convergence, bisector angles).	2D projected object geometry in images; parallax.	Data acquisition with optimal image-to-target geometry (further research needed)
Sun-to-image geometry	Highest	By positions of sensor and sun during imagery acquisition.	Imagery radiometry and its differences; efficiency and quality of image matching.	Imagery along-track path perpendicular to sun-to-target direction; along-track multi view imagery acquisition e.g. triple stereo imagery (further research needed)
Imagery spatial resolution	High	Sensor type and data acquisition parameters.	Image and object spatial geometry, object and it's parts detection and identification	Imagery with higher spatial resolution use
Poor initial stereo model absolute geo-referencing	High, Critical with external DTM use	Number and accuracy of measured GCP	Stereo model absolute vertical (DSM) and horizontal accuracy	Additional number of GCP, especially height points; Stereo measurements of GCPs

No significant differences were found between *Photomod* and *PCI Geomatica* photogrammetric software, both providing similar results of the extracted CHMs across the study area. The *Photomod* based models showed slightly better canopy detection results thanks to the modified SGM default settings. We should note however, that modifying and testing the new SGM settings required additional operator and machine time, and extra operator attention for further DSM filtering. The *PCI Geomatica* provides slightly better SGM results based on default settings than *Photomod,* an advantage for non-experienced users.

In terms of manual stereo digitizing/extraction of tree crowns in *Photomod,* and based on our stereo restitution experience, we have defined the following rules associated with SGM for regions with similar vegetation structures. If an experienced stereo operator cannot approximately identify (i.e. digitize in stereo) the shape, and accurately extract the height, of the crown (like on stereo model, **Figure 5.6a, 5.6b**), the SGM will fail with a 99% probability. However, if the operator can perform the stereo restitution of the approximate shape and height of the tree crown, the probability of image matching success will be > 30%. Omitting the necessary time for object extraction, the human visual capacity still has advantage over automated SGM techniques in such relatively sparse (~30% canopy cover) savannas with clumping and transparent Eucalypt vegetation.

5.5 Conclusions

The main aim of this study was to evaluate the potential for stereo imagery, from commercially available VHR satellites, to estimate canopy height variables in open canopy Australian tropical savannas. In this study, we only examined the SGM image matching algorithm, limited by sensor-to-target and sun-to-sensor geometry. We found that stereo dense matching using the SGM technique failed in all models of both GeoEye-1 (GE1) and WorldView-1 (WV1) stereo imagery. The results of this study show that the highest tree detection (completeness) rates (8 – 9 %) were achieved by using the NIR band of GE1 imagery, while the next best were PAN-based models. Both sets of stereo satellite imagery provided similar very low results (1 – 2 %). This study has been unable to demonstrate that WV1-GE1 cross-satellite (mixed) models could improve the quality of extracted DSM. Taken together, these results suggest that commercially available VHR satellites (0.5 m resolution) not well suited to estimating canopy height variables and AGB in open canopy Australian tropical savannas.

Despite the negative outcome, this study offers some insight into factors causing the poor SGM image matching. After comprehensive analysis of these factors, it was found that the problem is related to the clumping crown structure of the dominant overstorey Eucalypt trees, and their erectophile foliage, affecting the bidirectional reflectance distribution function, in combination with low sensor resolution and crown movement due to wind. These results provide key insights into possible future areas of research. We hope our findings and recommendations can improve the understanding of the complex factors affecting canopy detection performance by SfM image matching applied derived from VHR satellite stereo imagery.

Acknowledgments: This work was supported by Charles Darwin University and Darwin Centre for Bushfire Research, whose staff are gratefully thanked for their cooperation and research funding. The authors wish to acknowledge the financial support from the Bushfire and Natural Hazards Cooperative Research Centre, made available by the Commonwealth of Australia through the Cooperative Research Centre program. Jorg Hacker, AusCover facility of the Terrestrial Ecosystem Research Network (TERN) and Airborne Research Australia (ARA) are thanked for having collected and provided LiDAR data. For the field data collection, we thank Matt Northwood and Lindsay Hutley. The authors wish to express their thanks to Victor Adrov (Racurs) and PCI Geomatics for technical support. The authors would like to thank Dr Jeremy Russell-Smith (Darwin Centre for Bushfire Research) for providing valuable comments. We acknowledge the valuable long-term infrastructure at the Litchfield Savanna Super Site, which is part of the Australian Super Site Network (www.supersites.net.au), funded by TERN.

Chapter 6

Synthesis and general discussion

Page intentionally left blank

6.1 Summary

This final chapter provides an overview of the major results and outcomes from this research study, recapping the key findings, problematic and conclusions. In the next sections, the research findings, problems are summarized, synthesized and discussed in order of common and most important issues related to defined aims and objectives of this thesis. These sections include: summary of research outcomes (6.1); crown delineation and segmentation problematic (6.2); biomass uncertainty estimation (6.3); comparison the airborne LiDAR and optical sensors in terms of efficiency for biomass estimation (6.4); and consideration the spatial resolution of optical sensors for individual tree crown and canopy identification (6.5) in Australian mesic savanna. Research limitations and recommendations for future research are proposed in Sections 6.6 and 6.7.

The main aim of this dissertation was to assess the ability of VHR remote sensing data (LiDAR, airborne and VHR satellite imagery) to extract tree biophysical and vertical structural parameters to reliably estimate biomass and carbon stocks in Australian mesic savannas. Three research components were investigated to obtain the results. These components included the evaluation of Above-Ground Biomass (AGB) estimation uncertainty by using airborne LiDAR data; estimation of tree structural parameters from CHM derived by image-based matching technique from UAS data; and finally, an evaluation the potential for VHR stereo satellite imagery to estimate canopy height variables in Australian tropical savannas. The following series of research activities by using corresponding data sources were undertaken:

Reference data (refer Chapter3: Goldbergs et al. (2018a):

- Field data were collected from a 1 ha plot and every tree with a height > 2 m and DBH > 2 cm was measured. The DBH, tree height and tree species were recorded in the inventory;
- AGB of every reference tree was estimated using previously fitted species-specific allometric models with tree DBH as independent variable.

Airborne LiDAR data (refer Chapter3: Goldbergs et al. (2018a):

- The local maxima and watershed segmentation approaches were used to detect individual trees from LiDAR based canopy height models;
- Allometric relationships between field-derived individual tree AGB and corresponding LiDAR derived crown area and tree height were calculated;
- 300 rectangular 4 ha sample plots, 1200 1 ha plots, 4800 0.25 ha and 19,200 0.0625 ha (25 ×25 m) plots from throughout the entire LiDAR covered 12 km2 study area were established to determine the most appropriate metrics and scales for area-based estimations of AGB;
- estimations from individual tree LiDAR measurements are used as training/reference data for all established plots across entire study area to develop allometric equations related to LIDAR metrics;
- The errors of tree-level local maxima tree detection and individual tree AGB uncertainty were considered in the validation process, based on obtained tree detection rates and commission/omission errors ratio. The

obtained biases were introduced to every plot reference data across the study area.

UAS imagery (refer Chapter4: Goldbergs et al. (2018b):

- The light-weight mini-UAS quadcopter with an inexpensive consumer action GoPro camera was used for imagery acquisition across the study area (2.2 ha);
- The local maxima and watershed segmentation approaches were used to detect individual trees from the image derived CHMs, computed from extracted 3D dense point clouds;
- The influence of CHM spatial resolution on tree detection accuracy was analysed, and the results were validated against reference airborne LiDAR data.

VHR Stereo satellite imagery (refer Chapter5: (Goldbergs et al. 2019)):

- The potential of stereo imagery from commercially available VHR satellites was evaluated as an alternative for estimating canopy height variables by using semi-global dense matching (SGM) image-based technique;
- The completeness and vertical accuracy of extracted CHMs from GeoEye 1 and WorldView 2 satellite stereo pairs were assessed and compared against reference airborne LiDAR data.

The general results of the thesis are summarised and compared in Table **6.1.** In the next sections, the given research results are synthesized and discussed.

Table 6.1: A summary and comparison of the LiDAR and optical imagery, used in this research, for tree detection and height estimation.

	LiDAR	**UAS stereo photogrammetry [1]**	**VHR satellite stereo**
Tree detection and delineation methodology	Canopy Maxima and watershed segmentation	Canopy Maxima and watershed segmentation	CHM pixel-based comparison
Raw data spatial resolution	15 – 18 pts/m^2	GSD 0.04 m	GSD 0.5m
Optimal CHM resolution used	0.5 m	0.4 m	0.5 m
All tree detection rate	45-60 %	30-40 %	1-3 % (PAN band) 7-9 % (NIR band)
Dominant and co-dominant tree detection rate	75 %	70 %	-
Height estimation accuracy	N/A[2]	1.20m (SD)[3] -0.30 – 0.10 m (Mean bias))	-4 - -6 m (Mean bias)
AGB estimation accuracy	RMSE 3.40 Mg ha^{-1} SD 12% of plot AGB[4]	RMSE ~ 5 Mg ha^{-1} SD 17% of plot AGB	N/A[5]
DTM estimation Accuracy (LiDAR compared)	N/A	0.18 m (SD)	0.30 - 0.70 (SD)

[1] Gimbal flight only (refer to Chapter 4)
[2] Not available due to lack of accurate tree height field measurements (refer to Chapter 3)
[3] In comparison with LiDAR data
[4] Standard Deviation (SD) calculated based on 29.3 Mg ha^{-1} mean plot AGB across study area (12 km^2)
[5] AGB estimation was not possible due to severe underestimation of tree presence and canopy height (Chapter 5)

6.2 Crown delineation and segmentation

6.2.1 Individual tree detection and delineation

In this research, I applied canopy maxima and watershed tree crown detection and delineation approaches using LiDAR and stereo imagery data, focusing on the upper crown surface (CHM) and its spatial arrangement. The main reason for using the Canopy Maxima and watershed segmentation approaches is the speed and simplicity of processing. A disadvantage of these approaches is that they are limited by the CHM, which, due to interpolation, is unable to detect trees below the upper canopy. The issue is more pronounced in LiDAR data, where only the first returns per pulse are used for CHM creation, whereby a lot of information remains unclaimed. Canopy maxima and watershed segmentation performed far better for separating dominant and co-dominant trees than for small trees.

The most significant issue encountered by crown delineation algorithms is the problem of over-segmentation (commission errors), as these assume that each crown has only one dominant peak, versus under-segmentation (omission errors), where one or more abutting or overlapping tree canopies are identified as a single tree. This issue is of concern in Eucalypt stands with mixed canopy areas, where large canopies have a tendency to be subdivided, and small closely located canopies tend to be aggregated. This research confirmed that the problem could be partly minimized by using a CHM with a locally optimised spatial resolution after applying smoothing filters preserving local maxima (Gougeon and Leckie 2003). This research has demonstrated that detection of dominant and co-dominant trees remained stable by using 0.5 and 1 m (LiDAR), 0.4 - 1 m (UAS) CHM resolutions providing a high tree detection rate (>

70%). Thus, the above-described omission and commission errors could be minimized and partly compensated by concentrating on dominant and co-dominant tree detection.

The difficulty in delineating small trees is not only due to overstorey obscuration, but also due to tree size and shape, poor representativeness in point clouds and relatively coarse (0.4 -1 m) CHMs. The small trees could not be reliably identified with canopy maxima nor watershed segmentation approaches. Reference trees provided AGB calculations (Chapter 3), small trees (H < 10m) accounted for 15% of the total AGB in the study area. For this reason, I suggest that further research needs to be undertaken for dominant and co-dominant tree detection accuracy enhancement to minimize commission and omission errors.

6.2.2 The influence of Eucalypt structure on tree detection

In this study, I found that internal *Eucalypt* crown structure affected the efficiency of tree detection, for both active and optical sensors. The results of this study indicated that the problem is related to the clumping crown structure of the dominant Eucalypt overstorey, and their erectophile foliage, affecting the Bidirectional Reflectance Distribution Function (BRDF). These results match those observed in earlier studies (Culvenor 2000; Gerard and North 1997; Turner 2006). Eucalypt crowns mostly have multiple peaks; this is challenging for the canopy maxima approach which tries to detect the highest pixels within a localised search window based on the relationship between tree height and crown size (i.e., the higher the pixel the larger the search window). Eucalypt crowns are not uniform, having irregular crown edges, and highly variable size and shape, intra-crown gaps (Turner 2006), such that the canopy maxima approach leads to high commission errors. To improve the tree detection accuracy in this case, 3D approaches for single tree segmentation

(delineation) can be applied (Mongus and Žalik 2015). Ferraz et al. (2012) proposed a method applied directly to the 3D point clouds for the characterisation of multi-layered forests from LiDAR data using iterative clustering based on a mean shift algorithm. Further work is required to establish this in Australian savannas

Additionally, similar to Shendryk et al. (2016), I determined that the watershed segmentation approach did not improve tree detection efficiency nor accuracy, since crown shape and width estimates were poorly correlated with reference data. Again, it is highly probable that the key issue is due to highly fragmented crowns consisting of clumps of branches, interspersed with intra-crown gaps. In this case, the isolated branches are often classified as separate crown units, creating false local maxima and tree segments. As a result, applying smoothing filters to lower resolution CHMs is a compromise, that is, an 'efficiency threshold', which cannot fully eliminate the commission errors in tree detection by either the canopy maxima nor the watershed segmentation approaches. Therefore, I suggest that an area-based biomass estimation (ABA), incorporating errors from the ITC steps, could be one of the optimal solutions for estimation of AGB by LiDAR in Australian savannas.

6.3 Savanna biomass estimation

6.3.1 Hierarchical integration of individual tree and area-based approaches for biomass estimation by LiDAR

The ABA estimation method, with low-point-density data, is more efficient and cost-effective for both computation and laser data acquisitions. The calculation of point cloud height metrics is faster and technically easier compared to individual tree detection methods. The results of this study indicated that 1 ha and 4 ha sample plots provided more accurate estimates of AGB when using LiDAR cloud height metrics (Chapter 3). The area-based biomass estimation approach, which incorporated errors from the ITC steps, identified that the quadratic mean of canopy height (QMCH) was the best single independent variable for different plot sample sizes (e.g. for 4 ha plots RMSE = 3.4 Mg ha^{-1}, SD = 12% of plot AGB; and 1 ha plots RMSE = 4.0 Mg ha^{-1}, SD = 14% of plot AGB).

The larger plot size minimizes edge effects and co-registration errors, and maximizes the precision and accuracy of the output data. However, in practice, a large number of reference data are needed for a large sample plot, which can be costly and time consuming. The proposed two-phase framework reduces the need for extensive fieldwork by combining the advantages of both individual tree detection and ABA. The approach can be relatively easily performed by using the computationally fastest and simplest local maxima technique and manually digitised delineated tree crowns as the trained reference data. This study demonstrated that only a small area (1 ha in this case) of high-density data (>10 points m^{-2}) need to be used to estimate and update regression equations that relate laser data to field observations, and then generalise the prediction of AGB for the whole area using low-density LiDAR metrics.

6.3.2 Biomass uncertainty estimation based on hierarchical integration of individual tree and area-based approaches

The reasons for systematic errors of estimates based on the local maxima and watershed segmentation approaches are as following. Firstly, due to the vegetation structure (6.2.2) of tropical savannas, all trees cannot be detected by the ITC approach. The omission and commission errors, as described in Section 6.2.1, do not fully compensate for each other. Secondly, the number of stems is underestimated because obscured trees are less likely to be detected (Maltamo et al. 2004). Finally, this study has shown that the dominant and co-dominant trees are more readily correctly identified. As result, the total plot biomass is underestimated; or overestimated, in the case of a high proportion of commission errors.

Due to omission/commission errors, the reliability of tree detection was a major error source, biasing AGB estimation at the plot level when undertaking hierarchical integration of individual tree and area-based approaches. Thus, the errors of local maxima tree detection and individual tree AGB uncertainty must be considered in the process of upscaling AGB from tree to plot. This study provided a framework, describing how AGB uncertainty can be calculated and validated based on available reference field data or/and manually measured trees from the LiDAR point cloud. Total plot AGB should be corrected based on an uncertainty analysis of the local maxima tree detection approach. In this study, the overall systematic error in AGB estimation using the ITC local maxima approach was of the order of 10% underestimation compared to the reference data.

6.3.3 Biomass estimation from image-based derived 3D point clouds

In these analyses, I applied canopy maxima and watershed segmentation approaches to UAS image-based canopy height models in combination with LiDAR reference data to fit non-linear models for biomass estimation. The UAS data were compared with LiDAR data, as the spatial distribution of trees and the uncertainty in the ITC approach couldn't be assessed by the UAS data itself. Besides the omission/commission errors related to the efficiency of the individual tree detection approaches, the accuracy and completeness of CHMs generated from image-based 3D dense point clouds are also affected by: (1) the accuracy of the bundle-block adjustment (image geo-referencing); (2) sun-to-image and image-to-object geometry; (3) and the effectiveness of the chosen SfM matching algorithm. Thus, under similar data acquisition conditions (e.g. weather and the spatial resolution of the data), LiDAR data provide higher tree detection rates and more accurate estimates of tree biomass then corresponding image-based data. Despite this, this research concluded that UAS imagery, with gimbal, can be used as a standalone sensing technology for AGB estimation of the dominant and co-dominant trees in Australian tropical savannas, with a plot accuracy of 15% (without counting understorey trees). Possible area of future research would be investigation of UAS imagery acquisition using multiple viewing angles, in addition to nadir. Presumably, it will able to provide direct assess the spatial distribution of trees and improve ITC accuracy from image-based 3D dense point clouds.

This research also concluded that camera calibration is critical to tree height estimation accuracy. I anticipate that a camera with a larger sensor and detector pixel size could improve matching performance during individual tree detection and provide

better accuracy in tree height estimation due to its more stable internal sensor geometry and better radiometry. This is an important issue for future research.

6.4 LiDAR vs optical sensors

6.4.1 Data acquisition

In comparison to LiDAR, optical sensors are strongly influenced by solar illumination, sensor-to-target and sun-to-sensor geometry (i.e. BRDF). As a result, the shadows of the canopy can greatly limit matching efficiency. In contrast, LiDAR systems are not influenced by the presence of shadows or daylight, and therefore data can be acquired day or night. In Australian tropical savannas, it is important to bear in mind that wet season cloud, and dry season smoke haze, restrict the use of satellite-based sensors and make seasonal monitoring problematic (Collins et al. 2009).

Airborne sensors have wider swaths, a more effective field of view (FOV), and are more flexible in terms of image overlap in both the along-track and cross-track strip directions. Thus, for the same number of flying hours with LiDAR, large format airborne imagery can cover a much larger area. As an integrated part of data acquisition, the UAS requires operator presence at a field site, which then limits the UAS remote operating range and adds costs to field and travel activities.

6.4.2 Data geo-referencing

Thanks to the integration of accurate Global Positioning Systems (GPS) and Inertial Navigation Systems (INS), LiDAR provides direct 3D raw point (X,Y,Z) data with 5–20 cm vertical accuracy, 2-4 times better than planimetric, and an error of ca.

0.5–2 cm per 100 m of flying height for typical attitude errors and a scan FOV angle of 30 degrees (Baltsavias 1999b). Despite the fact that modern optical sensors are also equipped with GPS/IMU, allowing direct image geo-referencing, this research has shown that an integrated image orientation with in-field high-accuracy and signalized GCPs (with additional costs) is still required to achieve the corresponding vertical and planimetric accuracy with the LiDAR data.

Accurate image geo-referencing (aero-triangulation), used for tree/canopy attribute estimation, is based on GCP measurements, and thus is an additional processing step for any optical sensor. Since tree heights are based on above ground elevation, it is important that the extracted digital surface (DSM) and terrain (DTM) models used for CHM creation are appropriately accurate. This study has shown that errors incorporated into an image geo-referencing (orientation) process, for example due to cheap and inaccurate GPS/IMU or incorrectly measured GCPs, will be propagated into the DSM, DTM and finally into the CHM estimation.

6.4.3 Point cloud comparison

Overall, there are many more factors that can influence the results of image-derived 3D point clouds, thus making the prediction of the accuracy and error propagation much more complicated. Factors, like poor geo-referencing, low image texture, low radiometry differences between images, shadows, and the BRDF effect, do not affect LiDAR based 3D point clouds.

Previous studies have reported that LiDAR-based models (~10 pts m^{-2}) provide more accurate attribute estimations (such as maximum and mean tree height, volume and basal area) in coniferous forest than image-based models (Bohlin et al. 2012;

Järnstedt et al. 2012). The ability of LiDAR to penetrate the canopy could be essential in areas with rough terrain, or in riparian vegetation, which has much less transparency due to higher canopy cover. Additionally, small morphological features, such as cracks, lateral ridges, pressure ridges and step wise morphology can be recognizable in LiDAR models, providing the interpreter unprecedented detail.

However, with low LiDAR point density (< 1 pts m^{-2}), the advantage of photogrammetry is in break lines and mass point capture, whereas the sampling of LiDAR data is predetermined and measured points may not lie on break lines. The use of manual stereo restitution and verification is also a strength of photogrammetry. The potential advantage of optical sensors (mostly satellite) is related to the use of multispectral information for biomass estimation vegetation indices; it also enables visual interpretation of species, segmentation and other vegetation inventory attributes. A further study with more focus on spectral data use from imagery is therefore suggested.

6.4.4 Automation and data processing time

Due to additional processing steps, such as precise integrated image geo-referencing, 3D point cloud calculation and DTM filtering, the time required to acquire and process image data into a useable point cloud is much higher than for LiDAR. Thanks to the necessity for direct and precise 3D point cloud retrieval, LiDAR systems have a higher degree of automation and faster data delivery. Professional and freeware programs (*Lastools*, *Fusion*) provide full and integrated sets of tools for LiDAR data handling and processing. All LiDAR data post-processing, like point cloud classification and CHM creation, can be fully automated, without manual interaction,

in open and relatively flat areas like in the Australian tropical savannas. In most cases, these activities don't need advanced operator knowledge nor experience.

This research has shown that photogrammetric processes still need many manual and semi-automated interactions related to sensor orientation, optimal setting testing for image matching, DSM and DTM filtering, and careful accuracy assessment after each processing step. There are currently no freeware programs available for complete and comprehensive photogrammetric data processing and image handling. The photogrammetric workflow requires highly skilled photogrammetric ability and experience.

6.4.5 Cost-effectiveness

The evaluation of cost-effectiveness of remote sensing methods appears to be limited by the large number of variables to consider, including the project goals, the size of the study area, the final product accuracy, the spatial resolution of the RS data, the cost of data acquisition, software and hardware availability, data processing framework, consideration of workflow time, technical expertise of staff, etc. The comparison between satellite and airborne methods, such as UAS vs WorldView, is sometimes irrelevant because they are used for different tasks, related to different resolutions and cover areas.

Four main sources of expense are encountered during remote sensing: the cost of data acquisition; set-up costs (e.g. hardware and software); field survey time; and the time required for image processing (analysis) (Mumby et al. 1999). A general list is provided in **Table 6.2**. The data processing to data acquisition cost ratio can be raised significantly if accurate fine-scale mapping is required. If there are no set-up

costs, the total costs fall dramatically. Field survey (reference data collection), which is a necessary aspect particularly for aerial photography, constitutes a significant proportion of remote sensing cost, especially in remote vast Australian tropical savannas, including, beside field measurements, the staff travel time/allowance, RS equipment, vehicle lease, maintenance and fuel costs.

LiDAR data acquisition remains expensive in comparison with large format airborne photography (2-3 times) and satellite stereo data (at least 10 times). At the same time, factors like automation, relative simplicity in data handling and post-processing, accuracy of the final product, and processing time, increase the cost-effectiveness of using LiDAR substantially. Thus, LiDAR has become increasingly competitive compared to aerial photography and even VHR satellites. I have observed that project and production managers do not always prefer the least expensive remote sensing technique. In practice, the main requirements are related to equipment simplicity in handling and maintenance, and reliability and efficiency of data processing to achieve an acceptable degree of accuracy. The selection of technology for future savanna research and applications will depend on the objectives, the characteristics of the study and available budget.

Table 6.2: Cost-effectiveness of each remote sensing mapping approach, used in this study.

	LiDAR	**Airborne stereo photogrammetry**	**VHR stereo satellite**
Raw data acquisition ($/1km^2)	>1000	200 to 2000 (UAS case) UAS lease cost;	> 80
GCP field measurements	Optional	Mandatory (~$1000) per scene; plus, staff travel costs, equipment, vehicle lease and fuel cost	Mandatory (~$1000) per scene; plus, staff travel costs, equipment, vehicle lease and fuel cost
Software ($)	Freeware	$5,000 (Agisoft Photoscan, Photomod UAS)	$10,000 (Photomod, PCI Geomatica)
Post processing time and costs	Almost fully automatic; less processing steps and time	Semi-automatic processing; Manifold processing time than for LiDAR	Semi-automatic processing; Greater processing time; ~ $ 40 km^{-2} orthophoto and DTM creation
Skill required	Available scripts, basic expertise	Theoretical and practical photogrammetry expertise required;	Theoretical and practical photogrammetry expertise required;

6.5 Consideration of spatial resolution

6.5.1 LiDAR point density

The most important parameter describing the spatial resolution of a LiDAR point cloud is the point or pulse density. A pulse (pls) is a laser signal sent out from the lidar system towards the ground and a point (pts), referred to as a return or echo, is the signal reflected from the target back to the lidar system. Similar to the resolution of optical sensors, the point density of LiDAR data defines the number of measurements (samples) per area unit sampled, given as pls m^{-2} or pts m^{-2}.

The most important limitation of the monitoring and mapping of large forest areas by LiDAR is that it is not economically practicable to collect data with more than several laser pulses per square metre (Næsset and Gobakken 2008). Collecting higher point density data is costly, and processing these data can be problematic. Conversely, collecting LiDAR data, with lower point density over larger areas, encourages large area mapping but at the potential risk of losing accuracy. Previous studies have reported that accuracy remains relatively high until low pulse densities are used (e.g. 1 – 2 pulses m^{-2}) (Magnussen et al. 2013; Turner 2006). Coverage and lidar pulse density affect LiDAR acquisition cost (Baltsavias 1999a). As a result of the compromise between cost, coverage and density, large area data users must either order low pulse density data covering a large area or a higher pulse density data that concentrates on a subsection (Jakubowski et al. 2013).

If airborne LiDAR were to become standard for monitoring large areas of northern Australia, it is likely that only low densities of 1–3 points m^{-2} could be achieved,

allowing the establishment of the empirical relationship between plot-level derived LiDAR data metrics and the target plot-level inventory variable (e.g. AGB) by regression techniques. As this research was based on an average LiDAR point density of 15-18 points m^{-2}, the relevant question to be addressed is whether the low-point density (1–3 points m^{-2}), medium-point density (3 – 6 points m^2) and spaceborne LiDAR data can provide sufficient accuracy to reliably estimate the Eucalypt tree/canopy structure metrics (e.g. tree height, crown shape and canopy height metrics) and therefore to accurately predict the AGB Thus, the point density issue is an important issue for future research. This was not undertaken here given that simulation experiments based on LiDAR thinning can't adequately model the corresponding data acquisition parameters, such as flight altitude, LiDAR pulse energy, the footprint and the pattern.

6.5.2 Spatial resolution of imagery

This research has shown that determining the optimum image spatial resolution is critical for individual tree crown and canopy identification. Spatial resolution defines the level of spatial detail depicted in an image. It defines the smallest feature that can be resolved by the instrument and, in this sense, is directly related to ground sample distance (GSD). This research has demonstrated that tree detection efficiency is related to different spatial scales of image data, especially in comparison between UAS and stereo satellite imagery. In this comparison, the data differed in the ratio between the constant size of objects in a scene and the different spatial resolutions of the images (GSD 4 cm for UAS vs. 50 cm for satellite imagery). At a high spatial resolution (e.g. 4 cm), when the GSD is significantly smaller than the size of the image objects, many

neighbouring pixels, representing objects, are more likely to be matched, resulting in the extraction of an object's surface, for example the tree crown (**Fig 6.1**).

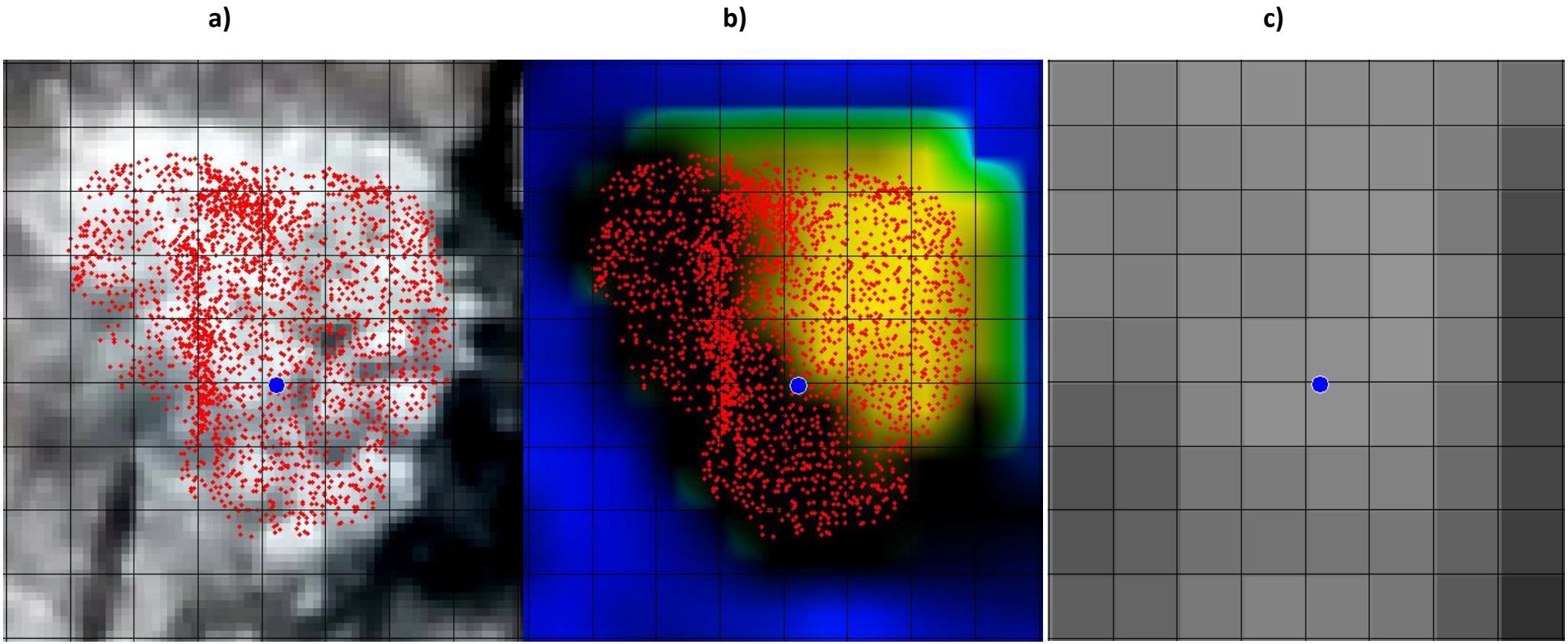

Figure 6.1: Spatial resolution: **a)** Successful extract of a single Eucalypt tree (height 13m, diameter=3m) from UAS imagery (GSD 4cm) represented by the 3D point cloud (red dots) with average point density 150 pts m^{-2}; **b)** corresponding CHM grid (40cm) used for canopy maxima and watershed segmentation tree detection algorithms; and **c)** corresponding WV1 image (50cm) with failed image matching failure. Black grid lines are spaced 50cm and the blue dot is the extracted local maxima from the UAS imagery.

As the GSD increases, the number of pixels comprising the object decreases, with the likelihood that neighbouring pixel similarity also decreases. In this case, the number of potential pixel matches decreases, reducing the capacity to estimate (fix) the object surface. Further increases in GSD result in the pixel value being influenced by multiple objects (foliage, ground etc), leading to an averaging of the spectral canopy response (brightness and contrast). Due to the clumped crown structure of Eucalypts, and their erectophile foliage, affecting the BRDF, relatively low satellite sensor resolution (GSD 50cm) leads to unsatisfactory image matching results.

This research set out to determine the number of matched points per tree or tree clump required for successful detection, using image matching techniques. The area parameter of all detected tree/canopy (UAS and stereo satellite research) segments was used to fulfil this task. A simple descriptive statistical analysis of the detected tree crown/canopy area (m^2) was used to evaluate the impact of sensor spatial resolution by comparison with reference tree area values (n = 2015, Chapter 3) (**Table 6.3**)

Table 6.3: Descriptive statistics (quantiles) of the areas of detected tree crowns/canopies based on watershed segmentation compared to the reference data. All values are given in m^2. UAS - 4cm GSD drone imagery (Chapter 4); GE1 NIR – GeoEye1 50cm GSD NIR band imagery (Chapter 5).

Quantiles	LiDAR reference data		UAS	GE1 NIR
%	All trees	Trees>10m	All trees	All trees
25	2.4	13.2	1.3	14.3
50	3.6	25.3	3.4	31.7
75	9.9	49.8	11.4	77.0
90	38.2	74.0	33.7	168.2

It is apparent from **Table 6.3** that UAS imagery, achieved a high individual tree detection rate and provided similar results to the LiDAR data, with only slight underestimation of crown areas, due to the difficulty of detecting trees with small crowns (< $3m^2$) and inaccurate crown edge detection. The most striking result to emerge from the satellite imagery, was the inability to detect trees with crown areas less than 10 m^2, accounting for about 75% of all live trees in the study area. It seems that the satellite imagery, at the given spatial resolution, was only capable of detecting dominant and co-dominant trees (H > 10m, crown > 15 m^2). Very high values for the GE1 imagery (75% and 90% quantiles) compared to the reference data, indicate the groups of merged crowns/canopy delineation instead of single/individual tree detection.

In this research, the stereo satellite imagery was unable to detect ~ 90% of trees (H > 10 m). To determine the number of matched points per tree, or tree clump, required for successful detection, it was assumed that 10% of detected trees represent the canopies with the greatest area, where factors such as clump structure, leaf orientation, wind etc, are neglected, with dependence only on spatial resolution. The 90 % percentile of the crown size of the reference trees (H>10m) is ~ $75m^2$, **Table 6.3**. Thus, 75 m^2 was defined as the threshold of successful tree detection. In the case of the of GE1 and WV1 imagery, 75 m^2 corresponds to 300 pixels (0.5m x 0.5m). This relationship between crown area and image resolution has ascertained the minimum number (300) of matched pixels required for successful tree crown detection, and extrapolated other crown areas (**Figure 6.2**).

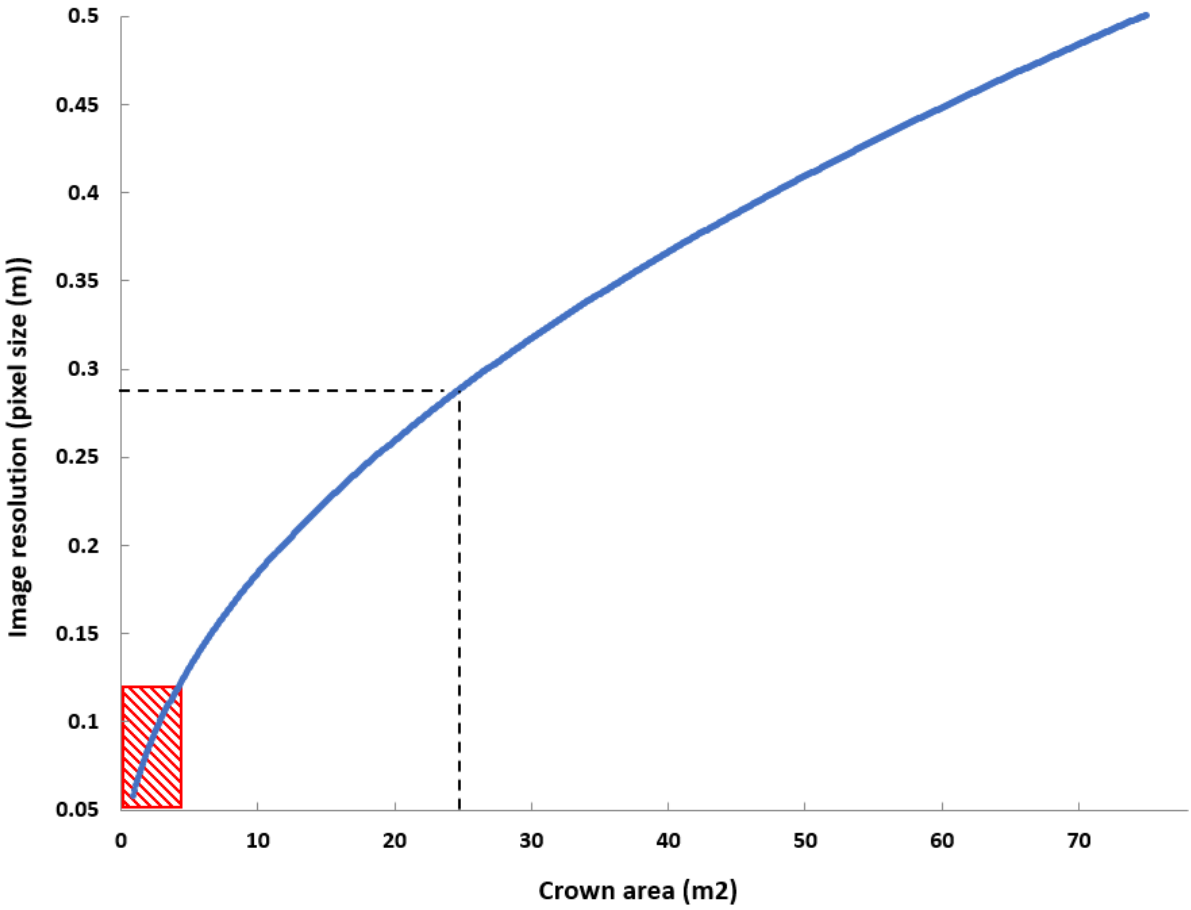

Figure 6.2: Relationship between the crown area and image spatial resolution based on 300 (minimum) matched pixels for successful tree (H > 10m) detection/delineation by using stereo satellite stereo imagery in Australian savanna. The red box represents 50% (Median) of all trees across the 4 ha validation plots (n = 2015, Chapter 3). The dashed black line represents 50% (Median) of trees (H > 10m) across 4 ha validation plots (n = 485).

These findings suggest that the pixel size of the optical imagery should be < 12 cm to detect/delineate at least 50% of all tree crowns (3.9 m^2) and < 30cm to detect 50% of dominant trees (H>10m, 25 m^2) by image matching techniques. It is important to bear in mind the possible bias in these responses after introducing the factors which have a direct impact on tree detection by image matching (**Table 7** from chapter 5).

The most important limitation lies in the fact that given relationship between crown area and image resolution based on specific tree detection rate using stereo satellite stereo imagery in Australian savanna. These findings suggest that another possible area of future research would be to investigate optical stereo imagery in a resolution range between 0.15 and 0.30 m (large format sensor airborne imaging) for estimating canopy structural parameters in open canopy Australian tropical savannas (**Figure 6.3**).

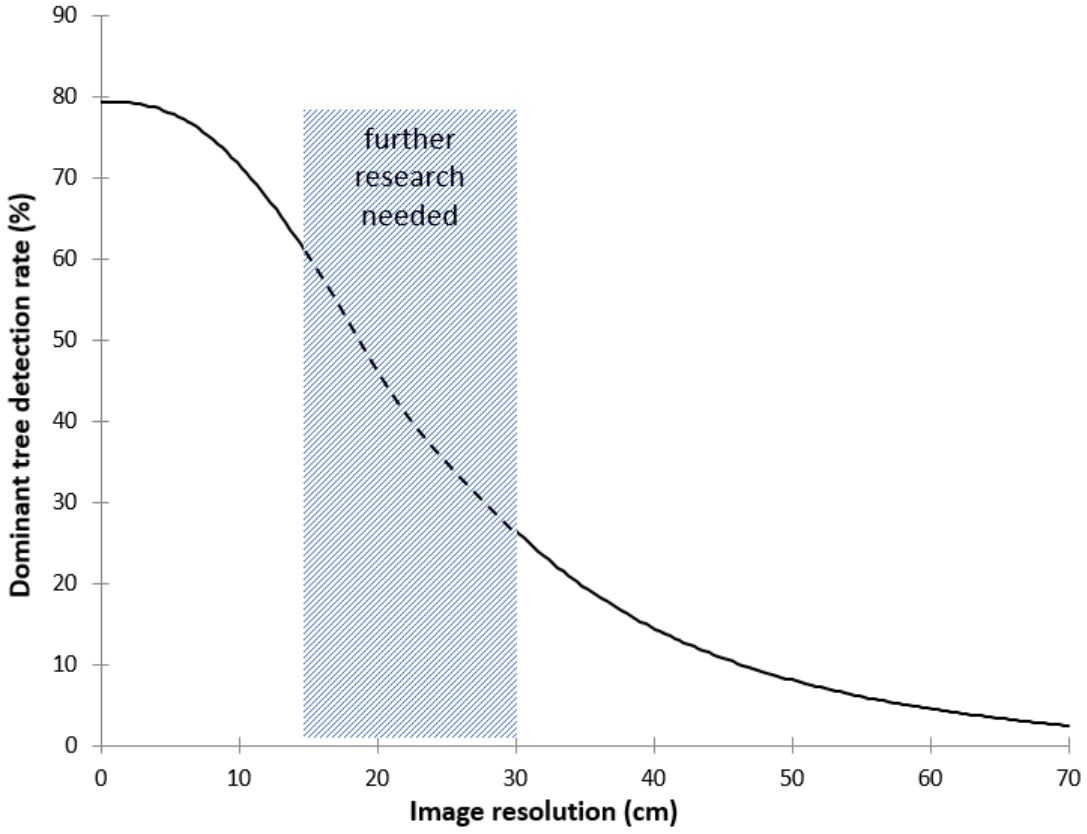

Figure 6.3: Dominant tree detection rate dependence on stereo image resolution. (Based on interpolation of UAS and satellite stereo image matching data in Australian tropical savannas).

It is important to bear in mind that the spatial arrangement and physical properties of the tree/canopy, sensor-to-target and sun-to-sensor geometry, sensor pixel size, and contrast of an object of interest compared with its surroundings, will

influence the electromagnetic radiation reflected from the scene and recorded by the sensor. My investigation of NIR band efficiency in terms of tree/canopy detection showed that the higher the contrast/brightness between crown and surrounding pixels, the less strict we have to be with the image resolution. If the contrast is low, the resampling will totally diminish point or line objects, so that they cannot be distinguished from the surroundings. For example, in the case of the GoPRO camera (Chapter 5), it can be expected that another camera with the same GSD resolution, but higher detector size like the Sony NEX series, can improve tree detection rates and provide better accuracy in tree height estimation due to its better radiometry. Further research is suggested focusing on AGB estimation accuracy by using UAS cameras with a bigger sensor detector (pixel) size. Also, the selection of the right pixel size will remain an issue to the application and project objectives.

6.6 Research limitations

A key limitation of the monitoring and mapping of vegetation in large remote areas with LiDAR is whether high-density data are necessary to obtain accurate results at the plot-scale. In the hierarchical integration of individual tree and area-based approaches for improved savanna biomass estimation, high-density LiDAR data (> 10 pulses m−2) are necessary to generalise the calibrated prediction of AGB for the whole area using low density LiDAR metrics. The quality of the AGB estimates depends on the size of the reference data used to construct and/or validate the allometric model. The main limitation of this study relates to the observation that AGB uncertainties can be applied only to local areas with similar Eucalypt dominated vegetation and LiDAR acquisition parameters.

There are many limitations with the single-tree detection methods used in this study. Depending on the ITC approach, this study demonstrated similar low detection rates of small trees (20-40%) using either LiDAR and UAS imagery data. The AGB estimation results in an overestimation/underestimation due to missing and false detected trees. Edge-detection using the watershed segmentation approach is also problematic due to Eucalypt crowns with numerous isolated branches extending beyond the core crown area. The only way to improve the accuracy of the AGB predictions is to improve the tree detection rates by using different methodological (e.g. parametric and non-parametric semi-ITC) approaches.

The main limitation of the UAS approach was the very small sensor (1.55 μm detector pixel size) of the GoPro camera, in combination with a small lens aperture, giving a low sensitivity to light (low signal to noise ratio and low dynamic range). Hence, this study does not recommend using the GoPro-derived imagery without basic radiometric pre-processing (contrast, sharpness, etc.). Another limitation is related to the fact that the self-calibrating bundle adjustment of non-metric cameras may not be able to derive lens radial distortion accurately enough, so that a systematic vertical error may remain even with sufficient numbers of GCPs, which leads to under/overestimation of tree heights and corresponding variation in plot AGB estimation.

In this research, the two sets of stereo satellite imagery had a very similar sensor-to-target and sun-to-sensor geometry, as they were acquired under similar seasonal and climatic conditions. This fact did not allow for a comprehensive analysis of the effect of image geometry differences (e.g. convergence, bisector and sun angles) and their influence on the quality of the extracted DSMs.

6.7 Practical implications and recommendations

This research has several practical applications to be applied in Australian mesic savannas. Firstly, it has established a two-phase AGB estimation procedure: (1) using estimations from individual tree LiDAR measurements as training/reference data; and then applying these data to (2) an area-based LiDAR estimation of AGB to create the allometric equations related to LIDAR metrics. The two-phase procedure can be easily applied in remote areas, where road networks are non-existent or sparse, and is a cost- and labour-effective method as it requires less measurement in the field to calibrate LiDAR estimates than previous remote sensing techniques. This method can be most effective in identifying individual dominant and co-dominant trees from CHM with 0.5–1 m resolution. AGB and the uncertainty of estimation can be quantified from LiDAR data by integrating both individual tree detection and area-based approaches. This provides a framework for regional savanna inventories, monitoring and mapping. The focus on dominant and co-dominant trees allows for minimizing uncertainty, associated with single-tree detection approaches (commission and omission errors) by providing sufficient (> 70%) tree detection rates.

The airborne LiDAR and image-based derived estimations accuracy of the tree parameters depend on the following two limitations. Firstly, the overlapping between a dominant target tree and its neighbours may have influenced the estimation of tree parameters (commission/omission errors). Secondly, the crown penetration (UAS) and the point density (airborne LiDAR) could be insufficient to describe individual tree crown shapes and tree components like stems and branches. Such error-causing problems possibly can be corrected, and more accurate results in the extraction of tree

parameters can be obtained using combination of LiDAR, UAS and Terrestrial Laser Scanner (TLS) data. Further work is required to establish this.

Whilst the initial cost of LiDAR data acquisition may appear high in comparison with VHR satellite and airborne large format imagery, factors like automation, relative simplicity in data handling and post-processing, accuracy of the final product, and processing speed increase the cost-effectiveness of using LiDAR substantially.

Recent trends in spaceborne LiDAR (Ice Cloud and Land Elevation Satellite (ICESat), Global Ecosystem Dynamics Investigation (GEDI)), and the combination of LiDAR with full colour imagery could provide an alternative methodology for better mapping of pan-tropical vegetation (Hajj et al. 2017). In an ideal scenario, LiDAR can be utilised within a multi-scale hierarchical framework, including other high (satellite based active (SAR and LiDAR) and passive (Sentinel-2) sensors) and medium resolution RS tools (e.g. Landsat), forming part of any regional savanna sampling or monitoring strategy. The key use of LiDAR would then be for data collection to establish local regression models, biomass mapping and dynamic change detection. Since active RS provides a straight forward procedure to estimate canopy vertical structure metrics, the errors and uncertainties associated with structural effects can be reduced in the combined approaches. The use of LiDAR within a multi-sensor framework provides an efficient method for understanding how scale impacts local to regional estimation of vegetation attributes.

A comprehensive change detection (with 2-3 years gap) pilot study would help to gain a better understanding of biomass dynamics and its changes due to factors such as fires, weed expansion (e.g. Gamba grass, *Andropogon gayanus*) and climate change.

Additionally, such a pilot study should focus on an assessment of low (1–3 points m^{-2}) and medium-point density (3 – 6 points m^{-2}) LiDAR data, and integration with VHR mono-satellites used for object-based tree crown delineation. Also, topography should be an additional parameter of interest due to challenges of data processing and the interactions with vegetation fuel characteristics and fire behaviour.

Although LiDAR data provide higher tree detection rates and more accurate estimates of tree heights, image matching was found to be an adequate low-cost alternative for the detection of dominant and co-dominant tree stands in local areas of tropical savannas. The main advantage of small and low-cost UAS is their ability to collect imagery with high spatial and temporal resolution. A stable and correct alignment of the images can be achieved by camera platform stabilisation during data acquisition.

The findings of this study suggest that the implementation of low-cost UAS imagery into the existing field data collection framework can enhance its performance and flexibility, and improve the final product output. It is recommended to use low-cost UAS image acquisition during each field campaign at least as a visual record. Further experimental investigations are needed to estimate the planimetric and vertical accuracy of image-based CHMs by using direct geo-referencing (no GCPs).

Despite the inadequacy of the stereo satellite imagery for canopy detection in Australian savannas, this research has offered some insights into the causes for the poor SGM image matching: the clumping crown structure of the dominant Eucalypt overstorey; the effect of erectophile foliage on BRDF; low sensor resolution and crown movement due to wind. The comprehensive analysis of the effect of the image geometry differences (e.g. convergence, bisector and sun angles) and their influence

on the quality of the extracted DSMs and along-track stereo satellite constellation, where the path direction and/or image-to-target is perpendicular to the sun-to-target direction (principal plane), are important issues for future research. As well, further research should be undertaken to investigate the dependency on image resolution for image matching efficiency in tropical savannas.

6.8 Contribution to Knowledge

This research has highlighted the efficiency of small footprint LiDAR and VHR optical remote sensing data (UAS and VHR stereo satellite imagery) to extract tree biophysical and vertical structural parameters for the purposes of accurately estimating biomass (RMSE <15 % of plot Mean AGB), and hence carbon stocks, in Australian mesic savannas.

The main contributions of this thesis to the body of scientific knowledge are:

- Understanding how uncertainty of biomass estimation varies with spatial scale by integrating both individual tree detection and area-based approaches.
- Area-based (ABA) biomass estimation, incorporating errors from the individual tree detection step identified that the quadratic mean of canopy height (QMCH) is the best single independent variable for AGB estimation.
- Large 1-4 ha ABA plot size choice is more suitable for accurate area biomass estimations across north Australia with airborne LiDAR.
- The detection of dominant and co-dominant trees by LiDAR and UAS remained stable by using 0.5 and 1 m CHM resolutions, providing a high tree detection rate (> 70%) for tropical *Eucalyptus*-dominated savanna, based on the canopy maxima and watershed segmentation routines.
- Light-weight and low-cost UAS imagery (<$2,000) can be used for the AGB estimation of the dominant and co-dominant trees in Australian tropical savannas, with a plot accuracy of 15% (without counting both small and understorey trees).

- Commercially available stereo VHR satellites (0.5 m resolution) are not well suited to estimate canopy height variables and AGB in open canopy Australian tropical savannas, due to severely underestimating tree presence and canopy height. The highest tree detection (completeness) rates (8 – 9 %) were achieved by using the NIR band of stereo satellite imagery.
- Despite the negative outcome from the use of stereo satellite imagery, this study offered insight into complex factors affecting canopy detection performance by SfM image matching related to the clumping crown structure of the dominant overstorey Eucalypt trees, and their erectophile foliage.

References

Agisoft (2011). PhotoScan community forum topic: Algorithms used in Photoscan. Available: http://www.agisoft.com/forum/index.php?topic=89.msg13780;topicseen#msg13780

Agüera-Vega, F., Carvajal-Ramírez, F., & Martínez-Carricondo, P. (2017). Assessment of photogrammetric mapping accuracy based on variation ground control points number using unmanned aerial vehicle. *Measurement, 98*, 221-227

Aguilar, M., Bianconi, F., Aguilar, F., & Fernández, I. (2014a). Object-Based Greenhouse Classification from GeoEye-1 and WorldView-2 Stereo Imagery. *Remote Sensing, 6*(5), 3554-3582

Aguilar, M.A., del Mar Saldana, M., & Aguilar, F.J. (2014b). Generation and quality assessment of stereo-extracted DSM from GeoEye-1 and WorldView-2 imagery. *IEEE Transactions on Geoscience and Remote Sensing*, *52*(2), 1259-1271.

Aguilar, M.A., del Mar Saldaña, M., Aguilar, F.J., & Lorca, A.G. (2014c). Comparing geometric and radiometric information from GeoEye-1 and WorldView-2 multispectral imagery. *European Journal of Remote Sensing, 47*(1), 717-738

Ahmadabadian, A.H., Robson, S., Boehm, J., Shortis, M., Wenzel, K., & Fritsch, D. (2013). A comparison of dense matching algorithms for scaled surface reconstruction using stereo camera rigs. *ISPRS Journal of Photogrammetry and Remote Sensing, 78*, 157-167

Asner, G.P., Clark, J.K., Mascaro, J., Vaudry, R., Chadwick, K.D., Vieilledent, G., Rasamoelina, M., Balaji, A., Kennedy-Bowdoin, T., Maatoug, L., Colgan, M.S., & Knapp, D.E. (2012a). Human and environmental controls over aboveground carbon storage in Madagascar. *Carbon Balance and Management, 7*(1), 1-13

Asner, G.P., Flint Hughes, R., Varga, T.A., Knapp, D.E., & Kennedy-Bowdoin, T. (2008). Environmental and Biotic Controls over Aboveground Biomass Throughout a Tropical Rain Forest. *Ecosystems, 12*(2), 261-278

Asner, G.P., & Mascaro, J. (2014). Mapping tropical forest carbon: Calibrating plot estimates to a simple LiDAR metric. *Remote Sensing of Environment, 140*, 614-624

Asner, G.P., Mascaro, J., Anderson, C., Knapp, D.E., Martin, R.E., Kennedy-Bowdoin, T., van Breugel, M., Davies, S., Hall, J.S., Muller-Landau, H.C., Potvin, C., Sousa, W., Wright, J., & Bermingham, E. (2013). High-fidelity national carbon mapping for resource management and REDD+. *Carbon Balance Manag, 8*(1), 7

Asner, G.P., Mascaro, J., Muller-Landau, H.C., Vieilledent, G., Vaudry, R., Rasamoelina, M., Hall, J.S., & van Breugel, M. (2012b). A universal airborne LiDAR approach for tropical forest carbon mapping. *Oecologia, 168*(4), 1147-1160

Australia., C.o. (2018). Carbon Credits (Carbon Farming Initiative—Emissions Abatement through Savanna Fire Management—Revocation) Instrument 2018. Australian Government. https://www.legislation.gov.au/Details/F2018L00558/Html/Text

Baltsavias, E., Gruen, A., Eisenbeiss, H., Zhang, L., & Waser, L.T. (2008). High-quality image matching and automated generation of 3D tree models. *International Journal of Remote Sensing, 29*(5), 1243-1259

Baltsavias, E.P. (1999a). Airborne laser scanning: basic relations and formulas. *ISPRS Journal of Photogrammetry and Remote Sensing, 54*(2-3), 199-214

Baltsavias, E.P. (1999b). A comparison between photogrammetry and laser scanning. *ISPRS Journal of Photogrammetry and Remote Sensing, 54*(2-3), 83-94

Barbati, A., Chirici, G., Corona, P., Montaghi, A., & Travaglini, D. (2009). Area-based assessment of forest standing volume by field measurements and airborne laser scanner data. *International Journal of Remote Sensing, 30*(19), 5177-5194

Becker, G., Coleman, E., Hetsch, S., Kazemi, Y., & Prins, K. (2006). Mobilizing Wood Resources: Can Europe's Forests Satisfy the Increasing Demand for Raw Material and Energy under Sustainable Forest Management? *Geneva Timber and Forest Discussion Papers, 48*

Beringer, J., Hacker, J., Hutley, L.B., Leuning, R., Arndt, S.K., Amiri, R., Bannehr, L., Cernusak, L.A., Grover, S., Hensley, C., Hocking, D., Isaac, P., Jamali, H., Kanniah, K., Livesley, S., Neininger, B., Paw U, K.T., Sea, W., Straten, D., Tapper, N., Weinmann, R., Wood, S., & Zegelin, S. (2011). SPECIAL—Savanna Patterns of Energy and Carbon Integrated across the Landscape. *Bulletin of the American Meteorological Society, 92*(11), 1467-1485

Beringer, J., Hutley, L.B., Abramson, D., Arndt, S.K., Briggs, P., Bristow, M., Canadell, J.G., Cernusak, L.A., Eamus, D., Edwards, A.C., Evans, B.J., Fest, B., Goergen, K., Grover, S.P., Hacker, J., Haverd, V., Kanniah, K., Livesley, S.J., Lynch, A., Maier, S., Moore, C., Raupach, M., Russell-Smith, J., Scheiter, S., Tapper, N.J., & Uotila, P. (2015). Fire in Australian savannas: from leaf to landscape. *Global change biology, 21*(1), 62-81.

Bohlin, J., Wallerman, J., & Fransson, J.E.S. (2012). Forest variable estimation using photogrammetric matching of digital aerial images in combination with a high-resolution DEM. *Scandinavian Journal of Forest Research, 27*(7), 692-699

Bosak, K. (2011). Secrets of UAV photomapping. *Pteryx*, Poland

Bradshaw, C.J.A., Bowman, D.M.J.S., Bond, N.R., Murphy, B.P., Moore, A.D., Fordham, D.A., Thackway, R., Lawes, M.J., McCallum, H., Gregory, S.D., Dalal, R.C., Boer, M.M., Lynch, A.J.J., Bradstock, R.A., Brook, B.W., Henry, B.K., Hunt, L.P., Fisher, D.O., Hunter, D., Johnson, C.N., Keith, D.A., Lefroy, E.C., Penman, T.D., Meyer, W.S., Thomson, J.R., Thornton, C.M., VanDerWal, J., Williams, R.J., Keniger, L., & Specht, A. (2013). Brave new green world – Consequences of a carbon economy for the conservation of Australian biodiversity. *Biological Conservation, 161*, 71-90

Breidenbach, J., Næsset, E., Lien, V., Gobakken, T., & Solberg, S. (2010). Prediction of species specific forest inventory attributes using a nonparametric semi-individual tree crown approach based on fused airborne laser scanning and multispectral data. *Remote Sensing of Environment, 114*(4), 911-924

Chave, J., Andalo, C., Brown, S., Cairns, M., Chambers, J., Eamus, D., Fölster, H., Fromard, F., Higuchi, N., & Kira, T. (2005). Tree allometry and improved estimation of carbon stocks and balance in tropical forests. *Oecologia, 145*(1), 87-99

Chave, J., Condit, R., Aguilar, S., Hernandez, A., Lao, S., & Perez, R. (2004). Error propagation and scaling for tropical forest biomass estimates. *Philosophical Transactions of the Royal Society of London. Series B: Biological Sciences*, *359*(1443), 409-420.

Chen, Q., Vaglio Laurin, G., & Valentini, R. (2015). Uncertainty of remotely sensed aboveground biomass over an African tropical forest: Propagating errors from trees to plots to pixels. *Remote Sensing of Environment, 160*, 134-143

Chen, X. (2002). Carbon balance of a eucalypt open forest savanna of Northern Australia. PhD thesis. *Northern Territory University*

Colgan, M., Asner, G., Levick, S.R., Martin, R., & Chadwick, O. (2012). Topo-edaphic controls over woody plant biomass in South African savannas. *Biogeosciences, 9*, 1809-1821

Colgan, M.S., Asner, G.P., & Swemmer, T. (2013). Harvesting tree biomass at the stand level to assess the accuracy of field and airborne biomass estimation in savannas. *Ecological Applications, 23*(5), 1170-1184

Collins, J.N., Hutley, L.B., Williams, R.J., Boggs, G., Bell, D., & Bartolo, R. (2009). Estimating landscape-scale vegetation carbon stocks using airborne multi-frequency polarimetric synthetic aperture radar (SAR) in the savannahs of north Australia. *International Journal of Remote Sensing, 30*(5), 1141-1159

Colomina, I., & Molina, P. (2014). Unmanned aerial systems for photogrammetry and remote sensing: A review. *ISPRS Journal of Photogrammetry and Remote Sensing, 92*, 79-97

Conrad, O., Bechtel, B., Bock, M., Dietrich, H., Fischer, E., Gerlitz, L., Wehberg, J., Wichmann, V., & Böhner, J. (2015). System for Automated Geoscientific Analyses (SAGA) v. 2.1.4. *Geoscientific Model Development, 8*(7), 1991-2007.

Cooke, P., Whitehead, P.J., & Russell-Smith, J. (2009). *Culture, Ecology, and Economy of Fire Management in North Australian Savannas : Rekindling the Wurrk Tradition*. Csiro Publishing.

Corona, P., & Fattorini, L. (2008). Area-based lidar-assisted estimation of forest standing volume. *Canadian Journal of Forest Research, 38*(11), 2911-2916

Culvenor, D.S. (2000). Development of a tree delineation algorithm for application to high spatial resolution digital imagery of Australian native forest. PhD thesis: *The University of Melbourne*

d'Angelo, P., & Reinartz, P. (2011). Semiglobal matching results on the ISPRS stereo matching benchmark. *Institute of Photogrammetry and GeoInformation, Leibniz Universität Hannover. High-Resolution Earth Imaging for Geospatial Information, Hannover*

DeWitt, J.D., Warner, T.A., Chirico, P.G., & Bergstresser, S.E. (2017). Creating high-resolution bare-earth digital elevation models (DEMs) from stereo imagery in an area of densely vegetated deciduous forest using combinations of procedures designed for lidar point cloud filtering. *GIScience & Remote Sensing, 54*(4), 552-572

Duncanson, L.I., Cook, B.D., Hurtt, G.C., & Dubayah, R.O. (2014). An efficient, multi-layered crown delineation algorithm for mapping individual tree structure across multiple ecosystems. *Remote Sensing of Environment, 154*, 378-386

Ediriweera, S., Pathirana, S., Danaher, T., & Nichols, D. (2014). Estimating above-ground biomass by fusion of LiDAR and multispectral data in subtropical woody plant communities in topographically complex terrain in North-eastern Australia. *Journal of Forestry Research, 25*(4), 761-771

Edson, C., & Wing, M.G. (2011). Airborne Light Detection and Ranging (LiDAR) for Individual Tree Stem Location, Height, and Biomass Measurements. *Remote Sensing, 3*(11), 2494-2528

Edwards, A.C., Maier, S.W., Hutley, L.B., Williams, R.J., & Russell-Smith, J. (2013). Spectral analysis of fire severity in north Australian tropical savannas. *Remote Sensing of Environment, 136*, 56-65

Edwards, A.C., Russell-Smith, J., & Maier, S.W. (2018). A comparison and validation of satellite-derived fire severity mapping techniques in fire prone north Australian savannas: Extreme fires and tree stem mortality. *Remote Sensing of Environment, 206*, 287-299

Englhart, S., Keuck, V., & Siegert, F. (2011). Aboveground biomass retrieval in tropical forests — The potential of combined X- and L-band SAR data use. *Remote Sensing of Environment, 115*, 1260-1271

Fatoyinbo, T. (2012). *Remote Sensing of Biomass – Principles and Applications*. Janeza Trdine Rijeka, Croatia

Fensham, R.J., & Fairfax, R.J. (2003). Assessing woody vegetation cover change in north-west Australian savanna using aerial photography. *International Journal of Wildland Fire, 12*(4), 359-367

Ferraz, A., Bretar, F., Jacquemoud, S., Gonçalves, G., Pereira, L., Tomé, M., & Soares, P. (2012). 3-D mapping of a multi-layered Mediterranean forest using ALS data. *Remote Sensing of Environment, 121*, 210-223

Ferraz, A., Saatchi, S., Mallet, C., Jacquemoud, S., Gonçalves, G., Silva, C., Soares, P., Tomé, M., & Pereira, L. (2016a). Airborne Lidar Estimation of Aboveground Forest Biomass in the Absence of Field Inventory. *Remote Sensing, 8*(8), 653

Ferraz, A., Saatchi, S., Mallet, C., & Meyer, V. (2016b). Lidar detection of individual tree size in tropical forests. *Remote Sensing of Environment, 183*, 318-333

Fox, I., Neldner, V., Wilson, G., & Bannink, P. (2001). The vegetation of the tropical Australian savannas. *Queensland Environment Protection Agency: Brisbane*

Franklin, S.E. (2001). *Remote sensing for sustainable forest management*. CRC Press

Frazer, G.W., Magnussen, S., Wulder, M.A., & Niemann, K.O. (2011). Simulated impact of sample plot size and co-registration error on the accuracy and uncertainty of LiDAR-derived estimates of forest stand biomass. *Remote Sensing of Environment, 115*, 636-649

Gaston, K.J., & Spicer, J.I. (2013). *Biodiversity: an introduction*. John Wiley & Sons

Gerard, F.F., & North, P.R.J. (1997). Analyzing the effect of structural variability and canopy gaps on forest BRDF using a geometric-optical model. *Remote Sensing of Environment, 62*(1), 46-62

Gobakken, T., & Næsset, E. (2005). Weibull and percentile models for lidar-based estimation of basal area distribution. *Scandinavian Journal of Forest Research, 20*(6), 490-502

Gobakken, T., & Næsset, E. (2009). Assessing effects of positioning errors and sample plot size on biophysical stand properties derived from airborne laser scanner data. *Canadian Journal of Forest Research, 39*(5), 1036-1052

Goldbergs, G., Levick, S.R., Lawes, M., & Edwards, A. (2018a). Hierarchical integration of individual tree and area-based approaches for savanna biomass uncertainty estimation from airborne LiDAR. *Remote Sensing of Environment, 205*, 141-150

Goldbergs, G., Maier, S., Levick, S., & Edwards, A. (2018b). Efficiency of Individual Tree Detection Approaches Based on Light-Weight and Low-Cost UAS Imagery in Australian Savannas. *Remote Sensing, 10*(2), 161

Goldbergs, G., Maier, S.W., Levick, S.R., & Edwards, A. (2019). Limitations of high resolution satellite stereo imagery for estimating canopy height in Australian tropical savannas. *International Journal of Applied Earth Observation and Geoinformation, 75*, 83-95

Goldstein, E.B., Oliver, A.R., deVries, E., Moore, L.J., & Jass, T. (2015). Ground control point requirements for structure-from-motion derived topography in low-slope coastal environments. *PeerJ PrePrints*

Goodwin, N., Turner, R., & Merton, R. (2005). Classifying Eucalyptus forests with high spatial and spectral resolution imagery: an investigation of individual species and vegetation communities. *Australian Journal of Botany, 53*(4), 337-345

Goodwin, N.R., & Collett, L.J. (2014). Development of an automated method for mapping fire history captured in Landsat TM and ETM+ time series across Queensland, Australia. *Remote Sensing of Environment, 148*, 206-221

Gougeon, F.A., & Leckie, D.G. (2003). Forest information extraction from high spatial resolution images using an individual tree crown approach. *Natural Resources Canada, Canadian Forest Service, Pacific Forestry Centre, Victoria, BC. Information Report BC-X-396E. 27 p.*

Goutte, C., & Gaussier, E. (2005). A probabilistic interpretation of precision, recall and F-score, with implication for evaluation. *European Conference on Information Retrieval* (pp. 345-359). Springer, Berlin, Heidelberg.

Grace, J., San, J., xe, Jos, xe, Meir, P., Miranda, H.S., & Montes, R.A. (2006). Productivity and Carbon Fluxes of Tropical Savannas. *Journal of Biogeography, 33*(3), 387-400

Greiner R, Stanley O, & Austin B (2012). *Sustainable Indigenous Livelihoods from north Australian land and water resources – Towards a research and development agenda and implementation strategy*. NAILSMA, Darwin.

Grodecki, J., & Dial, G. (2003). Block adjustment of high-resolution satellite images described by rational polynomials. *Photogrammetric Engineering & Remote Sensing, 69*(1), 59-68

Hajj, M., Baghdadi, N., Fayad, I., Vieilledent, G., Bailly, J.-S., & Minh, D. (2017). Interest of Integrating Spaceborne LiDAR Data to Improve the Estimation of Biomass in High Biomass Forested Areas. *Remote Sensing, 9*(3), 213

Handbook, A.S.a.L.S.F. (2009). *Australian Soil and Land Survey Field Handbook*. Collingwood, Vic: CSIRO Pub

Harrell, P.A., Kasischke, E.S., Bourgeau-Chavez, L.L., Haney, E.M., & Christensen, N.L. (1997). Evaluation of approaches to estimating aboveground biomass in Southern pine forests using SIR-C data. *Remote Sensing of Environment, 59*, 223-233

Hay, G., Marceau, D., Dube, P., & Bouchard, A. (2001). A multiscale framework for landscape analysis: object-specific analysis and upscaling. *Landscape Ecology, 16*(6), 471-490

Hay, G.J., Castilla, G., Wulder, M.A., & Ruiz, J.R. (2005). An automated object-based approach for the multiscale image segmentation of forest scenes. *International Journal of Applied Earth Observation and Geoinformation, 7*(4), 339-359

Heenkenda, M., Maier, S., & Joyce, K. (2016). Estimating Mangrove Biophysical Variables Using WorldView-2 Satellite Data: Rapid Creek, Northern Territory, Australia. *Journal of Imaging, 2*(3), 24

Heenkenda, M.K., Joyce, K.E., & Maier, S.W. (2015). Mangrove tree crown delineation from high-resolution imagery. *Photogrammetric Engineering & Remote Sensing, 81*(6), 471-479

Hernández-Stefanoni, J.L., Dupuy, J.M., Johnson, K.D., Birdsey, R., Tun-Dzul, F., Peduzzi, A., Caamal-Sosa, J.P., Sánchez-Santos, G., & López-Merlín, D. (2014). Improving Species Diversity and Biomass Estimates of Tropical Dry Forests Using Airborne LiDAR. *Remote Sensing, 6*(6), 4741-4763

Hirschmuller, H. (2008). Stereo Processing by Semiglobal Matching and Mutual Information. *Pattern Analysis and Machine Intelligence, IEEE Transactions on pattern analysis and machine intelligence, 30*(2), 328-341.

Hirschmüller, H. (2011). Semi-global matching-motivation, developments and applications. *Photogrammetric Week (Vol. 11, pp. 173-184). Wichmann Verlag Heidelberg, Germany.*

Höhle, J., & Höhle, M. (2009). Accuracy assessment of digital elevation models by means of robust statistical methods. *ISPRS Journal of Photogrammetry and Remote Sensing, 64*, 398-406

Huang, P.-H., Matzen, K., Kopf, J., Ahuja, N., & Huang, J.-B. (2018). Deepmvs: Learning multi-view stereopsis. *Proceedings of the IEEE Conference on Computer Vision and Pattern Recognition* (pp. 2821-2830)

Hung, C., Bryson, M., & Sukkarieh, S. (2012). Multi-class predictive template for tree crown detection. *ISPRS Journal of Photogrammetry and Remote Sensing, 68*, 170-183

Hutley, L.B., Beringer, J., Isaac, P.R., Hacker, J.M., & Cernusak, L.A. (2011). A sub-continental scale living laboratory: Spatial patterns of savanna vegetation over a rainfall gradient in northern Australia. *Agricultural and Forest Meteorology, 151*(11), 1417-1428

Hyyppä, J., Hyyppä, H., Leckie, D., Gougeon, F., Yu, X., & Maltamo, M. (2008). Review of methods of small-footprint airborne laser scanning for extracting forest inventory data in boreal forests. *International Journal of Remote Sensing, 29*(5), 1339-1366

Immitzer, M., Stepper, C., Böck, S., Straub, C., & Atzberger, C. (2016). Use of WorldView-2 stereo imagery and National Forest Inventory data for wall-to-wall mapping of growing stock. *Forest Ecology and Management, 359*, 232-246

Isenburg, M. (2014). "LAStools - efficient LiDAR processing software" (version 141017, unlicensed) http://rapidlasso.com/LAStools

Jacobs, M.R. (1955). Growth habits of the eucalypts. *Growth habits of the Eucalypts.*

Jakubowski, M.K., Guo, Q., & Kelly, M. (2013). Tradeoffs between lidar pulse density and forest measurement accuracy. *Remote Sensing of Environment, 130*, 245-253

James, M.R., & Robson, S. (2014). Mitigating systematic error in topographic models derived from UAV and ground-based image networks. *Earth Surface Processes and Landforms, 39*(10), 1413-1420

Järnstedt, J., Pekkarinen, A., Tuominen, S., Ginzler, C., Holopainen, M., & Viitala, R. (2012). Forest variable estimation using a high-resolution digital surface model. *ISPRS Journal of Photogrammetry and Remote Sensing, 74*, 78-84

Kaartinen, H., Hyyppä, J., Yu, X., Vastaranta, M., Hyyppä, H., Kukko, A., Holopainen, M., Heipke, C., Hirschmugl, M., & Morsdorf, F. (2012). An international comparison of individual tree detection and extraction using airborne laser scanning. *Remote Sensing, 4*(4), 950-974

Kandare, K., Orka, H.O., Chan, J.C.-W., & Dalponte, M. (2016). Effects of forest structure and airborne laser scanning point cloud density on 3D delineation of individual tree crowns. *European Journal of Remote Sensing, 49*(1), 337-359.

Kandel, Y.P., Fox, J.C., Arndt, S.K., & Livesley, S.J. (2011). LiDAR estimation of mean dominant height, quadratic mean canopy height and stem density in native sclerophyll forests. *Proceedings of SilviLaser, Hobart, Tasmania, Australia, Conference Secretariat*

Kanniah, K.D., Beringer, J., & Hutley, L.B. (2010). The comparative role of key environmental factors in determining savanna productivity and carbon fluxes: A review, with special reference to northern Australia. *Progress in physical Geography*

Kanniah, K.D., Beringer, J., & Hutley, L.B. (2011). Environmental controls on the spatial variability of savanna productivity in the Northern Territory, Australia. *Agricultural and Forest Meteorology, 151*(11), 1429-1439

Kanniah, K.D., Beringer, J., Hutley, L.B., Tapper, N.J., & Zhu, X. (2009). Evaluation of Collections 4 and 5 of the MODIS Gross Primary Productivity product and algorithm improvement at a tropical savanna site in northern Australia. *Remote Sensing of Environment, 113*, 1808-1822

Koch, B. (2010). Status and future of laser scanning, synthetic aperture radar and hyperspectral remote sensing data for forest biomass assessment. *ISPRS Journal of Photogrammetry and Remote Sensing, 65*, 581-590

Köhl, M., Magnussen, S.S., & Marchetti, M. (2006). *Sampling methods, remote sensing and GIS multiresource forest inventory*. Springer Science & Business Media

Konecny, G. (2014). *Geoinformation: remote sensing, photogrammetry and geographic information systems*. CRC Press

Korpela, I., Dahlin, B., Schäfer, H., Bruun, E., Haapaniemi, F., Honkasalo, J., Ilvesniemi, S., Kuutti, V., Linkosalmi, M., & Mustonen, J. (2007). Single-tree forest inventory using lidar and aerial images for 3D treetop positioning, species recognition, height and crown width estimation. In, *Proceedings of ISPRS workshop on laser scanning* (pp. 227-233)

Kumar, L., Skidmore, A.K., & Mutanga, O. (2010). Leaf level experiments to discriminate between eucalyptus species using high spectral resolution reflectance data: use of derivatives, ratios and vegetation indices. *Geocarto International, 25*(4), 327-344

Landsberg J, Gillieson D, & Salt D (2011). *Trees in savanna landscapes: finding the balance*. David Gillieson.

Lasky, J.R., Uriarte, M., Boukili, V.K., Erickson, D.L., John Kress, W., & Chazdon, R.L. (2014). The relationship between tree biodiversity and biomass dynamics changes with tropical forest succession. *Ecology Letters, 17*(9), 1158-1167

Lee, A.C. (2008). Utilising airborne scanning laser (LiDAR) to improve the assessment of Australian native forest structure. *Fenner School of Environment and Society, College of Medicine, Biology and Environment*: The Australian National University

Lee, A.C., & Lucas, R.M. (2007). A LiDAR-derived canopy density model for tree stem and crown mapping in Australian forests. *Remote Sensing of Environment, 111*, 493-518

Lefsky, M.A., Cohen, W.B., Harding, D.J., Parker, G.G., Acker, S.A., & Gower, S.T. (2002). Lidar remote sensing of above-ground biomass in three biomes. *Global Ecology and Biogeography, 11*(5), 393-399

Lefsky, M.A., Harding, D., Cohen, W.B., Parker, G., & Shugart, H.H. (1999). Surface Lidar Remote Sensing of Basal Area and Biomass in Deciduous Forests of Eastern Maryland, USA. *Remote Sensing of Environment, 67*, 83-98

Lehmann, C.E.R., Anderson, T.M., Sankaran, M., Higgins, S.I., Archibald, S., Hoffmann, W.A., Hanan, N.P., Williams, R.J., Fensham, R.J., Felfili, J., Hutley, L.B., Ratnam, J., San Jose, J., Montes, R., Franklin, D., Russell-Smith, J., Ryan, C.M., Durigan, G., Hiernaux, P., Haidar, R., Bowman, D.M.J.S., & Bond, W.J. (2014). Savanna Vegetation-Fire-Climate Relationships Differ Among Continents. *Science, 343*(6170), 548-552

Levick, S.R., Hessenmöller, D., & Schulze, E.-D. (2016). Scaling wood volume estimates from inventory plots to landscapes with airborne LiDAR in temperate deciduous forest. *Carbon Balance and Management, 11*(1), 1-14

Li, W., Guo, Q., Jakubowski, M.K., & Kelly, M. (2012). A new method for segmenting individual trees from the lidar point cloud. *Photogrammetric Engineering & Remote Sensing, 78*(1), 75-84

Lindberg, E., Holmgren, J., Olofsson, K., Wallerman, J., & Olsson, H. (2010). Estimation of tree lists from airborne laser scanning by combining single-tree and area-based methods. *International Journal of Remote Sensing, 31*(5), 1175-1192

Lu, D. (2006). The potential and challenge of remote sensing-based biomass estimation. *International Journal of Remote Sensing, 27*(7), 1297-1328

Lu, D., Chen, Q., Wang, G., Liu, L., Li, G., & Moran, E. (2016). A survey of remote sensing-based aboveground biomass estimation methods in forest ecosystems. *International Journal of Digital Earth, 9*(1), 63-105

Lucas, R.M., Ellison, J.C., Mitchell, A., Donnelly, B., Finlayson, M., & Milne, A.K. (2002). Use of stereo aerial photography for quantifying changes in the extent and height of mangroves in tropical Australia. *Wetlands Ecology and Management, 10*(2), 159-173

Lucas, R.M., Lee, A.C., & Bunting, P.J. (2008). Retrieving forest biomass through integration of CASI and LiDAR data. *International Journal of Remote Sensing, 29*(5), 1553-1577

Luhmann, T., Fraser, C., & Maas, H.-G. (2016). Sensor modelling and camera calibration for close-range photogrammetry. *ISPRS Journal of Photogrammetry and Remote Sensing, 115*, 37-46

Magnussen, S., Næsset, E., & Gobakken, T. (2013). Prediction of tree-size distributions and inventory variables from cumulants of canopy height distributions. *Forestry*, *86*(5), 583-595.

Maier, S.W. (2010). Changes in surface reflectance from wildfires on the Australian continent measured by MODIS. *International Journal of Remote Sensing, 31*(12), 3161-3176

Maier, S.W., & Russell-Smith, J. (2012a). Measuring and monitoring of contemporary fire regimes in Australia using satellite remote sensing. *Flammable Australia: fire regimes, biodiversity and ecosystems in a changing world*, 79-95

Maier, S.W., & Russell-Smith, J. (2012b). *Measuring and monitoring of contemporary fire regimes in Australia using satellite remote sensing*. CSIRO Publishing: Melbourne

Malenovský, Z., Rott, H., Cihlar, J., Schaepman, M.E., García-Santos, G., Fernandes, R., & Berger, M. (2012). Sentinels for science: Potential of Sentinel-1, -2, and -3 missions for scientific observations of ocean, cryosphere, and land. *Remote Sensing of Environment, 120*, 91-101

Maltamo, M., Mustonen, K., Hyyppä, J., Pitkänen, J., & Yu, X. (2004). The accuracy of estimating individual tree variables with airborne laser scanning in a boreal nature reserve. *Canadian Journal of Forest Research, 34*(9), 1791-1801

Maltamo, M., Næsset, E., & Vauhkonen, J. (2014). *Forestry Applications of Airborne Laser Scanning Concepts and Case Studies*. Springer

Mascaro, J., Detto, M., Asner, G.P., & Muller-Landau, H.C. (2011). Evaluating uncertainty in mapping forest carbon with airborne LiDAR. *Remote Sensing of Environment, 115*, 3770-3774

McGaughey, R.J. (2015). FUSION/LDV: Software for LIDAR data analysis and visualization - Version 3.50. *US Department of Agriculture, Forest Service, Pacific Northwest Research Station: Seattle, WA, USA*

McGill, R., Tukey, J.W., & Larsen, W.A. (1978). Variations of box plots. *The American Statistician, 32*, 12-16

Meyer, C.P., Cook, G.D., Reisen, F., Smith, T.E.L., Tattaris, M., Russell-Smith, J., Maier, S.W., Yates, C.P., & Wooster, M.J. (2012). Direct measurements of the seasonality of emission factors from savanna fires in northern Australia. *Journal of Geophysical Research: Atmospheres, 117*(D20).

Meyer, V., Saatchi, S.S., Chave, J., Dalling, J.W., Bohlman, S., Fricker, G.A., Robinson, C., Neumann, M., & Hubbell, S. (2013). Detecting tropical forest biomass dynamics from repeated airborne lidar measurements. *Biogeosciences, 10*(8), 5421-5438

Mitchell, A.L., Lucas, R.M., Donnelly, B.E., Pfitzner, K., Milne, A.K., & Finlayson, M. (2007). A new map of mangroves for Kakadu National Park, Northern Australia, based on stereo aerial photography. *Aquatic Conservation: Marine and Freshwater Ecosystems, 17*(5), 446-467

Miura, N., & Jones, S.D. (2010). Characterizing forest ecological structure using pulse types and heights of airborne laser scanning. *Remote Sensing of Environment, 114*, 1069-1076

Mongus, D., & Žalik, B. (2015). An efficient approach to 3D single tree-crown delineation in LiDAR data. *ISPRS Journal of Photogrammetry and Remote Sensing, 108*, 219-233

Montagu, K.D., Düttmer, K., Barton, C.V.M., & Cowie, A.L. (2005). Developing general allometric relationships for regional estimates of carbon sequestration—an example using Eucalyptus pilularis from seven contrasting sites. *Forest Ecology and Management, 204*(1), 115-129

Montesano, P.M., Neigh, C., Sun, G., Duncanson, L., Van Den Hoek, J., & Ranson, K.J. (2017). The use of sun elevation angle for stereogrammetric boreal forest height in open canopies. *Remote Sensing of Environment, 196*, 76-88

Moore, C., Beringer, J., Evans, B., Hutley, L., McHugh, I., & Tapper, N. (2015). The contribution of trees and grasses to productivity of an Australian tropical savanna. *Biogeosciences, 13*(8), 2387-2403.

Mumby, P.J., Green, E.P., Edwards, A.J., & Clark, C.D. (1999). The cost-effectiveness of remote sensing for tropical coastal resources assessment and management. *Journal of Environmental Management, 55*(3), 157-166

Næsset, E., & Gobakken, T. (2008). Estimation of above- and below-ground biomass across regions of the boreal forest zone using airborne laser. *Remote Sensing of Environment, 112*(6), 3079-3090

Næsset, E., & Økland, T. (2002). Estimating tree height and tree crown properties using airborne scanning laser in a boreal nature reserve. *Remote Sensing of Environment, 79*(1), 105-115

Neigh, C., Masek, J., Bourget, P., Cook, B., Huang, C., Rishmawi, K., & Zhao, F. (2014). Deciphering the Precision of Stereo IKONOS Canopy Height Models for US Forests with G-LiHT Airborne LiDAR. *Remote Sensing, 6*(3), 1762

Newton, A.C. (2007). *Forest ecology and conservation: a handbook of techniques*. Oxford University Press

O'Donnell, K. (2005). Tropical Savannas CRC-Tropical Savannas CRC home

O'Grady, A.P., Chen, X., Eamus, D., & Hutley, L.B. (2000). Composition, leaf area index and standing biomass of eucalypt open forests near Darwin in the Northern Territory, Australia. *Australian Journal of Botany, 48*(5), 629-638

O'Grady, A.P., Eamus, D., & Hutley, L.B. (1999). Transpiration increases during the dry season: patterns of tree water use in eucalypt open-forests of northern Australia. *Tree Physiology, 19*(9), 591-597

Paneque-Gálvez, J., McCall, M., Napoletano, B., Wich, S., & Koh, L. (2014). Small Drones for Community-Based Forest Monitoring: An Assessment of Their Feasibility and Potential in Tropical Areas. *Forests, 5*(6), 1481-1507.

Paul, K.I., Roxburgh, S.H., England, J.R., Ritson, P., Hobbs, T., Brooksbank, K., John Raison, R., Larmour, J.S., Murphy, S., Norris, J., Neumann, C., Lewis, T., Jonson, J., Carter, J.L., McArthur, G., Barton, C., & Rose, B. (2013). Development and testing of allometric equations for estimating above-ground biomass of mixed-species environmental plantings. *Forest Ecology and Management, 310*, 483-494

Persson, H.J., & Perko, R. (2016). Assessment of boreal forest height from WorldView-2 satellite stereo images. *Remote Sensing Letters, 7*(12), 1150-1159

Popescu, S., Wynn, R., & Nelson, R. (2003). Measuring individual tree crown diameter with lidar and assessing its influence on estimating forest volume and biomass. *Canadian journal of remote sensing, 29*(5), 564-577

Popescu, S., & Zhao, K. (2008). A voxel-based lidar method for estimating crown base height for deciduous and pine trees. *Remote Sensing of Environment, 112*(3), 767-781

Popescu, S., Zhao, K., Feagin, R., Gatziolis, D., Sheridan, R., Srinivasan, S., Ku, N., & Kulawardhana, R. (2013). From grass to forest biomass: uncertainty estimates with lidar remote sensing. *AGU Fall Meeting Abstracts*

Popescu, S.C., & Hauglin, M. (2014). Estimation of Biomass Components by Airborne Laser Scanning. In M. Maltamo, E. Næsset, & J. Vauhkonen (Eds.), *Forestry Applications of Airborne Laser Scanning: Concepts and Case Studies* (pp. 157-175). Dordrecht: Springer Netherlands

Popescu, S.C., Wynne, R.H., & Nelson, R.F. (2002). Estimating plot-level tree heights with lidar: local filtering with a canopy-height based variable window size. *Computers and Electronics in Agriculture, 37*(1-3), 71-95

Preece, N.D., Lawes, M.J., Rossman, A.K., Curran, T.J., & van Oosterzee, P. (2015). Modelling the growth of young rainforest trees for biomass estimates and carbon sequestration accounting. *Forest Ecology and Management, 351*, 57-66

Pulfrich, C. (1922). Die Stereoskopie im Dienste der isochromen und heterochromen Photometrie. *Naturwissenschaften, 10*, 751-761

QGIS (2017). QGIS Geographic Information System. Open Source Geospatial Foundation Project. *http://qgis.osgeo.org*

Reitberger, J., Schnörr, C., Krzystek, P., & Stilla, U. (2009). 3D segmentation of single trees exploiting full waveform LIDAR data. *ISPRS Journal of Photogrammetry and Remote Sensing, 64*(6), 561-574

Réjou-Méchain, M., Tymen, B., Blanc, L., Fauset, S., Feldpausch, T.R., Monteagudo, A., Phillips, O.L., Richard, H., & Chave, J. (2015). Using repeated small-footprint LiDAR acquisitions to infer spatial and temporal variations of a high-biomass Neotropical forest. *Remote Sensing of Environment, 169*, 93-101

Riaño, D., Meier, E., Allgöwer, B., Chuvieco, E., & Ustin, S.L. (2003). Modeling airborne laser scanning data for the spatial generation of critical forest parameters in fire behavior modeling. *Remote Sensing of Environment, 86*(2), 177-186

Richards, G.P., & Brack, C. (2004). A continental biomass stock and stock change estimation approach for Australia. *Australian Forestry, 67*(4), 284-288

Rogers, P., Jalal, P., Boyd, J., & Jalal, K. (2012). *An introduction to sustainable development*. Routledge.

Rombouts, J., Ferguson, I.S., & Leech, J.W. (2010). Campaign and site effects in LiDAR prediction models for site-quality assessment of radiata pine plantations in South Australia. *International Journal of Remote Sensing, 31*(5), 1155-1173

Russell-Smith, J., Murphy, B., Edwards, A., & Meyer, C.P. (2015). *Carbon Accounting and Savanna Fire Management*. Victoria, Australia: CSIRO publishing

Russell-Smith, J., Murphy, B.P., Meyer, C.P., Cooka, G.D., Maier, S., Edwards, A.C., Schatz, J., & Brocklehurst, P. (2009). Improving estimates of savanna burning emissions for greenhouse accounting in northern Australia: limitations, challenges, applications. *International Journal of Wildland Fire, 18*(1), 1-18

Russell-Smith, J., Yates, C., Edwards, A., Allan, G.E., Cook, G.D., Cooke, P., Craig, R., Heath, B., & Smith, R. (2003). Contemporary fire regimes of northern Australia, 1997–2001: change since Aboriginal occupancy, challenges for sustainable management. *International Journal of Wildland Fire, 12*(4), 283-297

Saatchi, S.S., Harris, N.L., Brown, S., Lefsky, M., Mitchard, E.T.A., Salas, W., Zutta, B.R., Buermann, W., Lewis, S.L., Hagen, S., Petrova, S., White, L., Silman, M., & Morel, A. (2011). Benchmark map of forest carbon stocks in tropical regions across three continents. *Proceedings of the National Academy of Sciences, 108*(24), 9899-9904

Saputra, M.R.U., Markham, A., & Trigoni, N. (2018). Visual SLAM and structure from motion in dynamic environments: A survey. *ACM Computing Surveys (CSUR), 51*(2), 37

Saugier, B., Roy, J., & Mooney, H.A. (2001). Estimations of Global Terrestrial Productivity-23: Converging toward a Single Number? *Terrestrial global productivity*.

Schull, M.A., Knyazikhin, Y., Xu, L., Samanta, A., Carmona, P.L., Lepine, L., Jenkins, J.P., Ganguly, S., & Myneni, R.B. (2011). Canopy spectral invariants, Part 2: Application to classification of forest types from hyperspectral data. *Journal of Quantitative Spectroscopy and Radiative Transfer, 112*(4), 736-750

Shendryk, I., Broich, M., Tulbure, M.G., & Alexandrov, S.V. (2016). Bottom-up delineation of individual trees from full-waveform airborne laser scans in a structurally complex eucalypt forest. *Remote Sensing of Environment, 173*, 69-83

Silva, C.A., Klauberg, C., Chaves e Carvalho, S.d.P., Hudak, A.T., & Rodriguez, L.C.E. (2014). Mapping aboveground carbon stocks using LiDAR data in Eucalyptus spp. plantations in the state of São Paulo, Brazil. *Scientia Forestalis. 42 (104): 591-604.*, *42*(104), 591-604.

Skowronski, N.S., Clark, K.L., Duveneck, M., & Hom, J. (2011). Three-dimensional canopy fuel loading predicted using upward and downward sensing LiDAR systems. *Remote Sensing of Environment, 115*(2), 703-714

St-Onge, B., Hu, Y., & Vega, C. (2008). Mapping the height and above-ground biomass of a mixed forest using lidar and stereo Ikonos images. *International Journal of Remote Sensing, 29*(5), 1277-1294

Statistics (2017). *Australian demographic statistics*. Australian Bureau of Statistics: https://www.abs.gov.au

Staver, A.C. (2018). Prediction and scale in savanna ecosystems. *New Phytologist, 219*(1), 52-57.

Stibig, H.J., Beuchle, R., & Achard, F. (2003). Mapping of the tropical forest cover of insular Southeast Asia from SPOT4-Vegetation images. *International Journal of Remote Sensing, 24*(18), 3651-3662

Straub, C., Tian, J., Seitz, R., & Reinartz, P. (2013). Assessment of Cartosat-1 and WorldView-2 stereo imagery in combination with a LiDAR-DTM for timber volume estimation in a highly structured forest in Germany. *Forestry, 86*(4), 463-473

Tang, L., & Shao, G. (2015). Drone remote sensing for forestry research and practices. *Journal of Forestry Research, 26*(4), 791-797

TERN (2012). Litchfield Savanna SuperSite. Available online: http://www.tern-supersites.net.au/supersites/lfld

Thomas, V., Treitz, P., McCaughey, J.H., & Morrison, I. (2006). Mapping stand-level forest biophysical variables for a mixedwood boreal forest using lidar: an examination of scanning density. *Canadian Journal of Forest Research, 36*(1), 34-47.

Tickle, P.K., Lee, A., Lucas, R.M., Austin, J., & Witte, C. (2006). Quantifying Australian forest floristics and structure using small footprint LiDAR and large scale aerial photography. *Forest Ecology and Management, 223*(1-3), 379-394

Tomaštík, J., Mokroš, M., Saloň, Š., Chudý, F., & Tunák, D. (2017). Accuracy of Photogrammetric UAV-Based Point Clouds under Conditions of Partially-Open Forest Canopy. *Forests, 8*(5), 151

Torresan, C., Berton, A., Carotenuto, F., Di Gennaro, S.F., Gioli, B., Matese, A., Miglietta, F., Vagnoli, C., Zaldei, A., & Wallace, L. (2017). Forestry applications of UAVs in Europe: a review. *International Journal of Remote Sensing, 38*(8-10), 2427-2447

Trumbore, S., Brando, P., & Hartmann, H. (2015). Forest health and global change. *Science, 349*(6250), 814-818

Turner, R.S. (2006). An airborne Lidar canopy segmentation approach for estimating above-ground biomass in coastal eucalypt forests. (*Doctoral dissertation, University of New South Wales*).

Ullman, S. (1979). The interpretation of structure from motion. *Proceedings of the Royal Society of London. Series B. Biological Sciences, 203(1153), 405-426.*

Valbuena, R., Mauro, F., Arjonilla, F.J., & Manzanera, J.A. (2011). Comparing airborne laser scanning-imagery fusion methods based on geometric accuracy in forested areas. *Remote Sensing of Environment, 115*(8), 1942-1954

Van der Werf, G.R., Randerson, J.T., Giglio, L., Collatz, G.J., Mu, M., Kasibhatla, P.S., Morton, D.C., DeFries, R.S., Jin, Y., & van Leeuwen, T.T. (2010). Global fire emissions and the contribution of deforestation, savanna, forest, agricultural, and peat fires (1997–2009). *Atmos. Chem. Phys., 10*(23), 11707-11735

Vastaranta, M., Holopainen, M., Yu, X., Haapanen, R., Melkas, T., Hyyppä, J., & Hyyppä, H. (2011). Individual tree detection and area-based approach in retrieval of forest inventory characteristics from low-pulse airborne laser scanning data. *Photogrammetric Journal of Finland, 22*(2), 1-13

Vastaranta, M., Kankare, V., Holopainen, M., Yu, X., Hyyppä, J., & Hyyppä, H. (2012). Combination of individual tree detection and area-based approach in imputation of forest variables using airborne laser data. *ISPRS Journal of Photogrammetry and Remote Sensing, 67*, 73-79

Vauhkonen, J., Ene, L., Gupta, S., Heinzel, J., Holmgren, J., Pitkänen, J., Solberg, S., Wang, Y., Weinacker, H., & Hauglin, K.M. (2011). Comparative testing of single-tree detection algorithms under different types of forest. *Forestry*, *85*(1), 27-40.

Wallace, L., Lucieer, A., Malenovský, Z., Turner, D., & Vopěnka, P. (2016). Assessment of Forest Structure Using Two UAV Techniques: A Comparison of Airborne Laser Scanning and Structure from Motion (SfM) Point Clouds. *Forests, 7*(3), 62.

Wallace, L., Lucieer, A., Watson, C., & Turner, D. (2012). Development of a UAV-LiDAR System with Application to Forest Inventory. *Remote Sensing, 4*(6), 1519-1543.

Werner, P.A., & Murphy, P.G. (2001). Size-specific biomass allocation and water content of above- and below-ground components of three Eucalyptus species in a northern Australian savanna. *Australian Journal of Botany, 49*(2), 155-167

Westoby, M.J., Brasington, J., Glasser, N.F., Hambrey, M.J., & Reynolds, J.M. (2012). 'Structure-from-Motion' photogrammetry: A low-cost, effective tool for geoscience applications. *Geomorphology, 179*, 300-314

White, J., Wulder, M., Vastaranta, M., Coops, N., Pitt, D., & Woods, M. (2013). The Utility of Image-Based Point Clouds for Forest Inventory: A Comparison with Airborne Laser Scanning. *Forests, 4*(3), 518-536.

Whiteside, T.G., & Bartolo, R.E. (2015). Use of WorldView-2 time series to establish a wetland monitoring program for potential offsite impacts of mine site rehabilitation. *International Journal of Applied Earth Observation and Geoinformation, 42*, 24-37

Whiteside, T.G., & Bartolo, R.E. (2016). Robust and repeatable ruleset development for hierarchical object-based monitoring of revegetation using high spatial and temporal resolution UAS data. proceedings.utwente.nl

Whiteside, T.G., Boggs, G.S., & Maier, S.W. (2011a). Comparing object-based and pixel-based classifications for mapping savannas. *International Journal of Applied Earth Observation and Geoinformation, 13*(6), 884-893

Whiteside, T.G., Boggs, G.S., & Maier, S.W. (2011b). Extraction of tree crowns from high resolution imagery over Eucalypt dominant tropical savannas. *Photogrammetric Engineering & Remote Sensing, 77*(8), 813-824

Whiteside, T.G., Maier, S.W., & Boggs, G.S. (2014). Area-based and location-based validation of classified image objects. *International Journal of Applied Earth Observation and Geoinformation, 28*, 117-130

Williams, R., Carter, J., Duff, G., Woinarski, J.Z., Cook, G., & Farrer, S. (2005a). Carbon accounting, land management, science and policy uncertainty in Australian savanna landscapes: introduction and overview. *CSIRO*

Williams, R., Hutley , L.B., Cook, G.D., Russell-Smith, J., Edwards, A., & Chen, X. (2004). Assessing the carbon sequestration potential of mesic savannas in the Northern Territory, Australia: approaches, uncertainties and potential impacts of fire. *Functional Plant Biology, 31*(5), 415-422

Williams, R.J., Myers, B.A., Muller, W.J., Duff, G.A., & Eamus, D. (1997). Leaf Phenology of Woody Species in a North Australian Tropical Savanna. *Ecology, 78*(8), 2542-2558

Williams, R.J., Zerihun, A., Montagu, K.D., Hoffman, M., Hutley, L.B., & Chen, X. (2005b). Allometry for estimating aboveground tree biomass in tropical and subtropical eucalypt

woodlands: towards general predictive equations. *Australian Journal of Botany, 53*(7), 607-619

Woinarski, J., Mackey, B., Nix, H., & Traill, B. (2007). *The nature of Northern Australia: it's natural values, ecological processes and future prospects*. ANU e Press

Wood, M., Keightley, E., Lee, A., & Norman, P. (2006). Continental Forest Monitoring Framework, Technical Report - Design and Pilot Study. *National Forest Inventory, Bureau of Rural Sciences, Canberra.*

Woodgate, W., Jones, S.D., Suarez, L., Hill, M.J., Armston, J.D., Wilkes, P., Soto-Berelov, M., Haywood, A., & Mellor, A. (2015). Understanding the variability in ground-based methods for retrieving canopy openness, gap fraction, and leaf area index in diverse forest systems. *Agricultural and Forest Meteorology, 205*, 83-95

Wu, J., & Qi, Y. (2000). Dealing with scale in landscape analysis: an overview. *Geographic Information Sciences, 6*(1), 1-5

Wulder, M. (1998). Optical remote-sensing techniques for the assessment of forest inventory and biophysical parameters. *Progress in physical Geography, 22*(4), 449-476

Yu, X., Hyyppä, J., Holopainen, M., & Vastaranta, M. (2010). Comparison of Area-Based and Individual Tree-Based Methods for Predicting Plot-Level Forest Attributes. *Remote Sensing, 2*(6), 1481

Yu, X., Hyyppä, J., Karjalainen, M., Nurminen, K., Karila, K., Vastaranta, M., Kankare, V., Kaartinen, H., Holopainen, M., Honkavaara, E., Kukko, A., Jaakkola, A., Liang, X., Wang, Y., Hyyppä, H., & Katoh, M. (2015). Comparison of Laser and Stereo Optical, SAR and InSAR Point Clouds from Air- and Space-Borne Sources in the Retrieval of Forest Inventory Attributes. *Remote Sensing, 7*(12), 15933-15954.
